

COMBINED CANCER THERAPY USING GOLD NANOPARTICLES

by

Celina Yang

M.Sc. Ryerson University, Toronto, Canada, 2014

B.Sc. University of Toronto, Toronto, Canada, 2011

A dissertation

presented to Ryerson University

in partial fulfillment of the

requirements for the degree of

Doctor of Philosophy

in the Program of

Biomedical Physics

Toronto, Ontario, Canada, 2018

© Celina Yang, 2018

Author's Declaration

I hereby declare that I am the sole author of this dissertation. This is a true copy of the dissertation, including any required final revisions, as accepted by my examiners.

I authorize Ryerson University to lend this dissertation to other institutions or individuals for the purpose of scholarly research.

I further authorize Ryerson University to reproduce this dissertation by photocopying or by other means, in total or in part, at the request of other institutions or individuals for the purpose of scholarly research.

I understand that my dissertation may be made electronically available to the public.

Celina Yang

Abstract

Combined cancer therapy using gold nanoparticles

Celina Yang
Doctor of Philosophy, Biomedical Physics
Ryerson University, 2018

This dissertation presents the effect of peptide-modified 10 nm gold nanoparticles (GNPs) with chemotherapeutic drugs, bleomycin and cisplatin, and 2 Gy of 6 MV X-ray irradiation in MDA-MB-231 cells. The GNPs were modified with a peptide sequence containing an 'RGD' amino acid motif. Bleomycin binds to the surface of the GNPs through a thiol bond and cisplatin has no known significant interaction with the GNP surface.

No significant toxicity was induced by introducing GNPs to MDA-MB-231 cells at the 0.3 nM concentration used throughout this dissertation. The surface modification with 'RGD' peptides increased accumulation of the GNP constructs 6~7 fold compared to the unmodified counterparts. There was no significant difference in the accumulation of GNPs in the presence of bleomycin or cisplatin. These results suggest that the presence of chemotherapeutics do not affect the accumulation of peptide modified GNPs into cells.

The effect of having GNPs with chemotherapeutics was examined. The presence of GNPs with bleomycin decreased the survival of MDA-MB-231 cells by 18 ± 3 % compared to treatment with the same concentration of free bleomycin. Treating cells with GNPs and cisplatin did not have a significant difference in survival compared to the same concentration of free cisplatin treatment. This suggests that conjugating chemotherapeutics onto the GNPs can result in a more efficient

delivery of the drug. If the drug does not bind to the GNP surface, having GNPs in the media does not interfere with the uptake of the drug.

The effect of radiosensitization in the presence of GNPs was studied by incubating cells with 0.3 nM GNPs prior to irradiation with 2 Gy of 6 MV X-rays. The survival fraction decreased by $19 \pm 6 \%$ compared to the irradiated control condition.

Lastly, the triple combined effect of GNPs, chemotherapeutics, and irradiation was investigated. The presence of GNPs had an advantage to the combined chemotherapy and radiation therapy. Based on results from these studies, GNPs can be used in addition to combined chemotherapy and radiation therapy for improved outcomes in cancer treatment.

Acknowledgements

Firstly, I would like to express my sincere and extreme gratitude to my supervisor, Dr. Devika Chithrani, for being an incredible mentor academically and personally. Her passion and drive in research has been a great example for me and helped me grow as a research scientist.

I would also like to extend my gratitude to my co-supervisor, Dr. Michael Kolios. His input guided this dissertation in a clear direction and his encouragement cultivated my confidence.

My supervisory committee members, Dr. Costin Antonescu and Dr. James Gräfe, have been available despite of their busy schedule. Discussions with them helped me expand my knowledge and allowed me to observe and tackle problems from various angles. Their inputs have made this dissertation progress efficiently.

Furthermore, I would like to thank Dr. Monique Van Prooijen for helping us with radiation experiments and Dr. Caterina Di Ciano-Oliveira for sharing her expertise on imaging and image analysis components. I also would like to mention and extend my gratitude toward Charmaine Cruje for sharing enjoyable conversations and aiding in proofreading and editing of my work.

Most importantly, I would like to thank my family and friends for their constant and extensive support: my mother for always being by my side and encouraging me to remain positive; my father for teaching me to be calm and persevere through any difficulties that come my way; my brother, Albert, for reminding me to look at the big picture and have humour in life; CHYKLS for inspiring me to explore beyond my comfort zone; and my husband, Sam, for having confidence in my abilities.

Table of contents

Author’s Declaration.....	ii
Abstract.....	iii
Acknowledgements.....	v
List of Tables	x
List of Figures.....	xi
Symbols & Abbreviations.....	xvii
Chapter 1 Introduction	1
1.1 Cell Biology of Cancer.....	1
1.2 Types of Cancer Treatment.....	3
1.3 Drug delivery using nanoparticles.....	5
1.4 Synthesis and Biocompatibility of GNPs.....	8
1.5 Accumulation of GNPs in tissue and cellular levels	11
1.5.1 Tumour Microenvironment and the Enhanced Permeability and Retention (EPR).....	11
1.5.2. Penetration of GNPs through the Extracellular Matrix (ECM).....	13
1.5.3 Cell – NP interaction, mechanisms of cellular uptake and pathway of NPs.....	16
1.5.4 Nuclear targeting.....	20
1.5.5 Exocytosis	22
1.6 Surface modification of GNPs with peptide sequences	24
1.7 Rationale for the use of 10 nm GNPs.....	26
1.8 DNA Damage.....	27
1.9 Chemotherapy	29
1.9.1 Action of bleomycin	29
1.9.2 Action of cisplatin.....	31
1.10 Radiation therapy	33
1.10.1 Use of radiation therapy in cancer treatment	33
1.10.2 High Z materials as radiosensitizers	34
1.10.3. Physical mechanism of GNP sensitization	36
1.10.4 Other mechanisms of GNP radiosensitization.....	40
1.11 Goals and specific aims.....	43
1.12 Overview of dissertation	44

Chapter 2 The use of chemotherapeutic drugs with peptide modified gold nanoparticles	46
2.1 Introduction	46
2.2 Methods	48
2.2.1 <i>Synthesis of colloidal gold nanoparticles</i>	48
2.2.2 <i>Preparation of peptide modified GNP constructs</i>	49
2.2.3 <i>Characterization of NPs</i>	49
2.2.4 <i>Hyperspectral imaging</i>	50
2.2.5 <i>Cell culture and GNP delivery</i>	50
2.2.6 <i>Quantification of GNP accumulation in cells</i>	50
2.2.7 <i>Clonogenic Assay</i>	52
2.2.8 <i>Statistical Analysis</i>	53
2.3 Results	54
2.3.1 <i>Characterization of GNPs</i>	54
2.3.2 <i>Effect of GNP accumulation with the presence of chemotherapeutics</i>	56
2.3.3 <i>Toxicity of GNPs</i>	57
2.3.4 <i>Nuclear entry of bleomycin conjugated GNPs (GNP-RGD-BLM)</i>	58
2.3.5 <i>Survival of cells treated with GNP -RGD-BLM in comparison to free BLM</i>	59
2.3.6 <i>Chemotherapeutic dose enhancement due to GNP-RGD-BLM</i>	60
2.3.7 <i>Survival of cells treated with GNP –RGD; CIS in comparison to free CIS</i>	61
2.4 Discussion	62
2.4.1 <i>Peptide modified GNP toxicity</i>	62
2.4.2 <i>GNP characterization</i>	63
2.4.3 <i>GNP accumulation</i>	64
2.4.4 <i>Presence of GNPs with chemotherapeutics in MDA-MB-231 cells</i>	66
2.5 Conclusions	68
Chapter 3 Gold nanoparticles as a radiosensitizer in radiation therapy	69
3.1 Introduction	69
3.2 Methods	70
3.2.1 <i>Synthesis of colloidal gold nanoparticles and peptide modification</i>	70
3.2.2 <i>Hyperspectral imaging</i>	71
3.2.3 <i>Cell culture and GNP delivery</i>	71

3.2.4 Setup for radiation therapy experiments	72
3.2.5 Immunofluorescence Assay for probing DNA damage.....	73
3.2.6 Clonogenic Assay	74
3.2.7 Statistical Analysis.....	74
3.3 Results	75
3.3.1 Gold nanoparticles as a radiosensitizer	75
3.4 Discussion	77
3.5 Conclusions	80
Chapter 4 Gold nanoparticles with combined chemotherapy and radiation therapy	81
4.1 Introduction	81
4.2 Methods.....	83
4.2.1 Sequence of combined treatment	83
4.2.2 Synthesis of colloidal gold nanoparticles.....	83
4.2.3 Preparation of peptide modified GNP constructs	84
4.2.4 Hyperspectral imaging	84
4.2.5 Cell culture and GNP delivery	85
4.2.6 Clonogenic Assay	85
4.2.7 Immunofluorescence Assay for probing DNA damage.....	86
4.2.8 Statistical Analysis.....	86
4.3 Results	87
4.3.1 Combined effect of gold nanoparticles, bleomycin and radiation.....	87
4.3.2 Combined effect of gold nanoparticles, cisplatin and radiation	90
4.4 Discussion	92
4.5 Conclusion.....	95
Chapter 5 Summary, discussion, and future work	97
5.1 Summary of GNP mediated combined therapy.....	97
5.2 Discussion	100
5.2.1 Significance of findings	100
5.2.2 Future directions	103
5.3 Future work – preliminary study.....	110
5.3.1 Materials and Methods	111

5.3.2 Preliminary results	114
5.3.3 Conclusion	116
Appendix.....	118
Supplementary.....	118
<i>Calculation to confirm TPS</i>	118
<i>In Vitro dosage in comparison to clinical dosage</i>	119
Bibliography	120

List of Tables

Table 4.1 Comparison of predicted effect using the Bliss Independence Criteria with experimental values.	94
Table 5.1 Summary of Survival fraction of MDA MB 231 cells of various treatment conditions.	99
Table 5.2 Values of Survival Fraction and Percentage Difference of Various Treatments	101
Table 5.3 Comparison of tumour control probability extended from experimental SF values	102

List of Figures

Fig. 1.1 TEM image of GNPs synthesized using Turkevich method. (A) 10 nm sized GNPs. The size is consistent with a colloidal shape (B) Larger GNPs have an increased variability in size and shape. 8

Fig. 1.2 Schematic figure representing enhanced permeability and retention. 11
Nanoparticles accumulate more in the tumour tissue than the normal tissue due to enhanced permeability from leaky and disorganized tumour vasculature, and due to the lack of lymphatic drainage. Free drugs are more likely to return to vasculature system than the nanoparticles conjugated with drugs.

Fig. 1.3 Differences in extracellular matrix (ECM) in MDA-MB-231 and MCF-7 tissue structures. (A) and (C), multicellular layer (MCL) tissue of MCF-7 cells at 10x and 60x magnification, respectively. (B) and (D), MCL tissue of MDA-MB-231 cells at 10x and 60x, respectively. Differences in the ECM structure can be seen at both magnifications. MCF-7 tissue had a much more organized ECM structure while MDA-MB-231 tissue has a disorganized ECM structure which allowed easy penetration of molecules into deeper tissues. Adapted from Yohan, D., *et al.*, *Elucidating the uptake and distribution of nanoparticles in solid tumors via a multilayered cell culture model*. Nano-Micro Letters, 2015. 7(2): p. 127-137. 13

Fig. 1.4 Schematic figure representing the comparison of GNP uptake in monolayer (left) and multilayer cell models (right). GNPs spread evenly regardless of size in monolayer cultures and 50 nm GNPs have a higher relative uptake per cell. In the MCL, 50 nm GNPs display poorer accumulation and penetration due to the prohibitive effects of the ECM. Adapted from Yohan, D., *Gold Nanoparticle Transport in Multilayered Cell Cultures*, in Biomedical Physics. 2015, Ryerson University: Toronto. 15

Fig. 1.5 Illustration of a cell, nucleus, and the nuclear pore complex. The structure of a cell is illustrated (top left), followed by the nucleus (top right) and the nuclear pore structure (bottom).	20
Fig. 1.6 Exocytosis of peptide modified GNPs. (A) Percent of NPs exocytosed for cells incubated with citrate-capped and peptide-capped GNPs. (B) Dynamics of exocytosis process following one and six hours. Error bars represent standard deviation of n=3. Adapted from Yang, C., et al., <i>Peptide modified gold nanoparticles for improved cellular uptake, nuclear transport, and intracellular retention</i> . <i>Nanoscale</i> 2014. 6(20): p. 12026-12033.	22
Fig. 1.7 Structure of CALNN pentapeptide. Molecular structure of CALNN peptide showing cysteine (C) in the N-terminus, Alanine (A) in the second position, Leucine (L) in the third position, and Asparagine (N) in the fourth and fifth position.	24
Fig. 1.8 Schematic diagram of the photoelectric effect. A photon with the energy $h\nu$ interacts with a K-shell electron.	37
Fig. 1.9 Schematic diagram of the Compton Effect.	38
Fig. 1.10 Regions of relative predominance of the three main forms of photon interaction with matter. Adapted from Podgorsak, E.B., <i>Radiation Oncology Physics: A Handbook for Teachers and Students</i> . 2005, Vienna: International Atomic Energy Agency.	39
Fig. 2.1 GNP Synthesis via the Turkevich method. In step 1, chloroauric acid is added to distilled water and brought to a boil. In step 2, sodium citrate is added to the mixture and acts as both a reducing and capping agent. After several minutes, the mixture changes colour, indicating the formation of GNPs. Adapted from Yohan, D., <i>Gold Nanoparticle Transport in Multilayered Cell Cultures</i> , in <i>Biomedical Physics</i> . 2015, Ryerson University: Toronto.	48

Fig. 2.2 Clonogenic assay flow chart. A flow chart schematic of the clonogenic assay method.	52
Fig. 2.3 Characterization of GNPs used in this study. (A) TEM image that indicates the core size of the GNPs used is 10 ± 0.89 nm (B) UV-Vis Spectra of GNP, GNP-RGD, GNP-RGD-BLM, GNP-RGD;CIS with no significant broadening, measured 46 hr post formulation. * indicates statistically significant difference (ANOVA, $p < 0.05$).	54
Fig. 2.4 Accumulation of GNP constructs in MDA-MB-231 cells. Improved accumulation was observed for cells modified with peptide (CALNN and RGD) modified GNPs compared to the unmodified (citrate stabilized) GNPs. Data are means \pm S.D. for $n = 10$ cell preparations over three independent experimental set-ups.	56
Fig. 2.5 Toxicity of 0.3 nM 10 nm sized GNPs in MDA-MB-231 cells. No toxic effects on MDA-MB-231 cells were observed after 16-hour incubation of 0.3 nM 10 nm sized peptide modified GNPs. No significant difference in survival fraction was observed from clonogenic assays. Data are means \pm S.E.M for $n = 6$ (Unpaired t-test, $p > 0.05$).	57
Fig. 2.6 Hyperspectral mapping of GNP distribution and protein probe for DNA DSBs (53BP1) in cells incubated with GNP and GNP-RGD-BLM. Different planes across the nuclei of the cells showed that there is localization of GNPs within the nucleus when they were conjugated with BLM. The cells incubated with citrated-capped GNPs were not found in the nucleus. The nucleus is stained with DAPI (blue), the GNP clusters are shown in red, the markers for DNA DSBs (53BP1) are shown in green. Adapted from Yang, C., J. Uertz, and D.B. Chithrani, <i>Colloidal Gold-Mediated Delivery of Bleomycin for Improved Outcome in Chemotherapy</i> . <i>Nanomaterials</i> , 2016. 6(3): p. 48.	58

Fig. 2.7 Comparison of cell survival for cells treated with GNP-RGD-BLM and equal concentrations of free BLM. MDA-MB-231 cells treated with GNP-RGD-BLM had an 18 ± 3 % decrease in survival compared to cells treated with same concentration of free BLM (633 nM). Data are means \pm S.E.M for n = 3. * indicates statistically significant difference (unpaired t-test, $p < 0.05$). 59

Fig. 2.8 Survival Fraction of MDA-MB-231 breast cancer cells treated with various concentrations of free bleomycin. MDA-MB-231 cells treated with various concentrations of bleomycin (0.25-2 fold of the concentration used for this study, where ratio of 1 corresponds to 633 nM). 60

Fig. 2.9 Comparison of cell survival for cells treated with GNP-RGD; CIS and equal concentrations of free CIS. MDA-MB-231 cells treated with GNP-RGD; CIS had no statistical significant change in survival fraction compared to cells treated with same concentration of free cisplatin (435 nM) Data are means \pm S.E.M. for n = 3. (Unpaired t-test, $p > 0.05$). 61

Fig. 3.1 Irradiation experiment setup with 6 MV X-rays. 72

Fig. 3.2 Comparison of cell survival for cells treated with saline and GNP-RGD with 2 Gy, 6 MV X-ray radiation. MDA-MB-231 cells treated with peptide modified GNPs had a 19 ± 6 % decrease in survival compared to control (treated with same volume of saline). Data are means \pm S.E.M. for n = 3. * indicates statistically significant difference (unpaired t-test, $p < 0.05$) 75

Fig. 3.3 DNA DSB probe protein (53BP1) for cells treated with GNP-RGD compared control with 2 Gy, 6 MV X-ray radiations. MDA-MB-231 cells incubated with peptide modified GNPs had a significant increase in 53BP1 count/2D projected area of nucleus to control (treated with same volume of saline). The nucleus is stained with DAPI shown in blue and the markers for DNA DSBs (53BP1) are shown in green. SD values display ranges of values in different nuclei. 76

Fig. 4.1 Sequence of combined treatment flow chart. A flow chart schematic of the combined treatment sequence. 83

Fig. 4.2 Comparison of cell survival fraction for cells treated IR GNP-RGD-BLM compared to IR BLM. MDA-MB-231 cells treated with peptide modified GNPs conjugated with 633 nM bleomycin (BLM) and treated with 2 Gy, 6 MV (IR-GNP-RGD-BLM) had a 32 ± 9 % decrease in survival compared to cells treated with same dosages of BLM and IR (treated with same volume of saline). Data are means \pm S.E.M. for $n = 4$. * indicates statistically significant difference (unpaired t-test, $p < 0.05$). 87

Fig. 4.3 Comparison of 53BP1 ratio for IR-BLM and IR-GNP-RGD-BLM. MDA-MB-231 cells treated with peptide modified GNPs conjugated with 633 nM BLM and treated with 2 Gy, 6 MV X-ray radiations. Scale bar = 10 μ m. The nucleus is stained with DAPI shown in blue and the markers for DNA DSBs (53BP1) are shown in green. SD values display ranges of values in different nuclei. 88

Fig. 4.4 Comparison of cell survival for cells treated with IR GNP-RGD; CIS compared to IR CIS. MDA-MB-231 cells treated with peptide modified GNPs and 435 nM cisplatin and treated with 2 Gy, 6 MV (IR-GNP-RGD; CIS) had a 30 ± 6 % decrease in survival compared to cells treated with same dosages of cisplatin and radiation (IR CIS) (treated with same volume of saline). Data are means \pm S.E.M for $n = 3$. * indicates statistically significant difference (unpaired t-test, $p < 0.05$). 90

Fig. 4.5 Comparison of 53BP1 ratio for IR-CIS and IR-GNP-RGD; CIS. MDA-MB-231 treated with peptide modified GNPs conjugated with 435 nM CIS and treated with 2 Gy, 6 MV X-ray radiations. Scale bar = 10 μ m. The nucleus is stained with DAPI shown in blue and the markers for DNA DSBs (53BP1) are shown in green. SD values display ranges of values in different nuclei. 91

Fig. 5.1 Summary of survival fractions of non-irradiated MDA-MB-231 cells under various treatment conditions. 97
Survival fraction of MDA-MB-231 cells treated with GNPs, chemotherapeutics (bleomycin and cisplatin) and GNP with chemotherapeutics. * indicates statistically significant difference between the pair (unpaired t-test, $p < 0.05$).

Fig. 5.2 Summary of survival fractions of irradiated MDA-MB-231 cells under various treatment conditions. 98
Survival fraction of MDA-MB-231 cells treated with GNPs, chemotherapeutics (bleomycin and cisplatin) and GNP with chemotherapeutics. * indicates statistically significant difference between the pair (unpaired t-test, $p < 0.05$).

Fig. 5.3 Accumulation of GNP constructs in monolayer MIA-Pa-Ca-2 cells. 114
Decreased accumulation was observed for cells modified with peptide (PEG and RGD) modified GNPs compared to the unmodified (citrate stabilized) GNPs.

Fig. 5.4 Accumulation of GNP constructs in various organs of SCID mice. 115
Accumulation of GNP constructs in various organs at 24, 48, 72 hrs post injection

Symbols & Abbreviations

ANOVA – Analysis of Variance

DDS – Dose Delivery System

DEF – Dose Enhancement Factor

DLS – Dynamic Light Scattering

DNA – Deoxyribonucleic acid

DSB – Double strand break

EPR – Enhanced permeability and retention

FBS – Fetal bovine serum

FS – Field Size

GNP – Gold nanoparticle

ICP-AES – Inductively coupled plasma – Atomic emission spectroscopy

IFP – Interstitial Fluid Pressure

LINAC – Linear Accelerator

LSPR – Local Surface Plasmon Resonance

MCL – Multicellular layers

MU – Monitor Unit (measure of machine output from a clinical accelerator for radiation therapy)

MV – Mega Voltage

NLS – Nuclear Localization Signal

NP – Nanoparticle

NPC – Nuclear Pore Complex

PEG – Polyethylene Glycol

PBS - Phosphate Buffered Saline

RGD – Arginine – Glycine – Aspartic acid

ROS – Reactive Oxygen Species

RME – Receptor-mediated endocytosis

SAM – Spectral angle mapping

S.E.M. – Standard Error of Mean

SF – Survival Fraction

TEM – Transmission electron microscopy

UV-VIS – Ultraviolet-Visible

Chapter 1

Introduction

1.1 Cell Biology of Cancer

Cancer is a common human genetic disease caused by accumulation of several mutations [1]. Breast cancer cells share a similar major genetic mutation spectrum and chromosome aberration profiles with tumours, despite having a high frequency of DNA alterations, which allow them feasible for tumour modelling [2]. Many types of cancer cells, including breast cancer cells, can be organized into malignant cancer stem cells that have extensive proliferative potential, and differentiated cancer cells that have limited proliferative potential [3]. The notion of cancer stem cells arise from similarities between somatic stem cells and cancer cells in that both self-renew [3]. While the differentiation of somatic stem cells is highly regulated, the cancer cell differentiation is poorly controlled [3]. This suggests that cancer is considered a disease resulting from mutations that convert normal stem cell self-renewal pathways into unregulated neoplastic proliferation [3]. Several signalling pathways that regulate normal stem cell self-renewal, including the Notch signaling pathway, are capable of causing neoplastic proliferation upon mutation [3]. Notch is a plasma membrane receptor that is involved in cell fate specification and in the maintenance of proliferative and differentiative balance in various cell lines [4, 5]. Notch is suggested to be one of the pathways involved in arise of breast cancer [3, 5].

In breast cancer cells, undifferentiated and differentiated cells cannot be distinguished by histology [3]. However, breast cancer cells may have distinct surface molecules. When human

breast cancer cells from nine patients were separated by the different surface molecules and injected into mice, only a small population of the cancer cells was able to induce tumour formation [6]. These cells expressed CD44, an adhesion molecule that binds to hyaluronate, but lacked CD24, an adhesion molecule that binds to P-selectin; reported as CD44⁺CD24⁻ cells [6]. While injection of 200 of these cancer cells was able to form tumours in mice, cancer cells with other phenotypes were not able to form tumours even with injection of thousands of cells [6]. The CD44⁺CD24⁻ cells not only produced more CD44⁺CD24⁻ cells but also gave rise to diverse non-tumourigenic breast cancer cells [6]. One of the classifications of subtypes of breast cancer can be based on molecular characteristics such as the status of predictive markers like the estrogen receptor (ER), progesterone receptor (PR) or the human epidermal growth factor 2 (HER2) [7]. The breast cancer epithelial cell line, MDA-MB-231 cells are classified as the ‘claudin-low’ or ‘triple negative’ type that lacks expression of ER, PR, and HER2 [2, 7]. The features of this cell line include having intermediate response to chemotherapy and having expressions associated with mammary cancer stem cells, such as the CD44⁺CD24⁻ phenotype [7].

MDA-MB-231 cells, were used for this dissertation as it was available for purchase from ATCC and have been investigated in previous gold nanoparticle (GNP) studies [8-12]. This cell line has been observed to have relatively good GNP uptake and significant radiosensitization [13]. For example, Jain *et al.* observed that the MDA-MB-231 cells had greatest uptake of GNPs among the type of cells (normal lung L132, prostate cancer DU145, breast cancer MDA-MB-231) used in uptake studies [8]. MDA-MB-231 cells are also a triple negative cell line that are known to be more aggressive, highly invasive with worse prognosis [2], therefore selected to study new options to further improve the currently used treatment modalities. Although this study is not targeted

specifically to the treatment of breast cancer, it is worthy to note some characteristics of the cell line used for the subsequent studies since many experimental results are dependent on the cell line.

1.2 Types of Cancer Treatment

According to the Canadian Cancer Society, the main types of cancer treatments include surgery, chemotherapy and radiation therapy [14]. The type of treatment a patient receives generally depends on the type of cancer and the advancement of cancer [14, 15]. The sources of radiation therapy include gamma or X-ray photons, ion-based electrons and protons [16, 17]. Although radiation therapy is considered effective and used in treatment of about 50 % of all cancer patients, a sufficient dose that can kill any tumour cell can also damage surrounding healthy tissue [18, 19]. A photon beam will irradiate some surrounding normal tissue no matter how well shaped or conformed to the dimensions of the tumour and this dose to normal tissue limits the amount of radiation a patient can receive [20]. Chemotherapy is also used as a major curative modality for few types of malignancies, palliative treatment for many types of advanced cancers, and adjuvant treatment before, during or after local treatment (surgery and/or radiotherapy) to eradicate micro-metastases and to improve local control of the primary tumour [21]. Chemotherapy involves administering pharmaceutical compounds that exert cytotoxic effects and disrupt the rapid overgrowth of malignant cells [22, 23]. However, the side effects caused by anti-tumour drugs also remain as one of the important problems to overcome in cancer treatment [24-26]. This is mainly induced by poor distribution of the anti-tumour agents and can be minimized by improving the bioavailability of the drug in the tumour region as well as confining them to the target region [26-29]. For most patients, a combination of treatments, such as surgery with chemotherapy and/or

radiation therapy is required. The integration of chemotherapy with local modalities of radiation therapy is a logical and reasonable approach that has greatly improved the cure rates of solid tumours [20, 30]. Clinically, combined chemotherapy and radiation therapy is commonly used. The chemotherapeutic agents can be used as a radiosensitizer or can be given systemically to eradicate distant micro-metastasis [20, 31].

The fundamental objective of all cancer therapeutics is to enhance tumour cell killing, while minimizing normal tissue toxicity to improve the therapeutic index [32]. Despite successful clinical application of combined radiation therapy and chemotherapy, the major limitation of combining chemotherapy and radiation therapy is the normal-tissue toxicity since either modality can cause major normal tissue toxicity [20, 32]. Due to the limitations of the current cancer treatment modalities, methods for improving the therapeutic results are continuously being researched. Gold nanoparticles (GNPs) are one of the materials that are used extensively in the field of nanomedicine and cancer research [33]. The enhanced tumour accumulation of biocompatible agents, such as GNPs, result in an improved therapeutic index [32]. Further improving bioavailability of GNPs through surface modification can potentially improve the therapeutic window of GNP mediated cancer therapy through co-delivery of chemotherapeutic agents and tumour-specific radiosensitization.

In this dissertation, the therapeutic enhancement of chemotherapy (Chapter 2), radiation therapy (Chapter 3) and combined therapy (Chapter 4) using peptide modified GNPs will be discussed.

1.3 Drug delivery using nanoparticles

Traditional delivery of drugs have limitations, such as a lack of targeted availability [34]. Therefore, a more efficient transport vehicle, such as nanoparticles (NPs), have been of interest [34]. NPs are sub-micrometer sized particles, often smaller than 200 nm, and exhibit unique physical and chemical properties [35-37]. Nanocarriers or Nanoscale drug delivery systems (DDS) have been used in research to overcome some problems with conventional anti-tumour drug delivery systems, such as non-specificity and severe side effects [38]. DDS can be made using a variety of materials including polymers (e.g. polymeric NPs, micelles, or dendrimers), lipids (e.g. liposomes), viruses (e.g. viral NPs), and metallic compounds (e.g. gold NP, silver NPs) and they are used to improve the pharmacological conventional free drug therapeutics [37, 39].

Polymer-based drug carriers can be categorized into polymer-drug conjugates, polymeric micelles, or dendrimers, based on the structure of the compound [37]. Polymer-drug conjugates use naturally occurring polymers, such as albumin, chitosan, and herapin; and synthetic polymers, such as N-(2-hydroxypropyl)-methacrylamide copolymer (HPMA), polystyrene-maleic anhydride copolymer, polyethylene glycol (PEG), and poly-L-glutamic acid (PGD) to deliver drugs [37]. Examples of polymeric NPs that are evaluated in clinical trial include Abraxane (serum albumin carrier with paclitaxel) [40], Xyotax (PGA-paclitaxel) [41], CT-2106 (PGA-camptothecin), PK1 (HPMA – doxorubicin) and PK2 (HPMA – doxorubicin – galactosamine) [37]. Polymeric micelles are a nanoscale hydrophobic core/ hydrophilic shell structure where the hydrophobic core is appropriate for encapsulating hydrophobic drugs while the hydrophilic shells are ideal for intravenous (i.v.) administration [37]. Dendrimers are hyperbranched macromolecules with regular patterns of repeated units, which are simple and easy to synthesize [37, 42]. Examples of dendrimer NPs are PAMAM - platinate (polyamidoamine conjugated to cisplatin) and PAMAM

– MTX (polyamidoamine with methotrexate) [43, 44]. The high ratio of surface groups to molecular weight volume have made dendrimers a promising carrier, but the toxicity issues associated with dendrimers are the limitations [45]. Other limitations of polymer-based NP systems include structural heterogeneity, particle instability, slow and non-uniform drug release and potential immunogenicity [46].

Liposomes are lipid bilayer colloidal structures with a central aqueous space and is one of the most common lipid-based carriers [37]. Liposomes are beneficial in solubilizing drugs and improving uptake by tumour than free drugs [47, 48]. There are several FDA approved liposomal drugs that are used, including DaunoXome (liposomal daunorubicin), DepoCyt (liposomal cytarabine), and Myocet (liposomal doxorubicin) [37, 49]. Doxil, a PEG-liposome containing doxorubicin, is approved for AIDS-related Kaposi's sarcoma, ovarian cancer and multiple myeloma [47, 49]. Doxil had an approximately 100-times longer half-life and reduced cardiotoxicity than free doxorubicin, but skin toxicity has been discovered that did not occur with doxorubicin [47]. Although liposomes improve the uptake of the drugs, they lack control for the time of drug release and lack effective intracellular delivery of drug molecules [47, 48]. Other limitations of liposomal NPs include particle instability, rapid clearance, and spontaneous membrane fusion with off target cells [46].

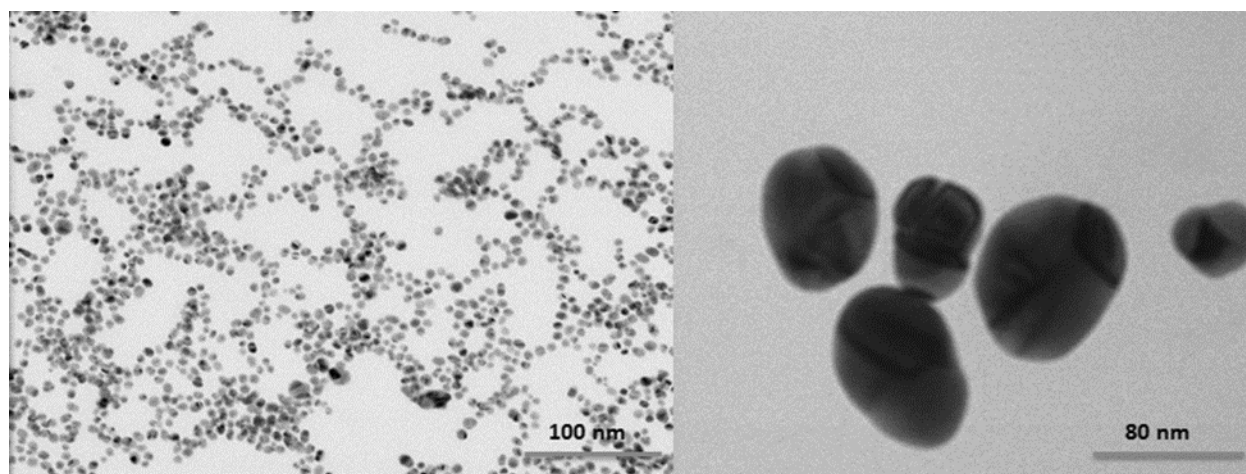
A variety of viral NPs (VNPs) have also been developed for biomedical and nanotechnology applications, including drug delivery, vaccination, imaging, and targeting [37, 38]. VNPs self assemble into discrete and monodisperse structures of precise shape and size that can be tailored at the atomic level [50]. This level of quality control and structural engineering cannot be yet achieved with synthetic NPs [50]. The sources of the VNPs are diverse, and some examples are plants (potato virus X [PVX], cowpea mosaic virus [CCMV], tobacco mosaic virus [TMV]),

bacteria (MS2, M13, Q β) and animals (adenovirus, polyomavirus) [38, 51]. The internal cavity of VNPs can be filled with drug molecules, imaging reagents, while the external capsid surface can be functionalized with targeting ligands to allow cell-specific delivery [37, 38, 51]. Although viral vectors are effective, the challenges to using VNPs are avoiding phagocyte-mediated clearance and stability with side effects such as immune response being a limitation [34, 46].

Some of the shortcomings of other NPs can be overcome by metallic NPs. There are various types of metallic NPs (e.g. silver NPs, gold NPs) and are utilized in biomedical sciences and engineering [52]. Metallic materials can be conjugated with various antibodies, ligands, and drugs allowing for applications in multiple fields including biotechnology, drug delivery, and diagnostic imaging [52]. Among many metallic NP systems, gold nanoparticles (GNPs) have been used extensively in the field of nanomedicine and cancer research [33]. The size and shape of GNPs can be easily controlled during synthesis and can be quantified in biological samples [53]. Moreover, the surface of GNPs can be easily functionalized with a variety of small molecules peptides, proteins, deoxyribonucleic acid (DNA) and ribonucleic acid (RNA) [54]. GNPs can also be incorporated with polymer- or lipid-based systems, such as liposomes, micelles, or dendrimers and the functionalization widened the application aspects of GNPs [55-57]. Moreover, the high surface area-to-volume ratio along with the large surface bio conjugation possibilities has made GNPs as an ideal platform for delivering pharmaceuticals for chemotherapy [58-60]. GNPs have also been used as a radiosensitizer in radiation therapy [33, 55, 61-63]. This allows the possibility of GNP mediated combined cancer therapy. The rationale for using GNPs in this dissertation is to utilize the drug carrying and radiosensitizing property of GNP for combined use with chemotherapy and radiation therapy.

The fundamental goal of NP-based platforms will be the successful delivery and monitoring of therapeutics to tumours while causing minimum damage to normal tissue and side effects to the patient [64]. The accumulation of GNPs from blood vessels to cell levels will be discussed in section 1.5.

1.4 Synthesis and Biocompatibility of GNPs



<Fig. 1.1> TEM image of GNPs synthesized using Turkevich method. (A) Approximately 10 nm sized GNPs. The size is consistent with a colloidal shape (B) Larger GNPs have an increased variability in size and shape.

One of the most common colloidal gold nanoparticle (GNP) synthesis protocols involve the citrate reduction of HAuCl_4 , developed by Turkevich *et al.* [65] and Frens [66] to form relatively controlled, and monodisperse GNPs of 10-60 nm diameters [67]. Varying the citrate versus gold concentration controls the size of GNPs synthesized [68]. Larger particles up to approximately 147 nm can be produced using this method at the cost of monodispersity and shape [66, 69]. The Turkevich method of GNP synthesis [65, 70], which is the method used for producing GNPs in the studies of this dissertation, produces monodisperse spherical GNPs suspended in

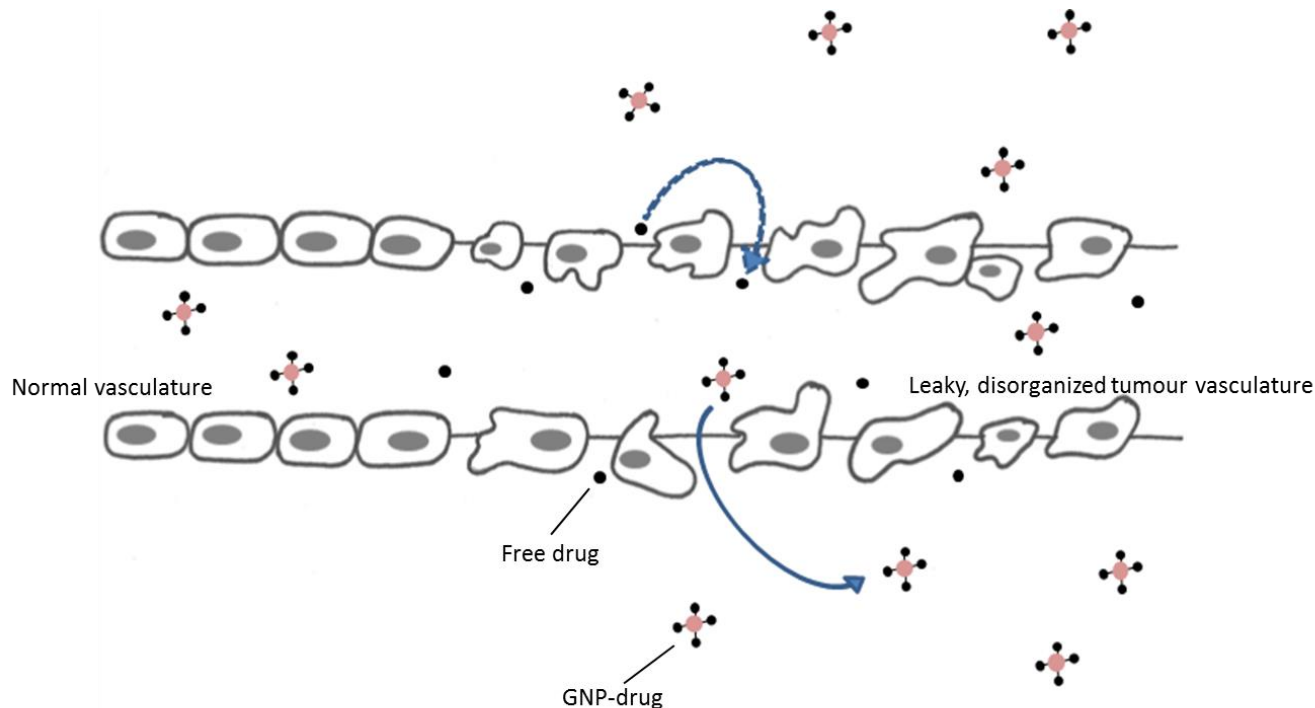
water. Sodium citrate, which is non-toxic, is commonly used as a reducing agent for this method of synthesis and varying this reaction parameter control for the size of the resulting GNPs [65, 71]. Fig. 1.1 shows the compensated monodispersity and colloidal shape for GNPs approximately 100 nm in diameter. For smaller than 10 nm GNPs, other reducing agents can be used. For example, GNPs of sizes 1-3 nm can be produced with the Brust-Schiffrin method [72]. This method involves reaction of chloroauric acid solution with tetraoctylammonium bromide (TOAB) solution in toluene as an anti-coagulant and sodium borohydride as reducing agent [72]. The simplest GNP solution contains the core material (gold), surface-bound stabilizing ligands, and potential left-over chemicals from the synthesis and observed toxicity from a GNP solution could be due to any of these components [73]. Many of the reagents used to produce smaller GNPs such as TOAB, toluene, sodium borohydride, are hazardous and some studies have reported that some precursors to GNPs may be toxic, but not the GNPs themselves [74, 75]. GNPs used throughout this dissertation is synthesized through the Turkevich method [65].

Biocompatibility is an important factor for a system to be used in clinical settings and a number of groups studying GNP cytotoxicity concluded that GNP biocompatibility depends on size, surface properties and concentration [74, 75]. Many experimental work has been done to confirm the non-toxicity of GNPs, but contradictory research results are also present [76]. The lack of general consensus on NP toxicity is due to different experimental methods employed, incubation conditions (concentrations and exposure time), variability of sizes and functionalities of GNPs, variability of cell lines, and different measures and assays for toxicity [76, 77]. For example, it has been reported that citrate capped GNPs were toxic to a human carcinoma lung cell line (A549) but not to a human liver cell line (HepG2) at the same dosages (120 nM) presenting that the toxicity is cell line dependent [76, 78]. As for the size dependence on toxicity, some studies have shown

that smaller GNPs have a smaller half maximal inhibitory concentration (IC_{50}) value (the concentration of the chemical that gives a decrease of 50 % of the cell viability) than larger GNPs, suggesting that smaller GNPs are toxic at less concentrations than the larger counterparts [74, 75, 78-86]. However, it remains unclear why certain sizes produce more toxicity than others and some reports suggest that the toxicity can be due to precursors to GNPs than the GNPs themselves [74-76]. Although there are contradictory reports on GNP toxicity dependence on size, it is better established that the accumulation and uptake of GNPs at both tissue and cellular level is size dependent [76] and it will be discussed in the next section. Owing to the numerous parameters that affect toxicity and the lack of standardized protocol of measurement, the assessment of toxicity can be rather complicated [76, 87].

1.5 Accumulation of GNPs in tissue and cellular levels

1.5.1 Tumour Microenvironment and the Enhanced Permeability and Retention (EPR)

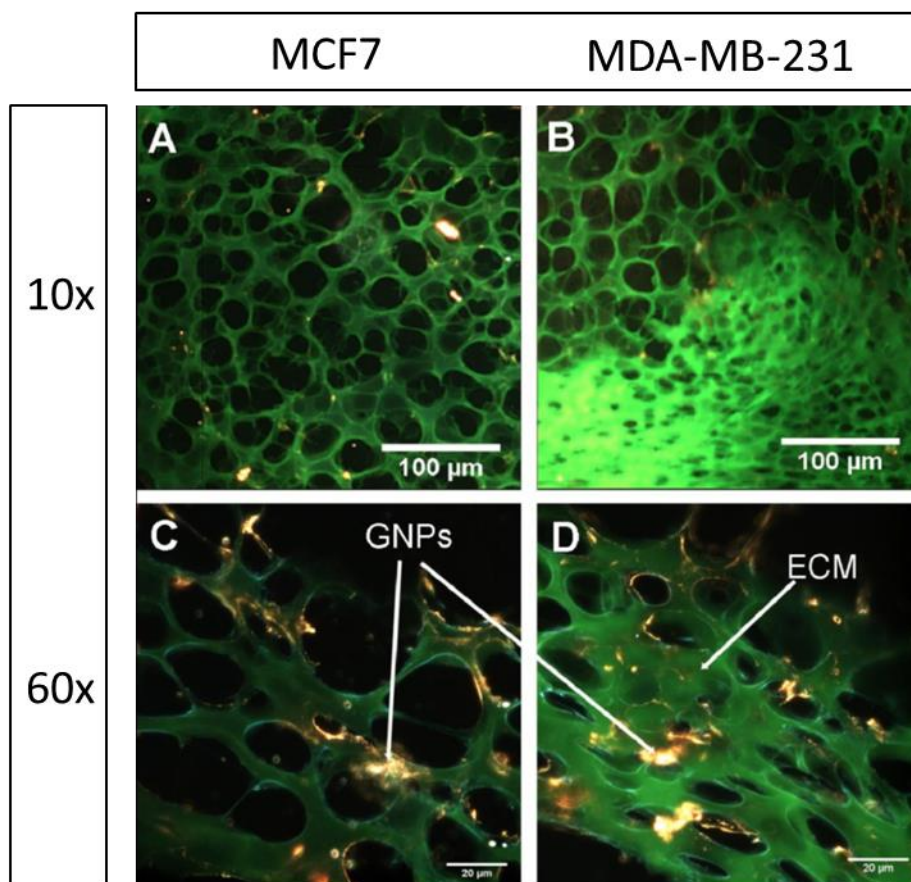


<Fig. 1.2> **Schematic figure representing enhanced permeability and retention.** Nanoparticles accumulate more in the tumour tissue than the normal tissue due to enhanced permeability from leaky and disorganized tumour vasculature, and due to the lack of lymphatic drainage. Free drugs are more likely to return to vasculature system than the nanoparticles conjugated with drugs.

Successful clinical translation of nanomedicine requires NPs to be accumulated in the tumour tissue [88]. Targeting of the tumour consists of passive and active targeting, but the active targeting occurs only after passive accumulation in tumours [89]. Delivery of NPs to solid tumours depends on the abnormal tumour environment that leads to Enhanced Permeability and Retention (EPR) [89]. In normal vasculature, the arterioles connect to the capillaries, and the blood vessel growth and regression are carefully regulated events [90]. However, tumour blood vessels have multiple structural and functional abnormalities due to the abnormal environment they grow in;

tumour blood vessels are dilated, have irregular shape, can be dead ended, and are leaky [90]. The endothelial cells of tumour vessels do not form a tight barrier and pericytes, cells that wrap around the endothelial cells, are loosely attached which make the vessels porous [91]. The gaps between endothelial cells can be as large as 10-1000 nm and the retention time of drugs conjugated onto NPs could be ten times higher than that of the free drugs because the free drugs are more likely to return to the vascular system [89, 92-94]. Nanoparticles of sizes larger than 1-2 nm will be restricted from exiting normal vasculature due to the tight endothelium of normal vasculature [47]. A schematic figure representing this process is shown in Fig. 1.2. These large gaps between endothelial cells of tumour micro-vessels lead to enhanced permeability of particles through diffusion and convection [91, 95]. Diffusion is the transport of small-sized molecules driven by concentration gradients, while convection is the collective movement of particles encompassing both diffusion and advection [91, 95]. Advection is the motion of particles along the bulk flow of fluid [95]. Along with these tumour abnormalities, functional lymphatic vessels lack from tumour vasculature that result in elevated interstitial fluid pressure (IFP) [96]. It has been studied that vascular permeability is inversely proportional to transported NP size [95]. Accumulation of NP systems in tumour tissue can result from the EPR effect, however, the therapeutic outcome based on the EPR effect can be inconsistent due to the heterogeneity associated with the tumour tissues [97]. The different results caused by the EPR effect will be further discussed in section 5.2.2.

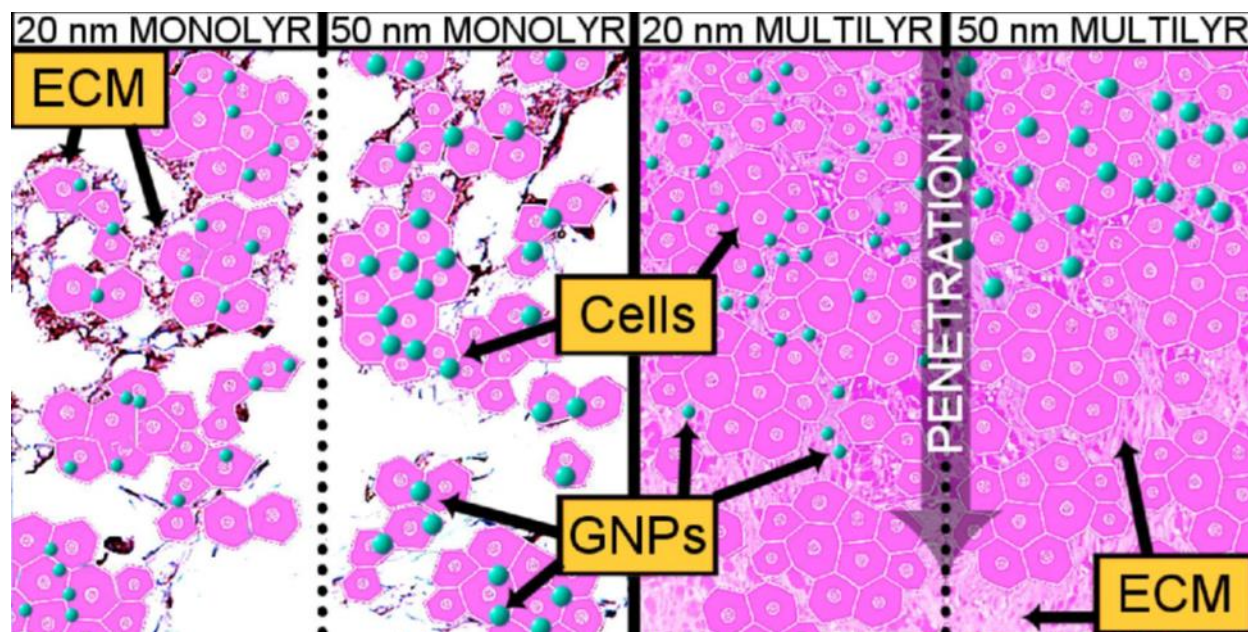
1.5.2. Penetration of GNPs through the Extracellular Matrix (ECM)



<Fig. 1.3> Differences in extracellular matrix (ECM) in MDA-MB-231 and MCF-7 tissue structures. (A) and (C), Multicellular layer (MCL) of MCF-7 cells at 10x and 60x magnification, respectively. (B) and (D), MCL tissue of MDA-MB-231 cells at 10x and 60x, respectively. Differences in the ECM structure can be seen at both magnifications. MCF-7 tissue had a more organized ECM structure while MDA-MB-231 tissue has a disorganized ECM structure that allowed easy penetration of molecules into deeper tissues. Adapted from Yohan, D., *et al.*, *Elucidating the uptake and distribution of nanoparticles in solid tumors via a multilayered cell culture model*. Nano-Micro Letters, 2015. 7(2): p. 127-137 [98].

Gold nanoparticles (GNPs) are expected to penetrate through the tumour tissue matrix once they leave the tumour blood vessels. Penetration of the GNPs through tissues is dependent on the size of GNPs and the tumour cell type [98]. A multicellular layer (MCL) model including the extracellular matrix (ECM) mimics a reasonable tumour microenvironment. MCL models were

used by Yohan *et al.* to study the GNP transport in tumour tissue in two breast cancer cell lines, MCF-7 and MDA-MB-231 [98]. Cell lines grown in three-dimensional culture displayed different cell morphology from that observed in two dimensions [7]. MCF-7 cells formed tightly cohesive structures displaying robust cell-cell adhesions while MDA-MB2-231 cells formed loosely cohesive grape-like structures that were consistent with more invasive phenotype they demonstrate *in vivo* [7]. The ECM for MDA-MB-231 cell MCLs was less organized than the ECM of MCF-7 cell MCLs. In addition, MDA-MB-231 cell layers were less compartmentalized than MCF-7 cell layers as shown in Fig 1.3 [98]. The more aggressive and invasive tumour cells like MDA-MB-231 secrete matrix-degrading proteinases that serve to break down collagen and attribute to the differences in ECM and cell layer organizations [99, 100]. It was observed that the GNPs penetrated deeper through the MDA-MB-231 MCL than the MCF-7 MCL as shown in Fig. 1.3. These results suggest that GNP penetration could be more efficient for a more aggressive cell lines such as MDA-MB-231 [98, 101].



<Fig. 1.4> Schematic figure representing the comparison of GNP uptake in monolayer (left) and multilayer cell models (right). GNPs spread evenly regardless of size in monolayer cultures and 50 nm GNPs have a higher relative uptake per cell. In the MCL, 50 nm GNPs display poorer accumulation and penetration due to the prohibitive effects of the ECM. Adapted from Yohan, D., *Gold Nanoparticle Transport in Multilayered Cell Cultures*, in *Biomedical Physics*. 2015, Ryerson University: Toronto [101].

Reports have shown that NPs of diameter of 20-50 nm showed the highest uptake although the size of highest uptake is cell line dependent [53, 102-104]. The proposed mechanisms behind this size preference will be discussed in the next section. The optimal size of GNPs that penetrate in multilayer environment, however, differ from the optimal size of most efficient cellular uptake at monolayer levels. It has been observed that 20 nm GNPs can better penetrate through multilayer cell structures than 50 nm GNPs [101]. It is suggested that GNP mobility through multilayer cell structures is inversely proportional to GNP size [101]. The schematic figure representing the comparison of size dependent GNP uptake in monolayer and multilayer cell cultures are shown in Fig. 1.4. Based on this particular study by Yohan *et al.*, it can be suggested that smaller GNPs are more optimal in tissue penetration once they leave tumour blood vessels than the larger

counterparts [101]. However, the uptake of smaller NPs can be lower once they reach single cell level [104]. Surface of smaller GNPs can be modified with peptide sequences to enhance the uptake of smaller NPs which will be discussed in section 1.6.

1.5.3 Cell – NP interaction, mechanisms of cellular uptake and pathway of NPs

Each cell type has unique molecular signatures and although the differences are generally subtle, cancerous cells can be differentiated from non-cancerous cells on the basis of biomarkers [105]. The differences between normal cells and cancer cells in terms of interaction of NPs can be predicted by NP uptake studies performed with the normal and cancer cells of the same type. Bajaj *et al.* exposed various types of cells with NP- fluorophore polymer complexes in which they are expected to interact with the cell surface through both electrostatic and hydrophobic interactions [105]. The group measured fluorescence intensities of the various cell types that were exposed to the NP complexes since the NP-cell interaction was expected to cause a displacement of the fluorophore polymers and generate a fluorescence response [105]. A higher change in fluorescence intensities were observed for MDA-MB-231 (metastatic breast cancer cell line) and MCF-7 (cancerous but non-metastatic breast cancer cell line) than the MCF-10A (normal breast cell line) [105]. Gal *et al.* also reported differences in internalization of 200-nm diameter particles in three types of breast cell lines [106]. Accumulation of NPs was significantly higher in MDA-MB-231 (high metastatic potential) and MDA-MB-468 cells (low metastatic potential) compared to MCF-10A cells (benign). This group suggested that the difference in accumulation is because normal cells form tight intra-connected colonies and therefore, NPs can be internalized mostly only at the

edge of a growing colony, while in malignant cells, the cell-cell and the cell-matrix connection is disturbed and therefore, NPs can be internalized into any cell on the tissue culture plate [106].

Cells internalize nutrients and signalling molecules to obtain energy and interact with other cells [107]. The two main endocytosis pathways employed by cells are phagocytosis and pinocytosis, and the pinocytosis route can be further subdivided as clathrin-mediated endocytosis, caveolae-mediated endocytosis, clathrin/caveolae-independent endocytosis, and micropinocytosis [97]. While phagocytosis is a triggered process that requires receptors to be activated to initiate the response, pinocytosis is a continuative process [108]. Eukaryotic cells continually ingest their plasma membrane in the form of pinocytic vesicles through endocytosis, which are later returned to the cell surface by exocytosis [108].

The major internalization pathway of unmodified GNPs in cells is reported to be an energy dependent process [104, 109-112] as the uptake of GNPs decreased in low temperature (4 °C) or other ATP-depleted environments, such as in cell pre-treated with sodium azide (NaN₃) [53, 110, 113-115]. However, Jiang *et al.* reported that the cellular uptake of NPs at reduced temperature had a strong size dependence, where no effects on uptake of 2 nm NPs were observed upon cooling cells to 4 °C and suggested that a different pathway is involved in the uptake of 2 nm NPs than from the uptake of larger counterparts [116]. Most NPs that are not modified are first coated with serum proteins and then met with the plasma membrane of cells [107]. Chithrani *et al.* hypothesized the uptake of GNPs is mediated by non-specific and instantaneous adsorption of serum proteins on the surface of GNPs [104]. This group also found that the uptake of transferrin coated GNPs was three times less than the uptake of unmodified (citrate-stabilized) GNPs and suggested that this is because a diverse set of serum proteins adsorb onto the surface of unmodified (citrate stabilized) GNPs which allow the GNPs to enter the cells through various corresponding

pathways of the adsorbed proteins [104]. Chithrani *et al.* further reported that the uptake of transferrin-coated GNPs was likely due to a clathrin-mediated process since pretreating cells with K^+ -depleted or sucrose-depleted (hypertonic treatment) medium drastically reduced the uptake of the transferrin-coated GNPs [53]. These pretreatment conditions are known to disrupt the formation of clathrin coated vesicles [53]. Jiang *et al.* however suggested that the endocytosis pathway may vary upon different NP size and surface functionalities [116]. When cells were treated with chlorpromazine (CPM) and sucrose, which inhibits clathrin-mediated endocytosis, the uptake of 2, 4, and 6 nm cationic GNPs were inhibited, while negligible inhibition effect was observed for zwitterionic and anionic GNPs with the exception of a modest inhibition effect for 2 nm anionic GNPs [116]. Liu *et al.* suggested that GNPs can be internalized through multiple pathways including caveole- and clathrin- mediated endocytosis as well as micropinocytosis [115].

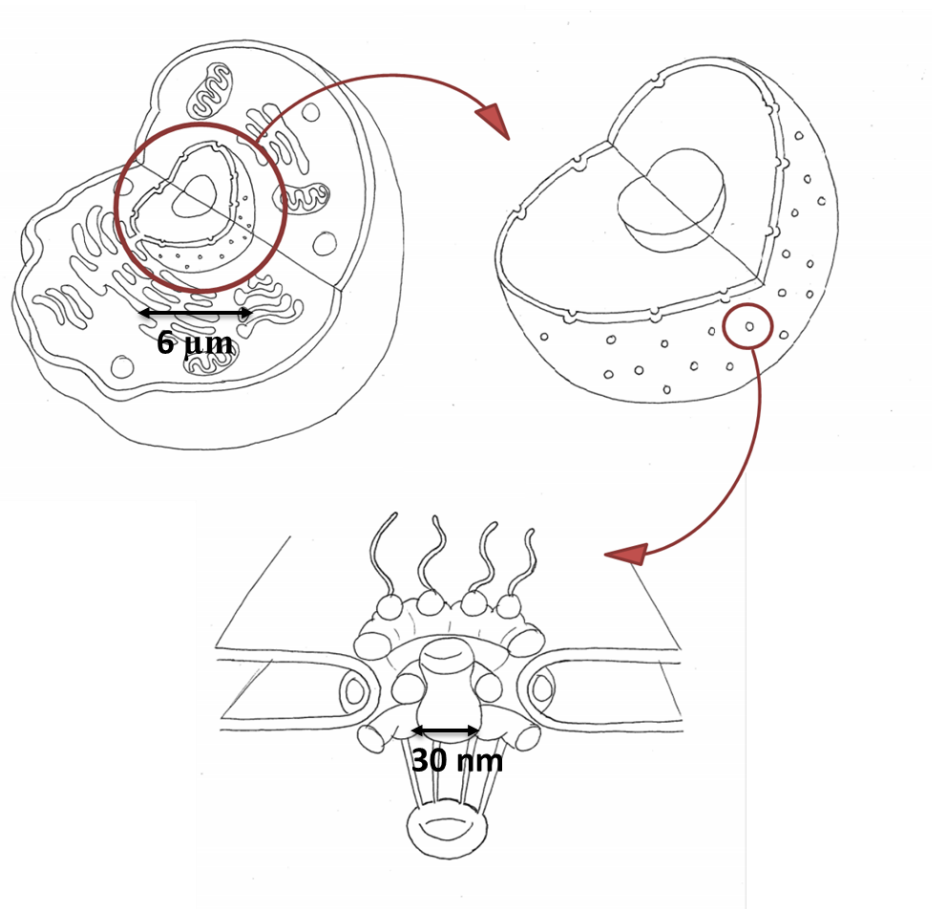
Once particles are internalized into the cell, an endosomal compartment is formed [34]. The endosomes are categorized sequentially as early endosomes that appear just beneath the plasma membrane, and late endosomes that appear closer to the Golgi apparatus and the nucleus [108]. The interior of endosomes is acidic (\sim pH 6) due to the H^+ -ATPase in the endosomal membrane and many internalized receptor proteins change their conformation and release their ligand in this acidic environment, however, some ligands remain bound to the receptors [108]. Some molecules and receptors in the endosomes are recycled back to the same plasma membrane they came from (recycling) through transport vesicles, some proceed to a different domain of the plasma membrane (transcytosis), or progress to lysosomes for degradation [108]. Subsequent trafficking post endocytosis of GNPs have not been well understood but recently Liu *et al.* attached a DNA tagged with fluorophore to GNPs to examine intracellular transport of GNPs through fluorescence and plasmonic images [115]. This group suggested that GNPs are eventually

transported to lysosomes by observing co-localization of the fluorescently-tagged GNPs and lysosomes stained with lysotracker [115].

The design of multifunctional nanocarriers to improve current therapeutic applications also requires a thorough understanding of the mechanisms behind NPs entering and leaving the cells. For drug delivery and radiation therapy applications, it is necessary to control and manipulate the accumulation of NPs for an extended period within the cell. It is difficult to produce particles for optimal cellular uptake, as the rate and mechanism of uptake is cell-type dependent, and vary between NPs with different size, charge and other surface properties [117]. Methods and materials to induce endosomal escape have been investigated for efficient cytoplasmic delivery of NPs and improve accumulation of particles once internalized [118]. Endosomolytic peptides, peptides that allow endosomal escape, derived from viruses and bacterial toxins or synthetic peptides with similar chemical properties have been examined in research [118]. There are several proposed mechanisms of trafficking across the endosomal membrane, and one mechanism is through endosomal membrane disruption by interaction of polymers or peptides [118]. The presence of arginine residues is a common motif of endosomal escape agents, such as cell-penetrating peptides (CPPs), which are short cationic amino acid sequences that have shown cytoplasmic localization [118, 119]. Arginine has a guanidinium functional group, which readily forms a complex with phosphate groups on phospholipids through a combination of hydrogen bonding and electrostatic interactions [118]. One of the most arginine-rich peptide sequences commonly used for inducing endosomal escape is the TAT peptide (derived from the Trans-Activator of Transcription protein in HIV). The TAT can be fused to proteins and polymers to induce endosomal escape, although the mechanism is not well understood [118]. Moreover, El-Sayed *et al.* reported that particles modified with arginine-rich peptides and lysine-rich peptides were able to escape the endosome [120]. The

peptides used to modify the GNPs in this dissertation contains oligolysine residues. The endosomal escape upon modification with cationic peptides were reported to be dependent on cell lines used, size of cargoes, and chemical composition of the capping layers [121].

1.5.4 Nuclear targeting



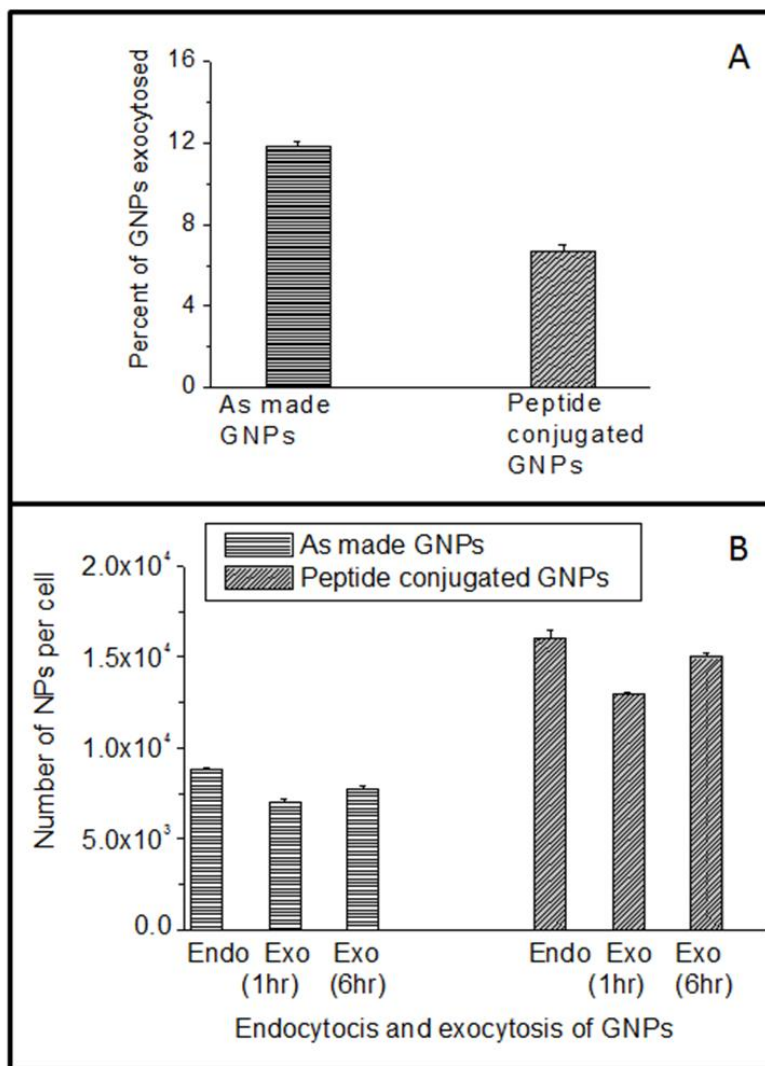
<Fig. 1.5> Illustration of a cell, nucleus, and the nuclear pore complex. The structure of a cell is illustrated (top left), followed by the nucleus (top right) and the nuclear pore structure (bottom).

Once the GNPs enter the cell, targeting the nucleus could be beneficial in improving therapeutic results further. The nucleus is an important target for NP applications as genetic information and the transcription machinery of the cell resides in the nucleus. Various therapies

that involve nuclear targeting have been used for treatment of diseases, such as gene therapy [122]. However, targeted nuclear delivery is challenging due to the biological barriers – the cellular membrane barrier and the nuclear envelope [123, 124]. The nucleoplasm and the genetic material in the nucleus are separated from the cytoplasm by the double membrane layer nuclear envelope [125, 126]. Nuclear pore complexes (NPCs), composed of various types of proteins and are embedded throughout the nuclear membrane, mainly mediate macromolecular transport into and out of the nucleus [125, 127, 128]. Fig. 1.5 is an illustration of a cell, nucleus, and the nuclear pore complex to represent the barriers of molecular nuclear entry.

Most nanomaterials and macromolecules, including GNPs, require some surface modifications for nuclear delivery [122]. For targeted nuclear delivery, the particle must enter the cell, escape the endosome, possess nuclear localization signals (NLSs) to interact with the NPC, and the whole complex should be small enough (less than 30 nm) to cross the nuclear membrane [124]. As discussed in the last section, 1.5.3, endosomal escape of GNPs can be achieved by modifying the surface with peptide sequences. Surface modification of GNPs with peptide sequences will be discussed further in section 1.6.

1.5.5 Exocytosis



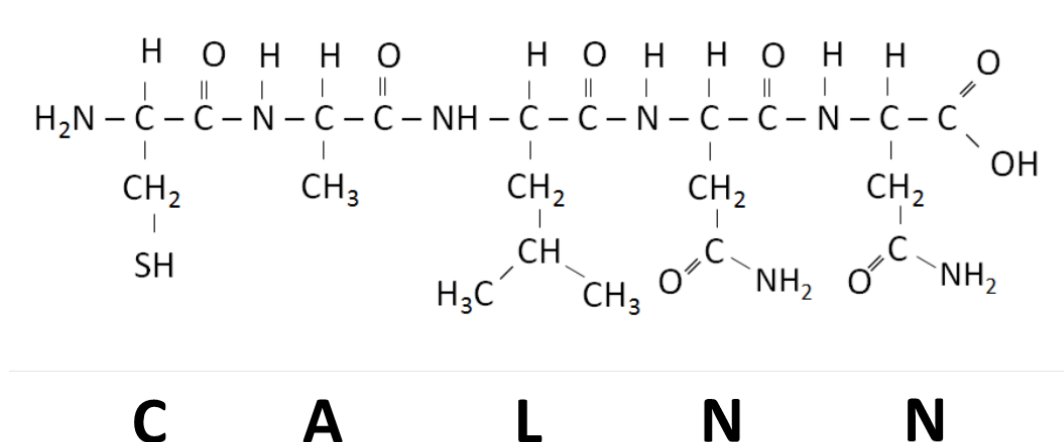
<Fig. 1.6> Exocytosis of peptide modified GNPs. (A) Percent of NPs exocytosed for cells incubated with unmodified (citrate capped) and peptide modified GNPs. (B) Dynamics of exocytosis process following one and six hours. Error bars represent standard deviation of $n = 3$. Adapted from Yang, C., *et al.*, *Peptide modified gold nanoparticles for improved cellular uptake, nuclear transport, and intracellular retention*. *Nanoscale* 2014. 6(20): p. 12026-12033 [129].

In general, nanoparticles administered into the body will be eventually cleared by the mononuclear phagocytic system (MPS) organs, such as the liver and spleen [107]. Compared to studies of NP endocytosis, limited number of studies have been performed on NP exocytosis [107, 130], however, previous work has shown that the exocytosis process also depends on the cell type,

NP size, and surface properties of NPs [130-132]. Hence, the assessment of exocytosis should be performed in relation to the parameters used in each study. Chithrani's group showed that the fraction of NPs exocytosed was lower by two-fold for cells targeted with peptide modified GNPs in HeLa cells (Fig. 1.6A) [129]. The cells were first exposed to GNP constructs, and then the cells were washed and supplied with fresh NP free medium. The accumulation of GNP constructs were measured at 1 hr or 6 hr after wash with phosphate buffered saline (PBS) and introduction to NP free medium [129]. The peptide on the surface of the GNPs causes endosomal membrane disruption and the peptide modified GNP constructs 'escapes' the endosomes and the residence time of the NPs in the cytoplasm increases [118]. The NPs escaping the endosomes and staying in the cytoplasm and nucleus was suggested to be the reason for the increased accumulation of GNPs in cells with less amount being exocytosed (Fig. 1.6A) [129, 131]. Particles that 'escape' the endosomes being excreted less was also observed with other types of NPs. For example, Wang *et al.* evaluated the excretion of CuO NPs in A549 human lung carcinoma cells and discovered that a portion of NPs, which were located in mitochondria and nucleus, could not be excreted by the cells [133]. Similarly, based on findings by Chu *et al.*, clusters of silica NPs in lysosomes are more easily exocytosed by H1299 human non-small lung carcinoma cells compared to single NPs in the cytoplasm [134]. It was also reported that a portion of the GNPs that are exocytosed can re-enter the cells. The percent of NPs re-entering the cells was 10 % and 15 % respectively, for unmodified (citrate-capped) and peptide modified GNPs as shown in Fig. 1.6B [129].

1.6 Surface modification of GNPs with peptide sequences

A mixture of several different peptide sequences can be used for stabilization and modification of gold nanoparticles (GNPs). Stabilization of GNPs is required prior to further modifications with other peptide sequences or conjugations with chemotherapeutics. In this dissertation, the GNPs were stabilized with a CALNN pentapeptide prior to modification with another peptide sequence containing a 'RGD' amino acid motif.



<Fig. 1.7> **Structure of CALNN pentapeptide.** Molecular structure of CALNN peptide showing cysteine (C) in the N-terminus, Alanine (A) in the second position, Leucine (L) in the third position, and Asparagine (N) in the fourth and fifth position.

A CALNN pentapeptide ligand has been used to convert citrate-stabilized GNPs into stable and water-soluble NPs [119]. Previously used strategies for stabilization of GNPs include usage of thiol ligands with hydrophilic terminal groups, such as polyethylene glycol (PEG), tiopronin, and bovine serum albumin (BSA). Various approaches have been used to produce stable GNP complexes, but the lack of generic protocols for functionalization of particles with biomolecules remained as a shortcoming [119]. GNPs often aggregate when thiol-containing amino acids or

peptides are added as capping agents, but modification with CALNN can result in a stable complex that can be further functionalized with other biomolecules [119, 135]. In order to have a nonaggregating particles, electrostatic aggregation should also be prevented by ensuring the particles have a net positive or net negative charge, leading to overall repulsive interactions [119]. The thiol group in the side chain of the N-terminal cysteine (C) makes a covalent bond to the surface of the GNP. The alanine (A) and leucine (L) in the second and third position of the CALNN sequence possess hydrophobic properties and promotes the self-assembly of the peptide. The leucine is larger than alanine which accounts for the curvature of the spherical core of the GNP. The amide group side chain of the asparagines (N) in the fourth and fifth position possess hydrophilic properties, thus, allowing the CALNN covered GNP complex to be hydrophilic [119]. The structure of CALNN is illustrated in Fig. 1.7.

The arginyl-glycyl-aspartic acid (RGD) tripeptide sequence is found in proteins such as fibronectin, citronectin, and type I Collagen [136, 137]. These three amino acids form the core structure recognized by cell surface receptors and can improve the intracellular retention of the NPs [129, 137]. The RGD peptide sequence is one of the principle adhesive ligand that is recognized by several integrin receptors, including $\alpha\beta3$, $\alpha\beta5$ and $\alpha\beta6$ [122, 138-141]. Integrins are main receptor proteins that cells use to bind and respond to the extracellular matrix (ECM) proteins, including collagens, fibronectin, and laminins [142]. Improved tumour targeting has been observed in studies using RGD-modified drug constructs because the integrin receptors are overexpressed on the surface of most types of cancer cells and RGD modified particles can enter the cytoplasm through receptor-mediated endocytosis [122, 141, 143-146]. Shayakhmetov *et al.* reported that vectors with deleted RGD motifs required 10 times more of the doses than the RGD motif possessing vectors to achieve a comparable effect [147]. This group also observed that the

deletion of RGD motif reduced the efficiency of a vector escape from endosomes or the kinetics of the endosomal escape was slower than the RGD possessing counterparts [147]. This finding leads to the possibility of RGD modified GNPs escaping the vesicles and remaining in the cytoplasm of the cell rather than exiting through exocytosis [129]. The reduced exocytosis of GNP molecules is suggested as one reason behind increased accumulation of RGD modified GNPs.

1.7 Rationale for the use of 10 nm GNPs

Gold nanoparticles (GNPs) can be synthesized in various sizes (2-100 nm) and shapes (spheres, rods, stars, etc) and the surface functionalization allows targeting into specific biological structures within the cell [63, 148-151]. Since various sizes of GNPs are available, and the optimal size varies for different purposes, several factors should be considered in selecting the size of GNPs appropriate for the aim of the study. The studies that will be discussed in this dissertation have an aim of using GNPs as a chemotherapeutic drug carrier and radiosensitizer at monolayer cell levels with a goal of translating the platform to multilayer cell levels with appropriate modifications in the future. Considering several factors, including toxicity, tissue penetration and cellular uptake, 10 nm sized colloidal GNPs were selected for the following studies. Reports have shown that NPs of diameter of 20 – 50 nm showed the highest uptake where the specific size of the highest uptake was found to be cell line dependent [53, 102, 103]. Many theoretical calculations support the size dependence on GNP uptake [152-154]. Despite having an optimal size of 20 – 50 nm for cellular accumulation, it has been suggested that smaller GNPs were better at penetration through the tissue matrix [101]. Moreover, since the action of many chemotherapeutics is on the DNA and there is higher radiosensitization when GNPs are targeted to the nucleus [129], a small

enough size of GNPs that has a potential to enter the nucleus of the cell was one of the criteria when selecting the size of GNP platform. Considering toxicity and biocompatibility, the smallest possible GNPs that could be synthesized with the Turkevich method of GNP synthesis [65, 70], 10 nm GNPs were selected. The cellular accumulation of 10 nm GNPs is predicted to improve by modifying the surface with peptide sequences containing the 'RGD' amino acid motif.

1.8 DNA Damage

The DNA of eukaryotic cells is constantly exposed to environmental and endogenous DNA damaging agents that impair DNA integrity and threaten genomic stability [155, 156]. Types of DNA damage include oxidative DNA damage, which refers to the oxidation of DNA bases, hydrolic DNA damage, which involves deamination or entire removal of individual bases, and single strand/double strand DNA strand breaks [155, 156]. In cells, Reactive Oxygen Species (ROS), such as superoxide (O_2^-), hydrogen peroxide (H_2O_2), hydroxy radicals (OH^\cdot), and singlet oxygen (1O_2), are formed as a byproduct of normal metabolism or external factors [157]. ROS can lead to several types of DNA damage, including oxidization of bases and single- and double-strand breaks [157]. Oxidation of purines commonly results in 8-hydroxypurines and oxidation of pyrimidines generates formamidopyrimidines [156]. Repair mechanisms of DNA oxidation include rapid degradation of the 8-hydroxypurine to prevent misincorporation during DNA replication and if misincorporation has already occurred, the 8-hydroxypurine in the DNA template is excised by a specific DNA glycosylase [156]. Hydrolic DNA damage generally occurs due to the glycosidic bond between bases and deoxyribose being hydrolyzed [156, 157]. The instability of this glycosyl bonds is measured by using DNA with ^{14}C -labelled purine or pyrimidine residues

[156]. The repair process is initiated by endonucleases breaking the DNA strand on the base-free sites, phosphodiesterase removing the sugar-phosphate residue, and filling the nucleotide gap by DNA polymerase and DNA ligase [156].

Of the many types of DNA damages, DNA double-strand breaks (DSBs) are considered the most harmful, because unrepaired DSBs are sufficient to trigger permanent growth arrest and cell death [158-160]. In addition, DSBs are potent inducers of gross chromosomal rearrangements such as deletions, translocations and amplifications. The source of endogenous damage is mostly derived from collapsed replication forks during the S phase of the cell cycle whereas exogenous lesions are caused by DNA-damaging agents such as ionizing radiation and DNA-damaging drugs [161]. Cells respond to DSBs by mounting a complex signaling network that coordinates DNA repair reactions with DNA damage checkpoint activation and chromatin reorganization [161]. This signaling network is called the DSB response and includes signaling events [161]. An important regulator of DSB signaling is 53BP1. 53BP1 was initially identified as a protein that binds to the central DNA binding domain of a transcription factor, p53 (also known as TP53), that blocks proliferation of cells harboring unrepaired or misrepaired DNA [162]. A wide range of genotoxic stresses, such as DNA damaging anti-cancer drugs or radiation promote nuclear accumulation of p53 and trigger p53-mediated transcriptional activation [162, 163]. As an early event in the recognition of the breaks, 53BP1 becomes hyper-phosphorylated and rapidly redistributes to distinct nuclear foci and co-localizes with phosphorylated H2AX (γ -H2AX) in mega-base regions surrounding the sites of DNA strand breaks. However, unlike H2AX, which has been reported to be phosphorylated in the synthesis (S) phase of the cell cycle, 53BP1 is phosphorylated at Serine 1778 in all asynchronously growing cells independent of cell cycle phase and thus can be used instead of γ -H2AX to better distinguish exogenous DNA damage from endogenous DNA damage

caused during DNA replication [159]. 53BP1 phosphorylation is nuclear, focal and dose-dependent at 30 min (initial DSBs) and decreases over time with kinetics that parallel the rate of DNA repair over time returning to baseline 16 hours post exposure [159, 164]. The 53BP1 foci detected after the 16-hour exposure are an indicator of the DNA DSBs that have a lower probability of being repaired. A single persistent DNA DSB may be sufficient to induce cell death through apoptosis [165, 166]. Apoptosis is typically described as a form of programmed cell death, known to be accompanied by the reduction of cellular volume, plasma membrane budding, phosphatidylserine (PS) externalization, and activation of caspases [167, 168].

1.9 Chemotherapy

Chemotherapy is also used as a major curative modality for few types of malignancies, palliative treatment for many types of advanced cancers, and adjuvant treatment before, during or after local treatment (surgery and/or radiotherapy) to eradicate micro-metastases and to improve local control of the primary tumour [21]. Chemotherapy involves administering pharmaceutical compounds, such as bleomycin or cisplatin, that exert cytotoxic effects to disrupt the rapid overgrowth of malignant cells [22, 23]. The action of bleomycin and cisplatin, the two chemotherapeutic agents used in this dissertation, will be discussed in this section.

1.9.1 Action of bleomycin

Bleomycin is one of the most potent natural anti-tumour drugs and has been used for chemotherapeutic agents in clinical treatments of some cancers, such as Hodgkin's disease, non-Hodgkin's lymphoma and testicular cancer [169, 170]. Bleomycin is a group of glycopeptide anti-

tumour antibiotics discovered by Umezawa *et al.* from the culture filtrate of *Streptomyces verticillus* [171]. It is a large molecule that crosses cell membranes slowly [172]. The mechanism of this drug is a deoxyribose oxidation that is similar to the free radical damage of DNA by chelating metals [26]. Bleomycin forms a complex with ferrous ion, Bleomycin-Fe²⁺, which undergo oxidation to Bleomycin-Fe³⁺ [173]. The bleomycin/ferrous iron complex binds to the DNA and this binding leads to insertion of the drug between base pairs, which is called intercalation, and unwinding of the double helix [172]. Oxidation of the complex is accompanied by the generation of reactive oxygen radical species which attach with the phosphodiester bonds of DNA – a second step in DNA strand break [170, 172, 173]. The therapeutic effectiveness, however, is limited due to the side effects of the drug, most notably pulmonary toxicity [26]. The usage of this anti-tumour drug could be widened if lower dosages could be delivered closer to the target and could be contained. Several NP systems had been used in the past for mediated delivery of bleomycin. For example, Georgelin *et al.* used core-shell magnetic NPs (CSMNs), NP which the core that consisted of citrate-coated maghemite (γ -Fe₂O₃, diameter around 7 nm) and the shell that consisted of silica and polyethylene glycol (PEG) chains, for cellular delivery of bleomycin [26]. Results from clonogenic assay showed that the cells incorporated with the drug and CSMN had 10 % clonogenic efficiency, while cells incorporated with the CSMNs only were able to reproduce normally at a 90 % clonogenic efficiency [26]. The complex was observed in the nucleus through transmission electron microscopy (TEM) [26]. Noting that the CSMN has no known nuclear targeting properties, this indicates that the bleomycin might have properties that allow itself to enter the nucleus [26]. Jain *et al.* used bleomycin as a radiomimetic agent and observed survival fraction (SF) was 0.39 in cells exposed to gold nanoparticles (GNPs) before the bleomycin exposure, which was close to a two-fold decrease than the SF of 0.62 for the bleomycin without

GNPs [8]. The sulfate ending of Bleomycin attaches onto the surface of GNPs. The simple conjugation makes it an ideal drug to use in a combinational experiment.

1.9.2 Action of cisplatin

Another successful anti-cancer drug that is widely used today is *cis*-diamminedichloroplatinum (II), also known as cisplatin [174]. Cisplatin has been known since 1845, its anti-tumour activity was established in 1970, and was approved by the FDA in 1978 [175-178]. Cisplatin is used to treat ovarian, cervical, head and neck, esophageal and non-small cell lung cancers, but best known for its usage in treatment of testicular cancer, with the cure rate that reaches over 90 % [179-183]. Although promising clinical trial results has been proven, one of the major side effects that come with cisplatin is severe renal toxicity [184]. The uptake pathway of this drug is known to be through passive diffusion [185]. Various mechanisms of cisplatin entry in cells have been postulated [186]. It had been suggested that active uptake of cisplatin is mediated by membrane-embedded proteins such as copper transporter CTR1 [187]. However, recent studies showed binding of platinum to cysteine-rich CTR1 protein is irreversible and it is unlikely that cisplatin can be transported into cells through CTR1 [188, 189]. Also, it was found that the rate of cisplatin entry did not depend on increased expression of CTR1 and the rate of the platinum drug uptake did not saturate [190]. These results suggest that cisplatin entry is not protein-mediated [190]. Eljack *et al.* showed that cisplatin is capable of passive diffusion across the lipid bilayer membrane [186]. The structure of cisplatin (*cis*-[PtCl₂(NH₃)₂]) has no net charge and is stable in a high chloride concentration (>100 mM) like the blood stream and the extracellular matrix [185, 186]. The small neutral compound is capable of diffusing across the cell membrane, and once the compound enters the cytoplasm the chloride ions dissociate from the platinum ion due to the decrease in chloride concentration in the

medium (approximately 4 mM), transforming the drug into an active form and allowing it to react with cellular targets [185, 186]. The dissociation results in positively charged complexes, $[\text{PtCl}_2(\text{NH}_3)_2(\text{OH}_2)]^+$ and $[\text{PtCl}_2(\text{NH}_3)_2(\text{OH}_2)_2]^{2+}$ which has a lower rate of permeation than the neutral cisplatin [186]. Although there is still a possibility of cisplatin uptake being facilitated, passive diffusion is considered a major uptake pathway of cisplatin into cells [186].

It is generally accepted that the primary target for cisplatin is the DNA by forming a cisplatin – DNA cross-link structure at the N7 position of guanine and adenine bases, resulting in distortion of the DNA [172, 174, 191, 192]. The formation of this cross-link structure destroys the helix stability of the DNA [174]. Since DNA replication and transcription are essential for cell division and protein production, the cisplatin binding to the DNA and distorting the DNA structure and interfering with normal functioning of this important cellular component would be considered cytotoxic [174]. Some studies showed that cisplatin inhibits DNA transcription, where transcription refers to the process where mRNA is produced from a DNA template. This cellular process is critical in protein synthesis [193, 194]. In these studies, cisplatin-treated cells progressed through the S phase of the cell cycle, where DNA synthesis happens and arrested in the gap 2 (G2) phase which is the second gap between the synthesis and mitosis. For cells treated with lower concentration of cisplatin, the G2 arrest was temporary. However, for cells treated with higher concentrations remained in the G2 arrest until cell death occurred [193].

The mechanism of cell death from cisplatin was found to be through apoptosis [195]. Apoptosis, which is also known as ‘programmed cell death’ is characterized by cell shrinkage and surface blebbing which was observed in Sorenson’s study [195]. One of the main reasons for cisplatin treatment failure pertains to resistance to the drug. The resistance is either intrinsic to certain cells or acquired through exposure to the compound [174]. Several studies have been

performed to understand the mechanism of resistance, but contradictory results have been found. Multiple mechanisms have been identified for cisplatin resistance, which include changes in intracellular accumulation of the drug, increased production of intracellular thiols to modulate toxicity, and increased capability of cells to repair damage from the cisplatin-DNA cross linkage [174]. It is one of the common drugs used with radiation [196] and has been previously used with GNPs and with MDA-MB-231 cells [9] that make it an ideal drug to use in a combined cancer therapy study.

1.10 Radiation therapy

1.10.1 Use of radiation therapy in cancer treatment

Radiation therapy is one of the most common treatment modalities for cancer, along with surgery and chemotherapy [14]. The sources of radiation therapy include gamma or X-ray photons, electrons and protons [16, 17]. In this dissertation, the studies use X-ray photons. In radiation therapy, energy is deposited along the path of the incident radiation and a series of events occur after irradiation of biological medium. These events can be categorized into physical, chemical, and biological stages [77]. The physical stage happens within the sub-femtosecond time frame, photons interact with medium, depositing energy [77]. The cells can be damaged directly by the ionizing energy fragmenting the DNA, or indirectly by ionizing energy creating secondary species such as low energy electrons (LEEs) or radicals that further damage DNA [77]. It has been shown by several studies that 70 % of DNA damage from X-rays is through production of free radicals and other reactive species and the rest is due to secondary electrons and direct DNA fragmentation [197-199]. These highly reactive radicals can rupture molecular bonds and oxidize DNA or

proteins of intracellular structures, which can affect the stability of cell membranes and organelles. Secondary electrons produced during ionization event can also cause DNA strand breaks through dissociative electron attachment [200]. The chemical stage happens within microseconds after irradiation and refers to damage due to secondary species as indirect damage [77]. The biological stage occurs from microseconds and forward which refer to damaged cells responding to the radiation exposure [77]. The DNA damage result in various lesions, such as base damage, single strand breaks (SSBs) or double strand breaks (DSBs). While base damage and SSBs are relatively effectively repaired by cell repair mechanisms, DSBs are more damaging to cells and are difficult to get successfully repaired especially when induced at high concentrations [201]. Although radiation therapy is considered effective and used in treatment of about 50 % of all cancer patients, a sufficient dose that can kill any tumour cell can also damage the surrounding healthy tissue [18]. A photon beam will irradiate some surrounding normal tissue regardless of how well shaped or conformed to the dimensions of the tumour [20]. This limits how much radiation a patient can receive and therefore a radiosensitizer, an agent that increase the cytotoxicity of radiation, targeted to the tumour area will be beneficial in improving therapeutic results of radiation [20]. A radiosensitizer may not have a direct anti-cancer effect or it may be one variety of anti-cancer drugs that exhibits antitumour effects alone in addition to radiosensitization [20]. Gold nanoparticles (GNPs) used for this study is predicted to be a radiosensitizer that does not have a direct anti-cancer effect.

1.10.2 High Z materials as radiosensitizers

Delivering the dose that eradicates tumour tissue while not disrupting surrounding healthy tissues has been a challenge and it is still being studied to reach the optimal and delicate balance

of treating tumour tissue while saving normal tissue. Many research groups are still in search to improve the current radiation based therapeutic techniques. High-Z materials have been used in research as radiosensitizers due to the production of secondary electron scattering from those high-Z materials [202, 203]. Some materials with a Z value higher than tissue ($Z \sim 7.5$) that were used as radiosensitizers in the past include iodine ($Z=53$), bulk metallic gold and micro diameter sized gold particles. Santos Mello *et al.* demonstrated that injecting iodine into the tumour suppressed re-growth rate of 80 % after radiation [204]. Nath *et al.* found introducing iodine into the DNA of the cell through iododeoxyuridine *in vitro* increased radio-sensitivity by a factor of three [205]. Iodinated compounds, however, can be cleared by the kidney rapidly and sometimes cause renal toxicity [206-208]. Regulla *et al.* developed a method to locally enhance radiation therapy by introducing a metal surface at the site of irradiation (US Patent 6,001,054) [209]. The solid metal surface, such as a metallic stent, was placed in the blood vessel adjacent to the tissue to be ablated. One of the drawbacks of this method is that placing bulk metal surfaces throughout all tumour vessels and tissues was impractical. Moreover, the radiation was restricted to less than 400 keV, which could not treat tumours at depth [55]. Skin cancers can be treated using this low photon energy range, but such tumours can be removed easily through surgery [55].

Herold *et al.* found a dose enhancement of a factor of 1.54 from a clonogenic assay when micrometer sized (1.5-3 μm diameter) gold particles were added in a stirred suspension prior to irradiating with 100-240 kV x-rays. This group also injected the same sized gold particles directly into tumour sites. Although reduction in tumour size did not occur, the plating efficiency of the extracted cells was lower than the control cells, 0.15 and 0.25 respectively. Histological data showed that the gold particles were mostly in the interstitial fluid while no particles were found in the tightly packed regions of tumour cells [210]. This implies the particles were non-uniformly

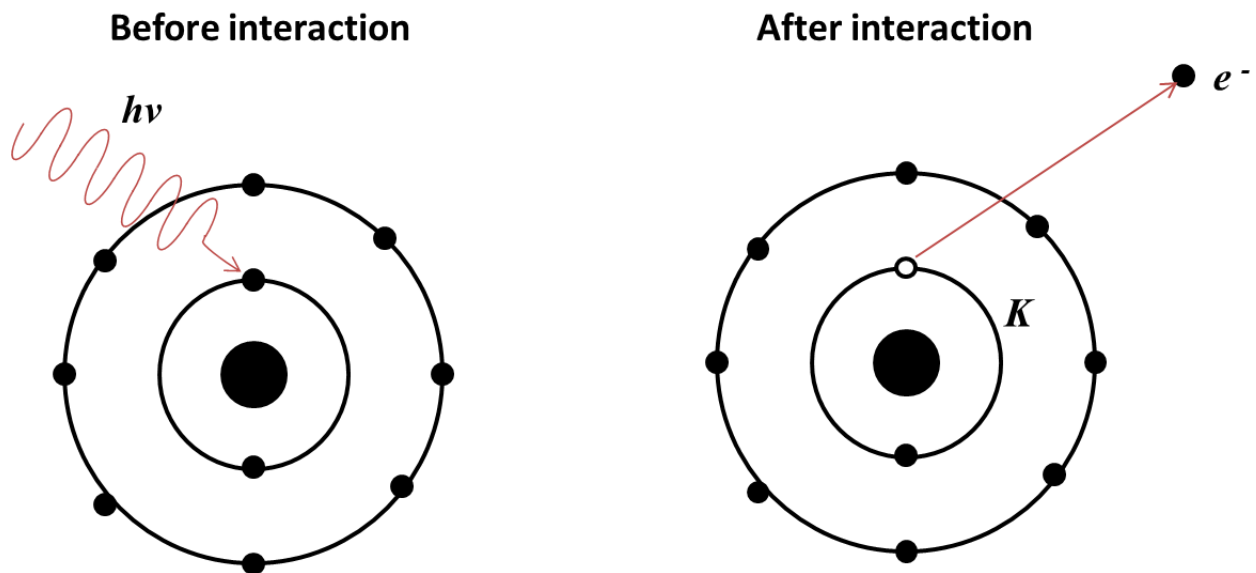
dispersed as the larger sized particles are unable to pass through the tightly packed regions. Consequently, NPs in the size range 2-100 nm have been used to deliver therapeutic systems into tumour tissues [55, 211, 212]. Our recent studies show that GNP uptake and their dose enhancement effects were dependent on the size of the NP [55, 131, 213]. Gold having a higher Z number than iodine can increase the absorption of radiation energy even more than iodine, while it is also biocompatible [74, 75, 204, 214-216] and can access the tumour cells as they are smaller than the typical cutoff size of pores in tumour vasculature [217].

The extent of sensitization with GNPs has been reported to depend on several factors including the beam energy. Monte Carlo studies predicted radiosensitization effects of GNPs under various radiation energy taking the secondary electrons and Auger electrons generated by GNPs with radiation into account [13, 218-222]. As the photoelectric cross-section strongly depends on the energy, irradiating GNPs with a low-energy photon beam would greatly increase the number of secondary electrons compared to GNPs irradiated with high energy beams. A number of cell studies have also examined the radiosensitization effects of GNPs and the enhancement by GNPs in cell studies reported to be greater than that estimated by physical calculations, even at high photon radiation where the Compton Effect dominates [55, 223]. Possible reasons behind the discrepancy between the Monte Carlo predications and cell study reports will be discussed in 1.10.4.

1.10.3. Physical mechanism of GNP sensitization

The physical mechanism for gold acting as a radiosensitizer is due to the larger energy absorbing properties of gold compared to soft tissues which enhance the physical dose in the presence of Au. However, this enhancement is known to be energy dependent. Bremsstrahlung X-

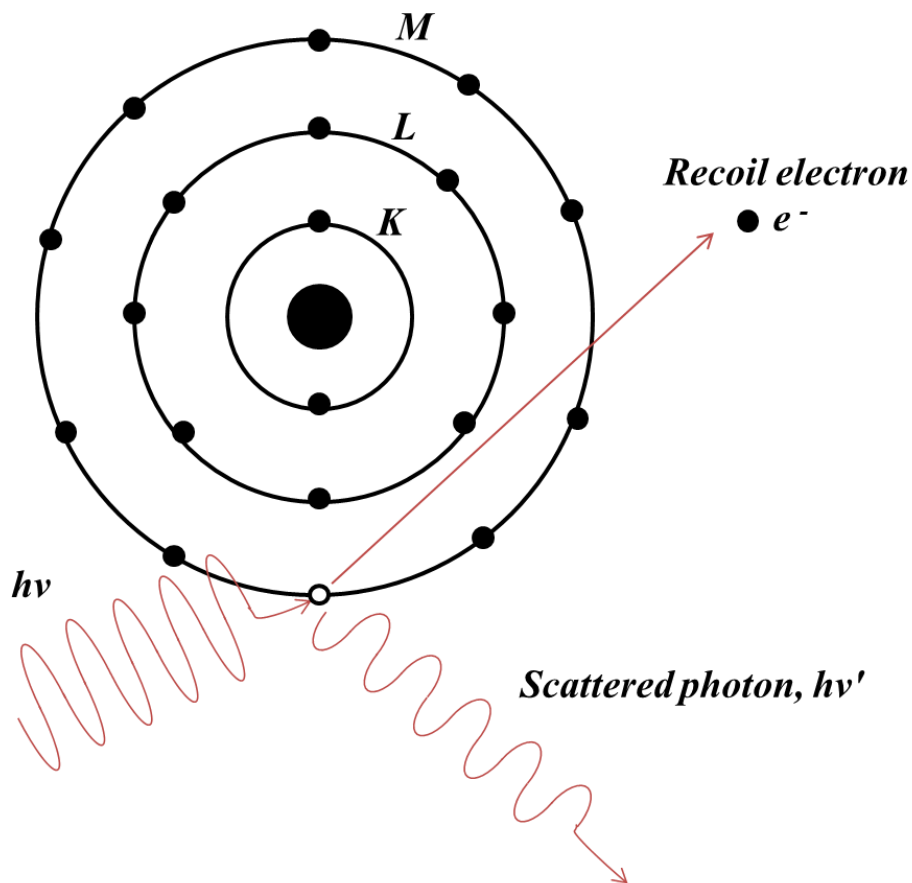
ray beams typically range between 100 kV and 25 MV which are produced with kinetic electron energies between 100 keV and 25 MeV decelerated in metallic targets [17]. While kinetic energies are transformed in the target into heat, a small fraction of the energy is emitted as X-ray photons [17]. These X-ray photons are used for the treatment. The deep seated tumours are treated with mega-voltage energy range from 4 MV to 25 MV and the kV energies are used for superficial tumours due to the lack of penetration [17]. The two main photon interactions with matter within the clinical photon based energy range are photoelectric, where photon interacts with a tightly bound electron and Compton, where photon interacts with a loosely bound electron.



<Fig. 1.8> Schematic diagram of the photoelectric effect. A photon with the energy $h\nu$ interacts with a K-shell electron.

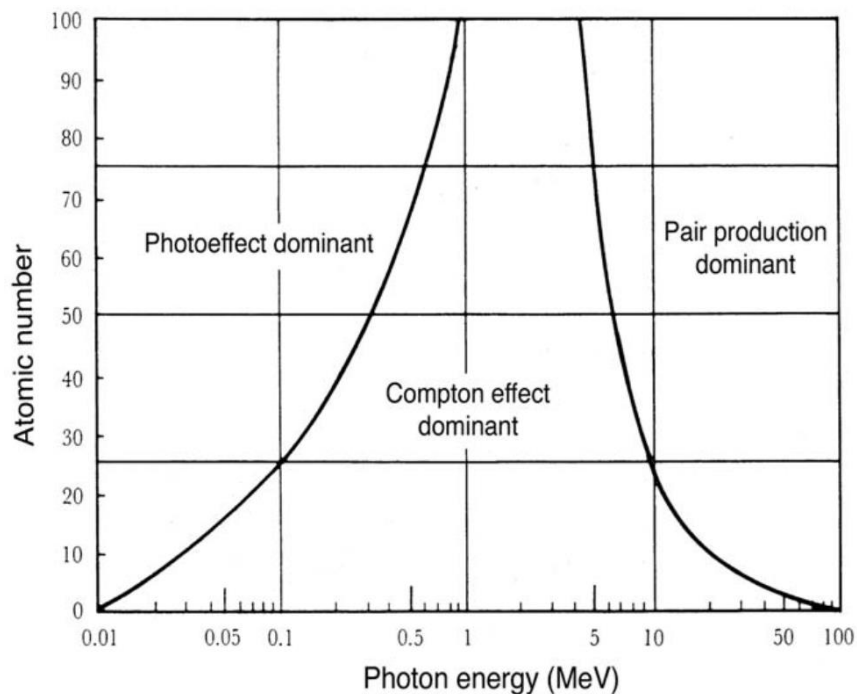
In a photoelectric event, the photon interacts with an electron from the inner shell. The photon is absorbed and the orbital electron with kinetic energy is ejected, leaving a vacancy (Fig. 1.8). The atomic cross section for the photoelectric effect has an atomic number Z dependence of

3~5, therefore, high-Z materials like gold ($Z = 79$) have a higher mass energy absorption coefficient in comparison to those with lower Z materials, such as biological tissue ($Z \sim 7.5$) that is composed of hydrogen, carbon, and oxygen [16, 77]. The photoelectric effect is also inversely proportional to $h\nu$ at a factor of up to 3 for energies less than 0.1 MeV [16]. Vacancies from the ejected electrons is usually followed by Auger cascades. Auger electrons have been shown to be effective in damaging DNA directly or indirectly by interacting with surrounding water molecules and producing hydroxyl radicals [200, 224]. It is therefore, predicted that the effect of radiation can be enhanced by introducing high-Z materials to the soft tissue.



<Fig. 1.9> Schematic diagram of the Compton Effect.

The Compton Effect is an interaction of photon energy, $h\nu$, with a loosely bound stationary electron and results in an ejection of the electron and a scattered photon that has a lower energy than the incident photon (Fig. 1.9). Unlike the photoelectric effect, the Compton effect is independent of the atomic number [16].



<Fig. 1.10> Regions of relative predominance of the three main forms of photon interaction with matter. Adapted from Podgorsak, E.B., *Radiation Oncology Physics: A Handbook for Teachers and Students*. 2005, Vienna: International Atomic Energy Agency [17].

However, the Compton effect dominates in most of the clinical energy ranges and even when considering gold ($Z = 79$) as an absorber, photoelectric effect does not dominate in the MeV range (Fig 1.10). However, kV energies lack penetration, therefore, MV X-rays are used for deep seated tumours and sensitization at higher energies would be more clinically relevant. Unlike the dose-based predictions of GNPs minimally radiosensitizing in MV ranges [222, 225], experimental studies have shown higher dose enhancement [11, 55, 226, 227]. The variation

between Monte Carlo prediction and experimental results indicate mechanisms other than physical mechanisms are also responsible for damage to cells upon radiation treatments.

A Monte Carlo study by Carter *et al.* revealed that DNA damage was caused mostly by low energy electrons (LEEs) that have effective ranges of 1-10 nm and DNA damage by long range photoelectrons that can travel up to micrometers were negligible [219]. These results suggest that physical radiosensitization results from the secondary LEEs of <100 eV generated from GNPs, which deposit energy within nanometer ranges of the GNP. However, most previous experimental studies using GNPs as a radiosensitizer were not targeted towards the nucleus. This suggests that radiosensitization mechanisms other than physical mechanisms are at play. Other mechanisms that are proposed for GNP radiosensitization is discussed in the next section.

1.10.4 Other mechanisms of GNP radiosensitization

Chemical sensitizations have also been proposed as mechanisms of GNP sensitizations. The physical, chemical and biological phases in response to radiation have been discussed in section 3.1.1. In the chemical phase, the presence of GNPs can induce DNA to be more susceptible to radiation-induced damage by weakening DNA bonds or interfering with reactions that fix the damage [228]. Yao *et al.* studied the DNA damage of GNP-DNA complexes induced by 10 eV electrons, an energy range where no secondary electrons are expected to be emitted from the GNPs, and observed that a positively charged 5 nm GNPs that binds strongly to DNA had the most damage up to 4.5 fold [229]. However, it requires GNPs to be in contact with the DNA which requires GNPs to be localized in the nucleus for this mechanism to be effective. Another chemical enhancement is attributed to the GNP catalyzed radical production. The interaction of molecular oxygen with the surface of GNPs facilitates the surface-mediated transfer of electrons for the

production reactive oxygen species (ROS). It has been shown that adding GNPs to water led to 1.46 fold increase in hydroxyl radicals and 7.68 fold increase in superoxide anions upon radiation with 100 kV X-rays. [230]. This enhancement to the already highly reactive environment formed by X-ray irradiation was attributed to the GNP induced emission of photoelectrons and Auger electrons that cause secondary radiolysis of water through charge transfer [231]. The production of the highly reactive free radicals causes a cascade of ionization which leads to further damages to the DNA.

Biological enhancements have also been suggested as a mechanism of action other than the physical mode [228]. DNA repair inhibition has been identified as one of the key biological pathways of radiosensitization, but the exact mechanism of biological cell response in the presence of GNPs still remain to be determined [228]. Previous studies demonstrated an inhibition of radiation-induced DNA damage repair with the presence of GNPs. Chithrani *et al.* reported that the incubation of HeLa cells with 50 nm citrate GNPs increased the number of γ H2AX and 53BP1 foci at 4 and 24 hrs post-IR at both 220 kV and 6 MV energies and suggested delayed DNA repair to be a key mode of radiosensitization [55]. Cui *et al.* also presented significant residual DNA damage from a γ H2AX immunofluorescence assay 24 hrs post IR on MDA-MB-231 cells radiated with 2 Gy and 4 Gy of 250 kV X-rays in the presence of 1.61 μ M or 3.21 μ M of 2.7 nm tiopronin GNPs in MDA-MB-231 cells [9]. Considering the association of DNA repair and radiation, inhibition of DNA damage response pathways is a plausible mechanism of dose enhancement with GNPs [228]. However, there are also reports on a lack of influence of GNPs on DNA repair kinetics. For example, Jain *et al.* observed no significant different in the number of 53BP1 foci, 1 hr or 24 hrs after with 1 Gy of 160 kV X-rays in cells MDA-MB-231 cells exposed to 12 μ M of 1.9 nm GNPs compared to the control group [8]. Contradictory outcomes for the effect of GNPs

on DNA damage upon irradiation reported by the various groups indicate that the role and mechanism of DNA repair inhibition in the presence of GNPs remain inconclusive in the field and further studies are required, taking the difference in parameters such as, physico-chemical properties of GNPs, cell line involved, incubation conditions, and radiation energy and dose, into account.

1.11 Goals and specific aims

Gold nanoparticles (GNPs) have been used either as a drug carrier or radiosensitizer. However, not many studies have used GNPs with chemotherapy and radiation therapy combined, utilizing both the drug carrying and radiosensitizing capability of GNPs. The goal of this dissertation is to study whether the use of GNPs with combined chemotherapeutics and radiation will have an improved effect in therapeutic results *in vitro*.

Hypothesis:

Combined use of chemotherapeutics and radiation in the presence of modified GNPs will result in a significant increase in tumour cell death than that of the same concentrations and dosages of chemotherapeutics and radiation in absence of GNPs in cells.

Specific Aims:

- 1) Investigate whether the presence of chemotherapeutic drugs can influence GNP accumulation in cells.
- 2) Investigate the effect of GNP mediated drug delivery.
- 3) Determine the radiosensitizing capability of the peptide modified GNP constructs with a clinically acceptable dose and energy of 2 Gy, 6 MV X-rays.
- 4) Determine the combined effect of chemotherapeutics and radiation in the presence of GNPs.

1.12 Overview of dissertation

The research presented in this dissertation uses peptide modified GNPs with chemotherapeutics (bleomycin or cisplatin), X-ray radiation (2 Gy, 6 MV), and combined use of chemotherapeutics and radiation in the presence of GNPs. To the best of the author's knowledge, this dissertation is the first demonstration of the results of combining chemotherapeutics and radiation with RGD-functionalized GNPs.

In Chapter 1, the concentration of the peptide modified GNPs used for this study has been investigated for toxicity to confirm that the improvement in therapeutic results in proceeding chapters is not a result due to GNP toxicity. The concentrations of GNPs used for studies discussed in this dissertation have been kept consistent at 0.3 nM.

In Chapter 2, the effect of GNP accumulation in MDA-MB-231 cells in the presence of chemotherapeutics (bleomycin or cisplatin) followed by the effect of GNP mediated drug delivery were investigated.

In Chapter 3, the radiosensitization effect of peptide modified GNPs was studied in MDA-MB-231 cells with 2 Gy, 6 MV X-rays. The radiation dose and energy were selected within the clinically relevant range for solid tumours.

In Chapter 4, combined effect of chemotherapeutics and radiation in the presence of peptide modified GNPs was studied. The same chemotherapeutics studied in Chapter 2, bleomycin (BLM) and cisplatin (CIS), were used concurrently with 2 Gy, 6 MV X-ray radiation. GNP-BLM and radiation combination were to observe the improvement with GNPs acting as both a drug carrier and a radiosensitizer. For the GNP, CIS, radiation combination, GNP acted as an additional radiosensitizer.

Chapter 5 summarizes the results, clinical significance and future work with preliminary data.

A part of chapter 2 (section 2.2.3) is published in *Nanomaterials* [232]. The rest of chapter 2, chapter 3, and chapter 4 are under review or submitted to peer-reviewed journals. The work in this dissertation has been presented at the SPIE BiOS conferences [233, 234].

Chapter 2

The use of chemotherapeutic drugs with peptide modified gold nanoparticles

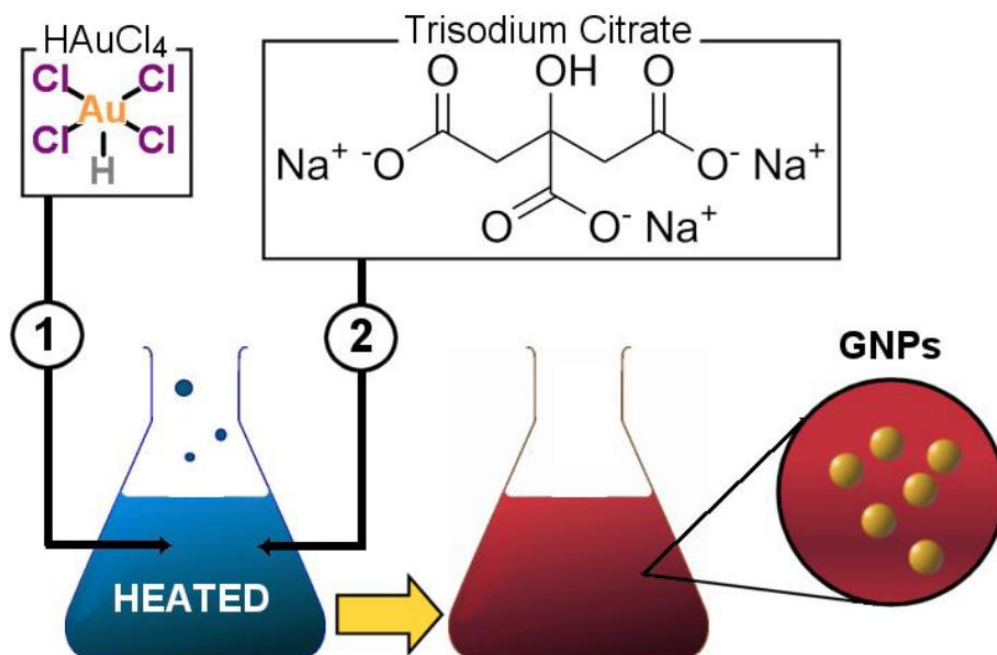
2.1 Introduction

Chemotherapy is used as a major curative modality for few types of malignancies, palliative treatment for many types of advanced cancers, and adjuvant treatment before, during or after local treatment (surgery and/or radiotherapy) to eradicate micro-metastases and to improve local control of the primary tumour [21]. Chemotherapy involves administering pharmaceutical compounds that exert cytotoxic effects and disrupt the rapid overgrowth of malignant cells [22, 23]. However, the side effects caused by anti-tumour drugs remain as one of the important problems to overcome in cancer treatment [24-26]. This is mainly induced by poor distribution of the anti-tumour agents and can be reduced by improving the bioavailability of the drug in the tumour region as well as confining them to the target region [26-29]. The use of nanoparticles (NPs) as drug carriers has been extensively documented in the last few decades and the advantages of NP-based drug delivery systems have been recognized by several previous studies [26, 47, 235-239]. Some NP-based therapeutic systems have already been introduced into the pharmaceutical market. For example, Doxil, a PEG-liposome containing doxorubicin, is approved for AIDS-related Kaposi's sarcoma, ovarian cancer and multiple myeloma [47, 49]. Liposomal drugs and polymer drug conjugates account for most of the FDA (Food and Drug Administration, USA) approved systems so far [240]. However, gold nanoparticle (GNP) based platforms are also being researched and have been used extensively in the field of nanomedicine and cancer research [33]. For example, a novel

nanomedicine that conjugated human tumour necrosis factor alpha (rhTNF) and thiolated PEG onto the surface of colloidal GNPs was recently tested in phase 1 clinical trial in cancer patients [241]. The size and shape of GNPs can be easily controlled during synthesis and can be quantified in biological samples [53]. Moreover, the surface of GNPs can be easily functionalized with small molecules, such as peptides and the surface functionalization widened the application aspects of GNPs [55-57]. The high surface area-to-volume ratio along with the large surface bio conjugation possibilities have made GNPs as an ideal platform for delivering pharmaceuticals for chemotherapy [58-60]. In this chapter, the effect of peptide modified GNPs with chemotherapeutic agents – one that attaches on the surface of GNPs, and one that has no interaction with GNPs – on MDA-MB-231 breast cancer cells will be observed. The sulfate ending of bleomycin attaches onto the surface of GNPs, while the cisplatin molecule has no known interaction with the GNPs. To the best of the group's knowledge, this is the first study to demonstrate the effect of 10 nm sized RGD modified GNPs at a relatively low concentration of 0.3 nM with chemotherapeutic agents.

2.2 Methods

2.2.1 Synthesis of colloidal gold nanoparticles



<Fig. 2.1> GNP Synthesis via the Turkevich method. In step 1, chloroauric acid is added to distilled water and brought to a boil. In step 2, sodium citrate is added to the mixture and acts as both a reducing and capping agent. After several minutes, the mixture changes colour, indicating the formation of GNPs. Adapted from Yohan, D., *Gold Nanoparticle Transport in Multilayered Cell Cultures*, in *Biomedical Physics*. 2015, Ryerson University: Toronto [101].

Gold nanoparticles were synthesized using the citrate reduction method [242]. First, 300 μl of 1 % chloroauric acid ($\text{HAuCl}_4 \cdot 3\text{H}_2\text{O}$) (Sigma-Aldrich) was added to 30 ml of double-distilled water and heated on a hot plate while stirring. Once it reached the boiling point, 1 ml of 1 % sodium citrate tribasic dehydrate ($\text{HOC}(\text{COONa})(\text{CH}_2\text{COONa})_2 \cdot 2\text{H}_2\text{O}$) (Sigma-Aldrich) was added. After the colour of the solution changed from dark blue to bright red, the solution was left to boil for another five minutes while being stirred. Finally, the GNP solution was brought to room temperature while being stirred. The method of GNP synthesis is illustrated in Fig. 2.1.

2.2.2 Preparation of peptide modified GNP constructs

Peptide modified GNP constructs were assembled by first conjugating the GNPs with a pentapeptide, H-Cys-Ala-Leu-Asn-Asn-OH (CALNN) (AnaSpec, San Jose, USA), with approximately 300 peptides/GNP ratio for stabilization purposes. The peptide with H-Cys-Lys-Lys-Lys-Lys-Lys-Gly-Gly-**Arg-Gly-Asp**-Met-Phe-Gly-OH (CKKKKKKGGRGDMFG) sequence (AnaSpec, San Jose, USA) was added with a 16 to 20 peptide/GNP ratio. This peptide modified GNP construct will be labelled and referred to as GNP-RGD in this dissertation.

Bleomycin (BioShop) was added to the GNP-RGD at approximately 780 bleomycin molecules/GNP ratio. Conjugation of the bleomycin molecules onto the GNP surface occurs through a gold-thiol bond. This construct will be labelled and referred to as GNP-RGD-BLM (BLM refers to bleomycin) in this dissertation.

Cisplatin (Tocris Bioscience) was added to GNP-RGD construct at approximately 620 molecule/GNP ratio. It was expected that cisplatin molecules do not have an interaction with the GNPs and remains in the mixture. This construct will be labelled and referred to as GNP-RGD; CIS (CIS refers to cisplatin). It is expected that the cisplatin does not attach onto the surface of the GNP-RGD, hence using a semicolon instead of a hyphen to indicate addition of cisplatin to the GNP-RGD solution.

2.2.3 Characterization of NPs

The core size and shape of the GNPs were obtained using transmission electron microscopy (TEM) using Hitachi H7000 TEM (Hitachi Coop., Tokyo, Japan) and the core size was measured with ImageJ software (NIH, Bethesda, USA). The UV-Vis spectra of the GNP constructs were obtained with Lambda 20 (Perkin Elmer, Waltham, USA).

2.2.4 Hyperspectral imaging

The CytoViva (CytoViva Inc., Auburn, USA) technology in combination with dark field microscopy was used to image GNP distribution within cells. The illumination of the microscope system utilized oblique angle illumination to create high resolution dark-field images. GNPs appear bright due to their high scattering cross-sections. This hyperspectral imaging of GNPs does not require optical labeling of the GNPs and it is also possible to extract spectral information from each pixel for verification purposes.

2.2.5 Cell culture and GNP delivery

MDA-MB-231 (breast cancer cell line) cells were obtained from ATCC and cultured in Dulbecco's Modified Eagle's Medium (DMEM) (Gibco), supplemented with 10 % Fetal Bovine Serum (FBS) (Gibco, USA origin) and 1 % penicillin-streptomycin (Gibco) at 37 °C humidified incubator with 5 % CO₂. The cells were exposed to either (1) Phosphate-Buffered Saline (PBS), (2) 0.3 nM of GNP-RGD, (3) 435 nM of CIS, (4) 0.3 nM of GNP-RGD and 435 nM of CIS, (5) 633 nM BLM, or (6) 0.3 nM of GNP-RGD and 633 nM of BLM for sixteen hours prior to clonogenic assays.

2.2.6 Quantification of GNP accumulation in cells

GNP accumulation in cells was quantified using Inductively Coupled Plasma Atomic Emission Spectroscopy (ICP-AES). Following sixteen hours of incubation with various GNP constructs, the cells were washed three times with PBS and the cells were suspended from the monolayer cultures with 0.25 % trypsin-EDTA (Gibco) for quantification of GNPs present per cell. Cells were counted with either a hemocytometer (Hausser Scientific, Horsham, USA) or a

Vi-CELL XR automated cell counter (Beckman Coulter, Brea, USA) and then treated with aqua regia (mixture of 37 % hydrochloric acid (HCl) (Sigma-Aldrich) and 70 % nitric acid (HNO₃) (Caledon Laboratories Ltd.) in a ratio of 3:1) in a silica oil bath. The samples were diluted and concentrations of gold (Au) atoms were measured in [mg/L] with the Optima 7300 DV ICP AES (Perkin Elmer, Waltham, USA). A calibration curve was obtained by measuring known concentrations of standard gold solutions prior to sample measurements.

The following equations were used to calculate the number of GNPs of each sample from the concentration of Au atoms measured from ICP-AES:

Number of Au atoms per GNP (U)

$$= \frac{\text{Number of Atoms per unit cell (*)} \times \text{Volume of GNP (sphere)}}{\text{Volume of unit cell}}$$

$$= \frac{4 \times \frac{4\pi (D/2)^3}{3}}{a^3} = \frac{2}{3}\pi \left(\frac{D}{a}\right)^3$$

where D = core diameter of GNP, a = length of a unit cell = 4.08 Å = 0.408 nm

* Gold nanoparticles synthesized through salt reduction methods assemble into Face-Centered Cubic (FCC) structures and FCC lattices contain 4 atoms per unit cell (a unit cell refers to the smallest repeating structure of any solid used to simplify the crystalline patterns solids arrange themselves to a lattice) [243].

Number of GNPs for each sample

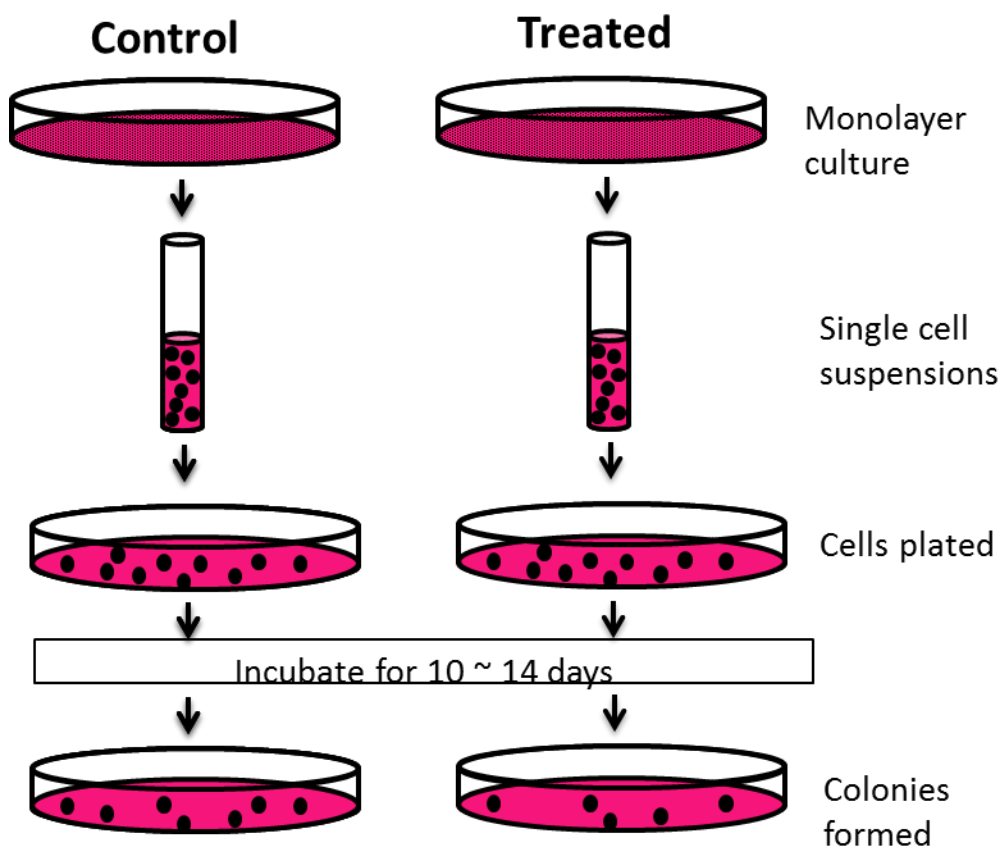
$$= \text{conc. measured from ICP AES} \left[\frac{g}{L} \right] \times \text{volume measured (L)}$$

$$\times \frac{1}{\text{molar weight of Au}} \left[\frac{mol}{g} \right] \times \text{Avogadro's number} \left[\frac{Au \text{ atoms}}{mol} \right]$$

$$\times \frac{1}{U} \left[\frac{GNP}{Au \text{ atoms}} \right]$$

The number of GNPs per cell is then determined by dividing the number of GNPs by the total number of cells for that sample. This calculation assumes a homogenous distribution of GNPs in the cell population [244].

2.2.7 Clonogenic Assay



<Fig. 2.2> Clonogenic assay flow chart. A flow chart schematic of the clonogenic assay method.

After the treatments, the cells were trypsinized and diluted to form single-cell suspensions. The required volumes of cell suspension solution were calculated for the control and treatment samples. The required volumes were placed on 60 mm tissue culture dishes and the dishes were rocked gently for even distribution of the cells. The cells were left in the 37 °C humidified incubator with 5 % CO₂ for 10-14 days for colonies to grow. The order of clonogenic assay is

represented in Fig. 2.2. Once colonies are formed, the dishes were stained and fixed with 0.1 % of methylene blue (BioShop) in 70 % ethyl alcohol (Fisherbrand) for 1 hr. The stained dishes were rinsed in lukewarm water and left to air-dry overnight. The air-dried control dishes were then counted. Colonies were defined as structures containing >50 cells. Then the plating efficiency (PE) was obtained.

$$PE = \frac{\text{Number of colonies counted}}{\text{Number of cells plated}}$$

The colonies of treatment samples were also counted and the survival fraction (SF) was obtained with the following equation:

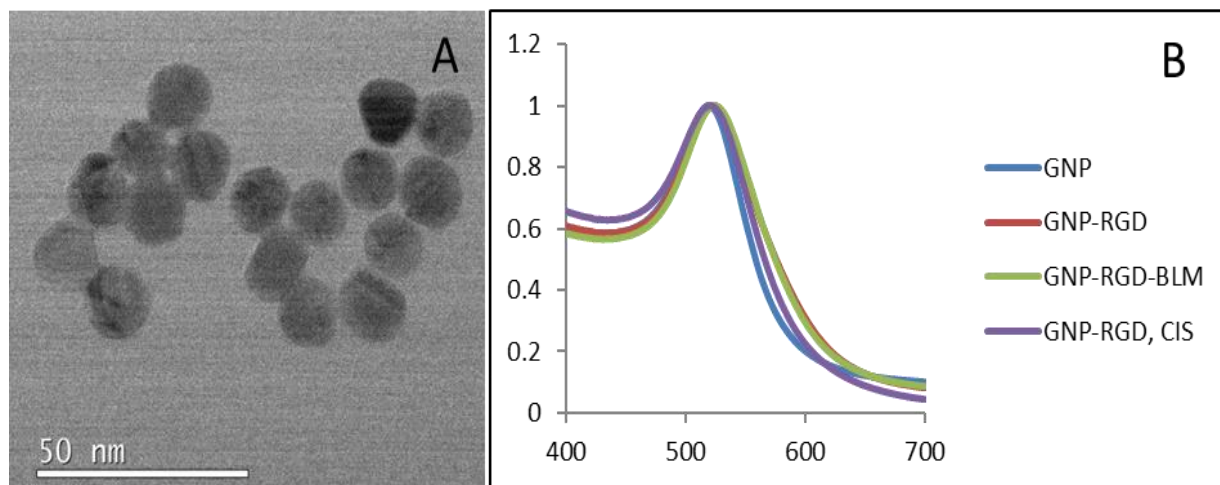
$$SF = \frac{\text{Number of colonies counted}}{\text{Number of cells plated} \times PE}$$

2.2.8 Statistical Analysis

Data for clonogenic assays are displayed as mean \pm standard error with at least three repeats. Statistical analyses were performed using the IBM SPSS Statistics (IBM Corporation, New York, USA). A two-sample t-test was used to measure statistical significance between pairs of results. For statistical analysis among three or more groups, one-way analysis of variance (ANOVA) was used and subsequent multiple comparisons with Bonferroni correction was performed in any statistical significance was detected by the ANOVA F-test. A p-value of less than 0.05 was considered to be significant.

2.3 Results

2.3.1 Characterization of GNPs

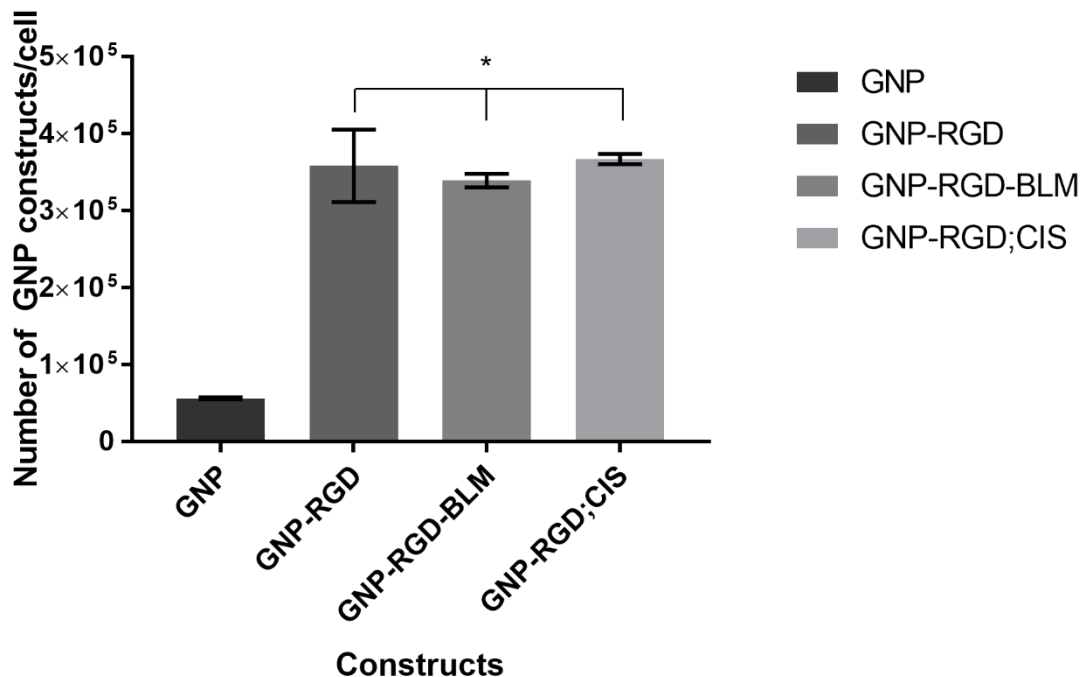


<Fig. 2.3> Characterization of GNPs used in this study. (A) TEM image that indicates the core size of the GNPs used is 10 ± 0.89 nm (B) UV-Vis Spectra of GNP, GNP-RGD, GNP-RGD-BLM, GNP-RGD; CIS with no significant broadening, measured up until 46 hr post formulation.

The shape and size of GNPs used for this study is determined with transmission electron microscopy (TEM) as shown in Fig. 2.3A. The approximate core diameter of these GNPs was 10 ± 0.89 nm, measured with the ImageJ software (NIH, Bethesda, USA) from at least 30 NPs synthesized from three different batches. Ultraviolet-Visible (UV-Vis) spectra were obtained to observe if broadening occurs with addition the of chemotherapeutics, bleomycin and cisplatin, to the GNP solutions. UV-Vis Spectroscopy measures the Local Surface Plasmon Resonance (LSPR) and it results in a strong absorbance band in the visible region, 500 nm to 600 nm. The peak wavelength of GNPs increases with the diameter of the particles and is often referred to as the red-shift. The size range of colloidal GNPs can also be determined by the peak SPR wavelength [245, 246]. UV-Vis measurements can also be used to evaluate the functionalization or aggregation of GNPs. When GNPs are successfully functionalized with ligands, the local refractive index at the

GNP surface will increase and result in a slight red-shift of the LSPR while maintaining the overall shape and intensity of the spectra. When GNPs are aggregated from irreversible inter-particle coupling, the LSPR will not only red-shift but the spectra will also broaden. Aggregated GNPs can also be detected visibly by the change in colour of the solution from red to blue. No significant broadening of spectra was observed for all samples up to 46 hrs post formulation as shown in Fig. 2.3B.

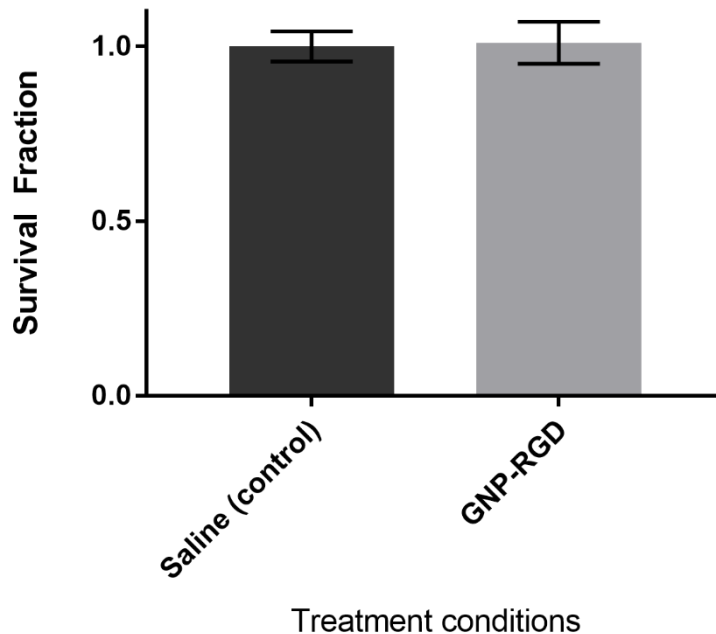
2.3.2 Effect of GNP accumulation with the presence of chemotherapeutics



<Fig. 2.4> Accumulation of GNP constructs in MDA-MB-231 cells. Improved accumulation was observed for cells modified with peptide (CALNN and RGD) modified GNPs compared to the unmodified (citrate stabilized) GNPs. Data are means \pm S.D. for $n = 10$ cell preparations over three independent experimental set-ups. * indicates statistically significant difference (ANOVA, $p < 0.05$)

The amount of GNP, GNP-RGD, GNP-RGD-BLM and GNP-RGD;CIS accumulated in MDA-MB-231 cells were measured and calculated after 16-hour. The number of GNPs accumulated per cell for GNP, GNP-RGD, GNP-RGD-BLM and GNP-RGD;CIS were $56,000 \pm 1200$, $358,000 \pm 47,000$, $339,000 \pm 8900$ and $367,000 \pm 6600$ respectively as shown in Fig. 2.4. All the peptide modified constructs had a significantly higher accumulation than the unmodified GNPs. The presence of the BLM and CIS did not significantly alter the accumulation of the peptide modified GNPs ($p > 0.05$).

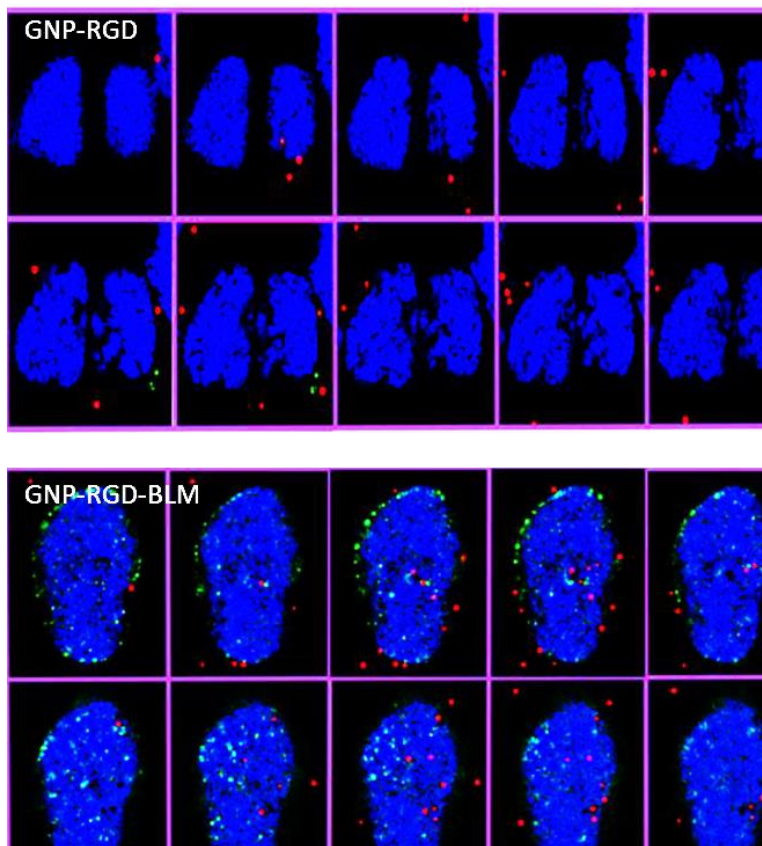
2.3.3 Toxicity of GNPs



<Fig. 2.5> Toxicity of 0.3 nM 10 nm sized GNPs in MDA-MB-231 cells. No toxic effects on MDA-MB-231 cells were observed after 16-hour incubation of 0.3 nM 10 nm sized peptide modified GNPs. No significant difference in survival fraction was observed from clonogenic assays. Data are means \pm S.E.M for n=6 (Unpaired t-test, $p > 0.05$).

Throughout the studies discussed in this dissertation, 0.3 nM of approximately 10 nm sized peptide modified GNPs were used. The cells that were incubated with 0.3 nM of 10 nm sized peptide modified GNPs did not demonstrate a decrease in survival fraction of MDA-MB-231 cells compared to the control group that were incubated with the same volume of phosphate buffered saline (PBS). Based on clonogenic assay results, the concentration of 0.3 nM of 10 nm sized peptide modified GNPs that were used in this study had no significant toxic effect on MDA-MB-231 cells when incubated up to 16 hours (Fig. 2.5).

2.3.4 Nuclear entry of bleomycin conjugated GNPs (GNP-RGD-BLM)

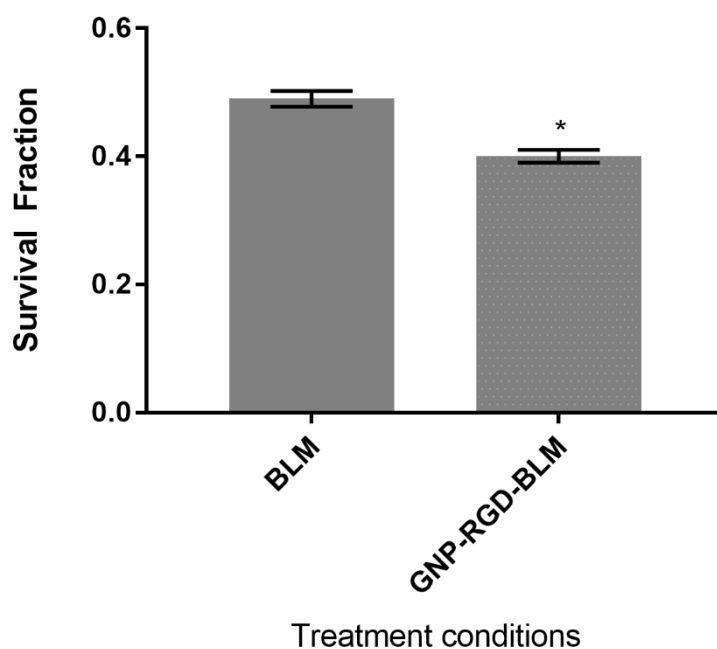


<Fig. 2.6> Hyperspectral mapping of GNP distribution and protein probe for DNA DSBs (53BP1) in cells incubated with GNP and GNP-RGD-BLM. Different planes across the nuclei of the cells showed that there is localization of GNPs within the nucleus when they were conjugated with BLM. The cells incubated with citrated-capped GNPs were not found in the nucleus. The nucleus is stained with DAPI (blue), the GNP clusters are shown in red, the markers for DNA DSBs (53BP1) are shown in green. Adapted from Yang, C., J. Uertz, and D.B. Chithrani, *Colloidal Gold-Mediated Delivery of Bleomycin for Improved Outcome in Chemotherapy*. *Nanomaterials*, 2016. **6**(3): p. 48 [232].

As shown in the top panel of Fig. 2.6, cells incubated with GNP-RGD (marked in red) were not found in the nucleus (stained with DAPI and marked in blue in Fig. 2.6). No overlap of GNP-RGD and the nucleus was observed, indicating that GNP-RGD constructs do not enter the nucleus. However, GNP-RGD-BLM constructs (marked in red in the bottom panel of Fig. 2.6) were observed to overlap with the nucleus (marked in blue) from hyperspectral imaging (HSI).

Fluorescently tagged 53BP1, that probes for the DNA double strand break (DSB), was assayed (marked in green). The cells incubated with GNP-RGD-BLM constructs had more DNA damage compared to the cells incubated with GNP-RGD, based on the 53BP1 probed. The efficacy of GNP-RGD-BLM compared to free bleomycin in cells will be shown from cell survival fractions in the next section, 2.3.4.

2.3.5 Survival of cells treated with GNP -RGD-BLM in comparison to free BLM

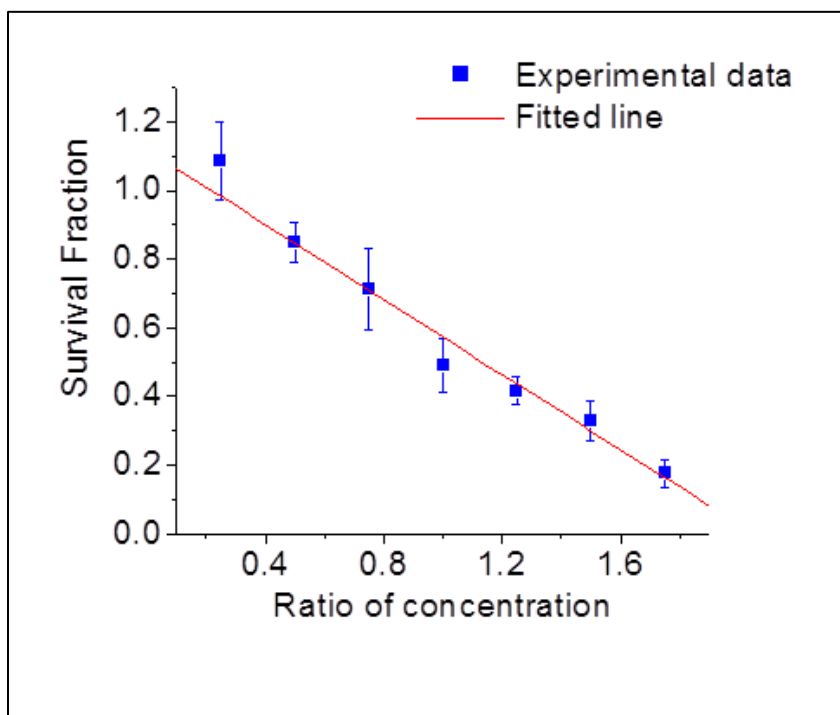


<Fig. 2.7> Comparison of cell survival for cells treated with GNP-RGD-BLM and equal concentrations of free BLM. MDA-MB-231 cells treated with GNP-RGD-BLM had an 18 ± 4 % decrease in survival compared to cells treated with same concentration of free BLM (633 nM). Data are means \pm S.E.M for $n = 3$. * indicates statistically significant difference (unpaired t-test, $p < 0.05$).

The MDA-MB-231 cells incubated with GNP-BLM had an 18 ± 4 % ($p < 0.05$) decrease in survival fraction compared to the group that were incubated with the same amount of drug without the GNP, with survival fraction of 0.40 ± 0.010 and 0.49 ± 0.012 , respectively as shown

in Fig. 2.7. The concentration of bleomycin used for this study was 633 nM. This concentration was the maximum amount that could be added to the peptide modified GNP solution without any significant aggregation observed through UV-VIS spectra. The effect of bleomycin was improved with the presence of GNP-RGD, indicated from reduced cell survival.

2.3.6 Chemotherapeutic dose enhancement due to GNP-RGD-BLM

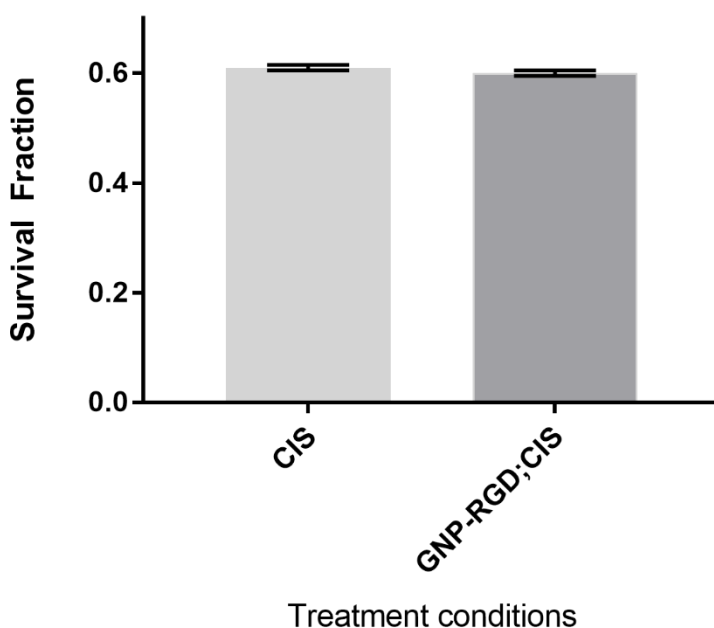


<Fig. 2.8> **Survival Fraction of MDA-MB-231 breast cancer cells treated with various concentrations of free bleomycin.** MDA-MB-231 cells treated with various concentrations of bleomycin (0.25-2 fold of the concentration used for this study, where ratio of 1 corresponds to 633 nM).

The concentration of bleomycin used in this dissertation was kept at 633 nM. This concentration was the maximum amount that could be added to the peptide modified GNPs without any significant aggregation. To establish a dose enhancement factor (DEF), the survival fraction of MDA MB 231 cells treated with various concentration of bleomycin (0.25-2 times of 633 nM

– the concentration used throughout the experiment) were plotted with a linear trend line of $y = -0.5806x + 1.1608$, $R^2 = 0.9729$ (Fig. 2.8). The survival fraction (SF) of cells incubated with GNP-RGD-BLM was 0.40. This SF was compared against this trend line and the DEF was calculated to be 1.31.

2.3.7 Survival of cells treated with GNP –RGD; CIS in comparison to free CIS



<Fig. 2.9> Comparison of cell survival for cells treated with GNP-RGD; CIS and equal concentrations of free CIS. MDA-MB-231 cells treated with GNP-RGD; CIS had no statistical significant change in survival fraction compared to cells treated with same concentration of free cisplatin (435 nM) Data are means \pm S.E.M for $n = 3$. (Unpaired t-test, $p > 0.05$).

The MDA-MB-231 cells incubated with GNP-RGD;CIS had no statistically significant difference in cell survival fraction compared to cells incubated with the same concentration of free cisplatin (CIS), with SF of 0.60 ± 0.005 and 0.61 ± 0.005 , respectively ($p > 0.05$) (Fig. 2.9). The concentration of cisplatin used for this study was 435 nM. This concentration was the maximum

amount that could be added to peptide modified GNPs without the solution showing signs of aggregation. This indicates that the presence of peptide modified GNPs do not significantly improve or interfere with the action of cisplatin when the drug is not attached onto the surface of GNP constructs. This suggests that GNPs can be still used in combined chemotherapy and radiation therapy as a radiosensitizer in the presence of cisplatin without interfering with the action of cisplatin. Cisplatin is also known to act as a radiosensitizer and the effect of two radiosensitizers (GNP and cisplatin) with radiation will be discussed in Chapter 4.

2.4 Discussion

2.4.1 Peptide modified GNP toxicity

New nano-scaled systems that are studied to be used with existing treatment modalities should be carefully probed for unwanted effects. A number of groups studying GNP cytotoxicity concluded that GNP biocompatibility depends on size, surface properties and concentration [74, 75]. Non-toxicity of GNPs has been reported by several groups. For example, Connor *et al.* found that GNPs of various sizes (4, 12, 18 nm) and capping agents (citrate, cysteine, glucose, biotin, and cetyltrimethyl ammonium bromide) were nontoxic to K562 (human leukemia cell line) cells up to micromolar concentrations based on MTT assays [75]. Sukla *et al.* observed lysine capped 35 nm GNPs did not show detectable cytotoxicity up to 100 μ M concentration in RAW265.7 macrophage cells based on MTT assays [74]. Despite the many reports on non-toxicity of GNPs, contradictory research results are also present [76]. It has been reported by Zhang *et al.* that PEGylated 12.1 nm sized GNPs incubated in HeLa cells had an IC_{50} of 0.477 mM [83]. The lack of general consensus on NP toxicity is due to different experimental methods employed, incubation

conditions (concentrations and exposure time), variability of sizes and functionalities of GNPs, variability of cell lines, and different measures and assays for toxicity [76, 77].

In this study, 0.3 nM concentrations of 10 nm GNPs had no signs of toxicity to MDA-MB-231 cells with clonogenic assay results. This concentration is relatively lower than what other groups have used for GNP studies, and since toxicity is highly dependent on the incubation concentration, the non-toxic result from clonogenic assays is reasonable.

2.4.2 GNP characterization

The approximate core diameter of GNPs used in this study determined by TEM was approximately 10 nm as shown in Fig. 2.3A. Reports have shown that NPs of diameter of 20 – 50 nm showed the highest cell uptake although the size of highest uptake is known to be cell line dependent [53, 102, 103]. Despite having 20 -50 nm optimal size for cellular accumulation, it has been suggested that smaller GNPs were better at penetration through the tissue matrix [101]. Although this study is has been performed *in vitro*, it has a future goal of implementing in multi-layer models, therefore, the smallest possible GNPs that could be synthesized with the Turkevich method of GNP synthesis [65, 70], 10 nm GNPs, were selected to be used in this study. Moreover, since the action of many chemotherapeutics is on the DNA and there is higher radiosensitization when GNPs are targeted to the nucleus [129], a small enough size of GNPs that has a potential to enter the nucleus of the cell was another factor that was considered when selecting the size of GNP platform.

In this study, bleomycin or cisplatin was added to the peptide modified GNPs prior to incubation to the MDA-MB-231 cells. Ultraviolet-Visible (UV-Vis) spectra were obtained to observe if aggregation occurs with the addition of the chemotherapeutic agents. UV-Vis

spectroscopy measures the local surface plasmon resonance (LSPR) and it results in a strong absorbance band in the visible region, 500 nm to 600 nm. The peak wavelength of GNPs increases with the diameter of the particles and is often referred to as the red-shift. The size range of colloidal GNPs can also be determined by the peak SPR wavelength [245, 246]. UV-Vis measurements can also be used to evaluate the functionalization or aggregation of GNPs. When GNPs are successfully functionalized with ligands, the local refractive index at the GNP surface will increase and result in a slight red-shift of the LSPR while maintaining the overall shape and intensity of the spectra. When GNPs are aggregated from irreversible inter-particle coupling, the LSPR will not only red-shift but the spectra will also broaden. Aggregated GNPs can also be detected visibly by the change in colour of the solution from red to blue. Addition of cisplatin or bleomycin to the peptide modified GNP solution resulted in no significant broadening the UV spectra up to 46 hrs post formulation (Fig. 2.3B). This signifies that the addition of cisplatin or bleomycin at that concentration does not de-stabilize the GNP complex.

2.4.3 GNP accumulation

The accumulation of unmodified GNPs, RGD peptide modified GNPs, RGD peptide modified GNPs with BLM, and RGD peptide modified GNPs with cisplatin in MDA-MB-231 cells was measured as part of this study. The surface modification of GNPs with RGD peptides increased the cell accumulation by 6-7 fold compared to the unmodified counterparts. The arginyl-glycyl-aspartic acid (RGD) tripeptide sequence is found in proteins such as fibronectin, citronectin, and type I collagen [136, 137]. The RGD peptide sequence is one of the principle adhesive ligand that is recognized by several integrin receptors, including $\alpha\beta3$, $\alpha\beta5$ and $\alpha\beta6$ [138-140]. Improved tumour targeting has been observed in studies using RGD-modified drug constructs

because the integrin receptors are overexpressed on tumour cells [143-146]. Shayakhmetov *et al.* reported that vectors with the RGD motif deleted required 10 times more doses than the RGD motif possessing vectors to achieve a comparable effect [147]. Therefore, the 6-7 times improvement in accumulation of RGD modified GNPs is reasonable. The addition of bleomycin or cisplatin to the GNP-RGD solution did not have any statistically significant effect in accumulation of GNPs within cells. This suggests presence of the bleomycin on the surface of GNPs does not affect accumulation of the GNP constructs and the cisplatin molecules that have no known interaction with the GNP constructs do not compete with the uptake of the GNP constructs.

The incubation time of the GNP constructs for all subsequent studies in this dissertation was 16 hrs (overnight incubation). Chithrani *et al.* reported that the accumulation of GNPs are dependent on the incubation time, which plateaued for all sizes studied (14, 50, 74 nm) between 4 - 7 hrs post incubation in HeLa cells [104]. It is suggested by this time point, the rate of endocytosis of GNPs is in equilibrium with the rate of exocytosis [104]. It has also been reported by Coulter *et al.* that GNP uptake occurred in a time dependent manner with a steady increase in number of NP per cell up to the 6 hr post introduction, reaching a plateau at 6 hrs measured up to 24 hr time point in MDA-MB-231 cells, DU145 cells, and L132 cells [247]. The 16-hr incubation time was selected for this and subsequent studies so that it is after the plateau point. The 16-hr incubation was kept consistent throughout the studies.

There is emerging evidence from experiments done in collaboration with an analytical chemistry laboratory that the recovery rate values from the ICP-AES experiments may not be accurately measuring the absolute concentration of GNPs [248]. However, even in the case that the results from the ICP-AES experiments do not represent the absolute amount of GNP

accumulation, the trend of surface-modification dependent accumulation remains the same and it does not change the conclusion that modifying the GNP surface with RGD improved accumulation to MDA-MB-231 cells. Further studies will address the accuracy of the ICP-AES experiments that were conducted using methods and protocols that are standard in the field.

2.4.4 Presence of GNPs with chemotherapeutics in MDA-MB-231 cells

The effect of GNPs with two different chemotherapeutic drugs incubated in MDA-MB-231 cells is observed through clonogenic assays. The key property of effective therapeutic results is the loss of reproductive integrity of cancer cells [249]. This is assayed most easily by assessing their ability to generate progeny in a colony-forming assay [249]. While the MDA-MB-231 cells incubated with GNP-BLM had a $18 \pm 4 \%$ ($p < 0.05$) decrease in survival fraction compared to the group that were incubated with the same amount of drug without the GNP, with survival fraction of 0.40 ± 0.010 and 0.49 ± 0.012 , respectively; the MDA-MB-231 cells incubated with GNP-RGD; CIS had no statistically significant change in SF compared to cells incubated with the same concentration of free cisplatin (CIS), with SF of 0.60 ± 0.005 and 0.61 ± 0.005 , respectively ($p > 0.05$) from clonogenic assays.

The clinical efficacy of bleomycin is suggested to stem from their ability to mediate single- and double-strand DNA breaks [250, 251]. The mechanism is reported to be deoxyribose oxidation, where bleomycin forms a complex with a ferrous ion, Bleomycin-Fe²⁺, which then undergoes oxidation to become Bleomycin-Fe³⁺ [26, 173]. The bleomycin/ferrous iron complex binds to the DNA and this binding leads to insertion of the drug between base pairs, which is called intercalation, and unwinding of the double helix [172]. Oxidation of the complex is accompanied by the generation of reactive oxygen radical species which attach with the phosphodiester bonds

of DNA [170, 172, 173]. In this study, bleomycin was conjugated onto the surface of GNPs prior to incubation with MDA-MB-231 cells. The localization of GNP-RGD-BLM within the nucleus was shown using the Hyper Spectral Imaging (HSI) technique, as shown in Fig. 2.6. This shows that peptide modified GNPs can carry BLM to its biological target, DNA, without the mediation of nuclear penetration molecules. These results were consistent with a previous study where core-shell magnetic NPs (CSMN) with no known nuclear targeting properties were found in the nucleus when conjugated with bleomycin [26]. The usage of BLM could be expanded if BLM dosages could be delivered closer to the biological target, such as the nucleus and could be contained. When the chemotherapeutic agent, bleomycin, was conjugated onto the surface of the peptide modified GNPs prior to exposure to MDA-MB-231 cells, the cell survival decreased by $18 \pm 4 \%$ ($p < 0.05$). This indicates that the peptide-modified GNPs can be an effective carrier of bleomycin. No significant difference is cell survival for cells treated with CIS and GNP-RGD;CIS were found as shown in Fig. 2.9. This suggests that having GNP constructs in the cell do not interfere with the action of cisplatin, when the chemotherapeutic agent is not conjugated onto the surface of GNP-RGD. This implies that GNPs can still be used in combined chemotherapy and radiation therapy as a radiosensitizer without interfering with the action of an unconjugated chemotherapeutic agent. The use of GNPs with the two chemotherapeutic agents in combination with radiation will be discussed in Chapter 4.

The drug concentrations used in the above studies have been calculated to be 1~10 % of the clinical recommended dosages listed by Cancer Care Ontario, an advising body of the Ontario government to cancer and to access to care for key health services. The calculations used is shown in the supplementary section. However, it is also recognized that the effect from clinical drug dosages cannot be directly paralleled to the effect of same dosages in *in vitro* studies. Moreover,

when chemotherapy is given to a patient, a drug dose is selected based on clinical trials that have determined average dose as per unit of body surface area that gives some toxicity [21]. At this dose, some patients may have no detectable effect on normal tissues, while others may have severe or even lethal toxicity on normal tissues [21]. Hence, in a clinical setting, the prescribed drug dosage is based on each individual patient.

2.5 Conclusions

This work demonstrates the accumulation GNP constructs in MDA-MB-231 cells in the presence of chemotherapeutic drugs, bleomycin or cisplatin. Bleomycin has a capability of conjugating onto the GNP surface through a thiol bond, while cisplatin has no known significant interaction with GNPs. Upon modification with peptides, the GNP accumulation in cells increased 6-7 folds, compared to the unmodified counterparts. The presence of chemotherapeutic agents did not significantly affect GNP accumulation in cells. The cells incubated with GNP-RGD-BLM had a lower survival than cells treated with free BLM, while cells incubated with GNP-RGD;CIS had no significant difference in survival compared to cells treated with free cisplatin. Peptide modified GNPs can act as a carrier to agents that conjugate on the surface. It can also be used with a chemotherapeutic agent that has no known interaction with the GNPs without interfering with the action of the agent. This could signify that GNPs can be used in combined chemotherapy and radiation therapy by possibly acting as a drug carrier and a radiosensitizer or just as a radiosensitizer.

Chapter 3

Gold nanoparticles as a radiosensitizer in radiation therapy

3.1 Introduction

Radiation therapy is one of the most common treatment modalities for cancer, along with surgery and chemotherapy [14]. The sources of radiation therapy include gamma or X-ray photons, ion-based electrons and protons [16, 17]. Although radiation therapy is considered effective and used in treatment of about 50 % of all cancer patients, a sufficient dose that can kill any tumour cell can also damage surrounding healthy tissue [18]. A photon beam will irradiate some surrounding normal tissue no matter how well shaped or conformed to the dimensions of the tumour [20]. This limits how much radiation a patient can receive and therefore a radiosensitizer targeted to the tumour area will be beneficial in improving therapeutic results [20]. A radiosensitizer may not have a direct anti-cancer effect or it may be one variety of anti-cancer drugs that exhibits anti-tumour effects alone in addition to radiosensitization [20]. Gold nanoparticles (GNPs) are radiosensitizers and the dose enhancement is attributed to the production of secondary electrons scattering from the surface of the high-Z material, compared with soft tissue [202, 203]. This has been confirmed by direct dose measurements [252, 253] and Monte Carlo modeling [218, 254]. The extent of sensitization with GNPs depends on several factors including the beam energy, in which greater radiation sensitization have been observed for cells irradiated with lower energy beams [55, 211]. The sensitization is known to come from the photoelectric effect, which is dominant at kV energies, in which photon absorption has a $\sim Z^4$ relationship with

the target material [8]. However, although some cancer patients are treated at kV energies, megavoltage (MV) X-rays are used for most radiotherapy regimes to provide adequate dose deposition to central tumours [8]. Monte Carlo modeling has predicted negligible physical dose enhancement with GNPs at MV energies in which Compton effects, that have no relationship with Z, are dominant [13, 218-222]. Contrary to theoretical predictions, a number of groups reported experimental results of GNP sensitization in the MV energy ranges [8, 55, 223]. The extent of sensitization with GNPs was reported to depend on several factors including the beam energy, size and surface modification of the NPs, type of cells, and the radiation dose. In this study, sensitization of peptide modified GNPs incubated in breast cancer cells, MDA-MB-231, at a relatively low incubation concentration (0.3 nM) to what have been used in the past will be observed at a clinically relevant 6 MV energy.

3.2 Methods

3.2.1 Synthesis of colloidal gold nanoparticles and peptide modification

GNPs of size 10 nm were synthesized using the citrate reduction method [65]. First, 300 μ l of 1 % chloroauric acid ($\text{HAuCl}_4 \cdot 3\text{H}_2\text{O}$) (Sigma-Aldrich) was added to 30 ml of double-distilled water and heated on a hot plate while stirring. Once it reached the boiling point, 1 ml of 1 % sodium citrate tribasic dehydrate ($\text{HOC}(\text{COONa})(\text{CH}_2\text{COONa})_2 \cdot 2\text{H}_2\text{O}$) (Sigma-Aldrich) was added to form NPs of diameter 10 nm. After the colour of the solution changed from dark blue to bright red, the solution was left to boil for another five minutes while being stirred. Finally, the GNP solution was brought to room temperature while being stirred. Peptide modified GNP constructs were assembled by first conjugating the GNPs with a pentapeptide, H-Cys-Ala-Leu-Asn-Asn-OH

(CALNN) (AnaSpec, San Jose, USA), with approximately 300 peptides/GNP ratio for stabilization purposes. The peptide with H-Cys-Lys-Lys-Lys-Lys-Lys-Lys-Gly-Gly-**Arg-Gly-Asp**-Met-Phe-Gly-OH (CKKKKKKGGRGDMFG) sequence (AnaSpec, San Jose, USA) was added with a 16 to 20 peptide/GNP ratio. This peptide modified GNP construct will be labelled and referred to as GNP-RGD in this dissertation.

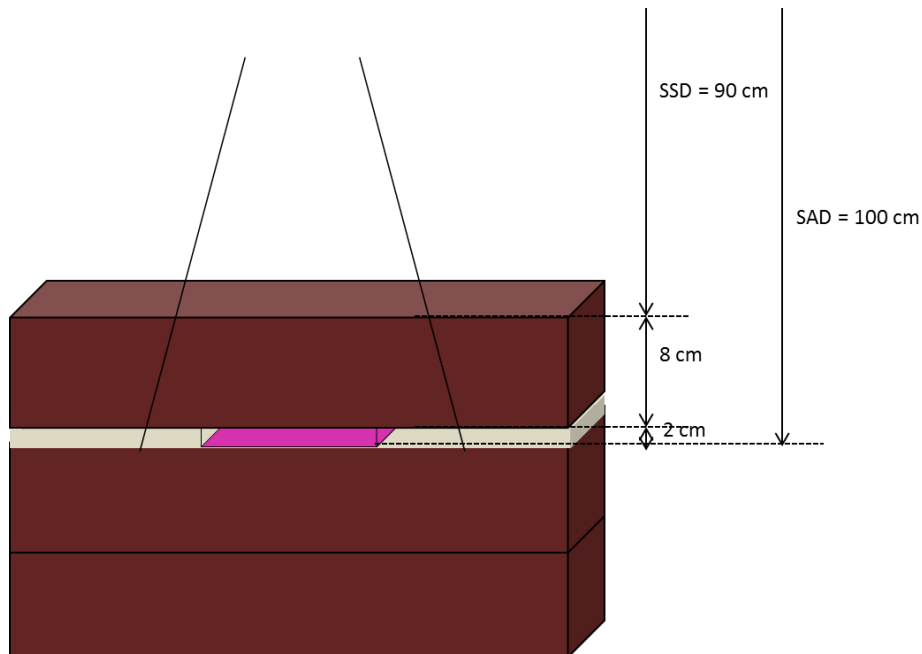
3.2.2 Hyperspectral imaging

The CytoViva (CytoViva Inc., Auburn, USA) technology in combination with dark field microscopy was used to image GNP distribution within cells. The microscope is a dark-field imaging system that uses oblique angle lighting. NPs appear bright due to high scattering cross-sections of GNPs. This hyperspectral imaging of GNPs in cells and tissues does not require optical labeling of the GNPs. It is also possible to extract spectral information from each pixel for verification purposes.

3.2.3 Cell culture and GNP delivery

MDA-MB-231 (breast cancer cell line) cells were obtained from ATCC and cultured in Dulbecco's Modified Eagle's Medium (DMEM) (Gibco), supplemented with 10 % Fetal Bovine Serum (FBS) (Gibco, USA origin) and 1 % penicillin-streptomycin (Gibco) at 37 °C humidified incubator with 5 % CO₂. The cells were exposed to either Phosphate-Buffered Saline (PBS) or 0.3 nM of GNP-RGD for sixteen hours prior to radiation and clonogenic assays.

3.2.4 Setup for radiation therapy experiments



<Fig. 3.1> Irradiation experiment setup with 6 MV X-rays.

The cells were grown in 6-well tissue culture dishes and incubated with GNP constructs 16 hours prior to radiation with a 2 Gy single fraction of 6 MV X-rays with Agility™ Linac (Elekta Oncology Systems, Stockholm, Sweden), at a dose rate of 600 MU/min, and field size of 20 x 20 cm². The machine was calibrated following the AAPM TG51 protocol [255] to deliver 1 cGy/MU at 1.5 cm depth for a 10 x 10 cm² field. PMMA bolus and superflab with equal thickness to the culture dish, was used to surround the culture dish with water equivalent material in lieu of air to ensure tissue equilibrium. Solid water was placed under and above the dish to account for the backscatter and to set the monolayer source-to-axis distance (SAD) to 100 cm at a depth of 10 cm. Since the culture dishes contain air gaps within the dishes, the setup was scanned in CT to verify the dose distribution in a treatment planning system (TPS). The number of monitor units calculated by Pinnacle required to deliver 200 cGy to the cell depth was 225 MU. A manual calculation was

performed to confirm the TPS calculation. The calculation is shown in the appendix as supplementary. The schematic of the radiation setup is shown in Fig. 3.1.

3.2.5 Immunofluorescence Assay for probing DNA damage

Cells were grown in coverslips (#1.5 18 mm) in 6 well dishes. After the overnight treatment under different experimental conditions, the cells were rinsed three times with PBS. The cells were then treated with 2 % paraformaldehyde/PBS/0.2 % and Triton X-100 for 20 min followed by treatment with 0.5 % NP40 for 20 min. Cover slips were left in 2 % BSA/1 % donkey serum in PBS for 1 hr. Cells were washed with PBS three times for 5 min between each treatment. Following this, the coverslips were fixed with a primary antibody (53BP1 Ser 1778. 1:200; Cell Signalling Technologies) overnight. The coverslips were then washed with 0.5 % BSA/0.175 % Tween 20/PBS (secondary wash) for 5 min three times before being treated with an optically labeled secondary antibody (anti-rabbit IgG Alexa 488. 1:500; Life Technologies) for 45 min. The coverslips were washed with the secondary wash before being treated with 0.1 µg/mL of DAPI for 10 min. The coverslips were then finally washed with PBS for 5 min three times and mounted onto glass slides after adding a drop of antifade solution. The edges were sealed and stored at 4 °C in the dark. The slides were then imaged with a LSM 700 confocal microscope (Carl Zeiss Microscopy, Jena, Germany) and analyzed with the Imaris software (Bitplane, Zurich, Switzerland).

3.2.6 Clonogenic Assay

After the treatments, the cells were trypsinized and diluted to form single-cell suspensions. The required volumes of cell suspension solution were calculated for the control and treatment samples. The required volumes were placed on 60 mm tissue culture dishes and the dishes were rocked for even distribution of the cells. The cells were left in the 37 °C humidified incubator with 5 % CO₂ for 10-14 days for colonies to grow. Once colonies are formed, the dishes were stained and fixed with 0.1 % of methylene blue (BioShop) in 70 % ethyl alcohol (Fisherbrand) for 1 hr. The stained dishes were rinsed in lukewarm water and left to air-dry overnight. The air-dried control dishes were then counted. Colonies were defined as structures containing >50 cells. Survival fractions were then calculated relative to non-irradiated control cells. Survival fraction (SF) was obtained with the following equation:

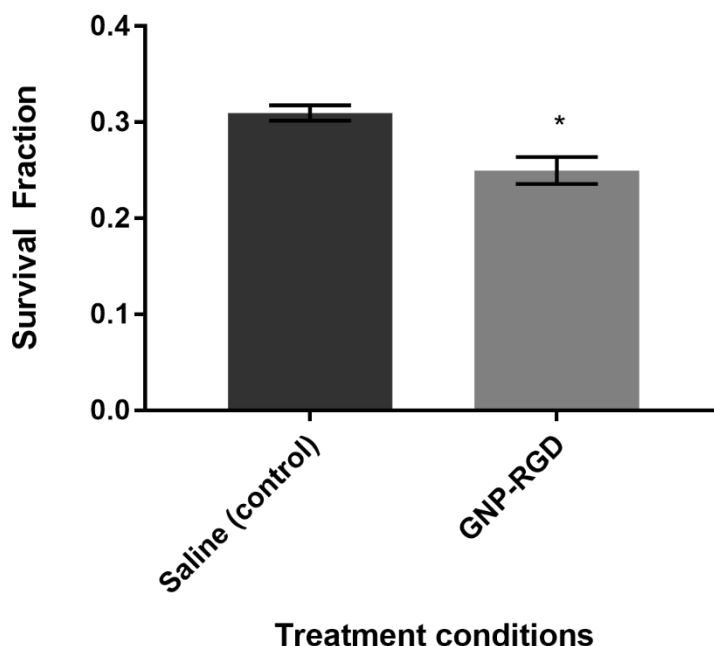
$$SF = \frac{\text{Number of colonies counted}}{\text{Number of cells plated} \times PE}$$

3.2.7 Statistical Analysis

Statistical analyses were performed using the IBM SPSS Statistics (IBM Corporation, New York, USA). A two-sample t-test was used to measure statistical significance between pairs of results. A p-value of less than 0.05 was considered to be significant.

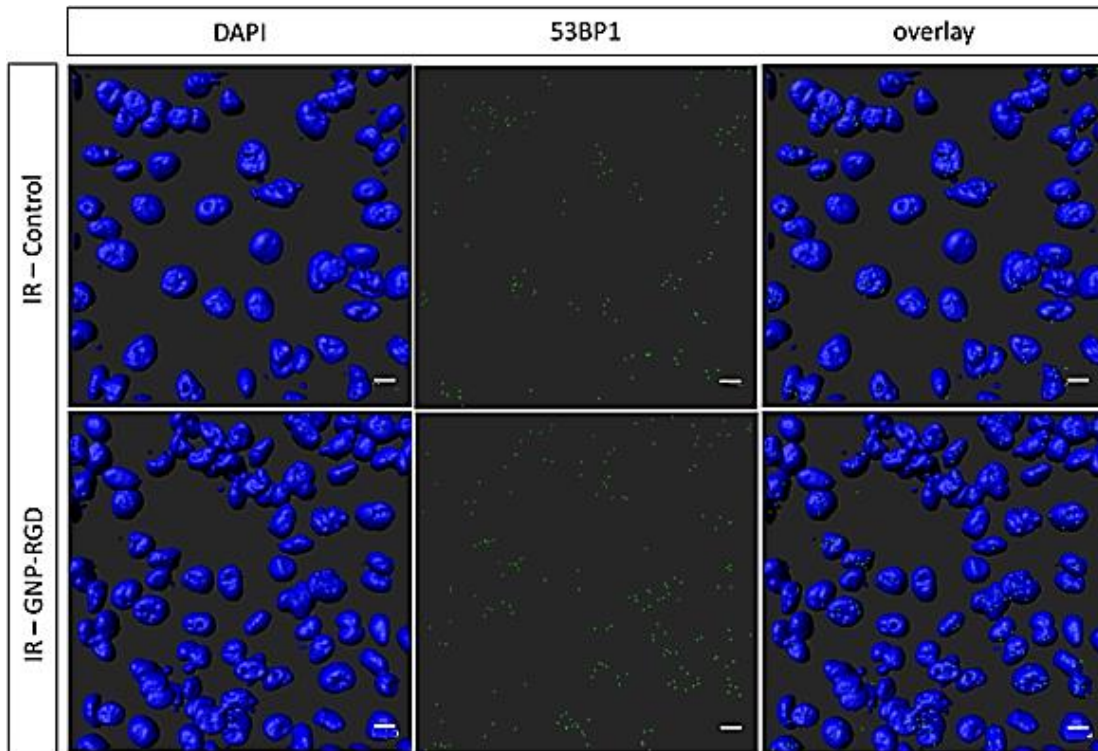
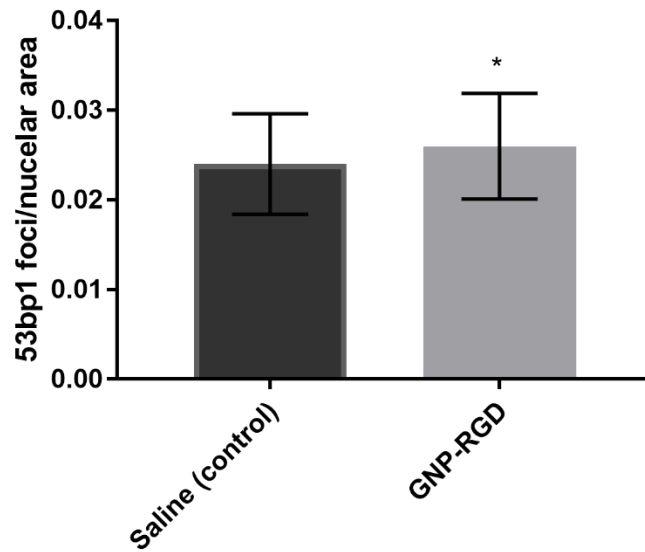
3.3 Results

3.3.1 Gold nanoparticles as a radiosensitizer



<Fig. 3.2> Comparison of cell survival for cells treated with saline and GNP-RGD with 2 Gy, 6 MV X-ray radiation. MDA-MB-231 cells treated with peptide modified GNPs had a 19 ± 6 % decrease in survival compared to control (treated with same volume of saline). Data are means \pm S.E.M. for $n = 3$. * indicates statistically significant difference (unpaired t-test, $p < 0.05$).

The survival fractions of cells after 16-hour incubation with GNP complexes and single fraction of 2 Gy, 6 MV radiations with a linear accelerator (LINAC) were calculated from clonogenic assays. The cells that were irradiated with peptide modified GNPs (GNP-RGD) had a 19 ± 6 % ($p < 0.05$) decrease in survival compared to the irradiated control group with the survival fraction of 0.31 ± 0.008 and 0.25 ± 0.014 , respectively (Fig. 3.2).



<Fig. 3.3> DNA DSB probe protein (53BP1) for cells treated with GNP-RGD compared control with 2 Gy, 6 MV X-ray radiations. MDA-MB-231 cells incubated with peptide modified GNPs had a significant increase in 53BP1 count/2D projected area of nucleus to control (treated with same volume of saline). The nucleus is stained with DAPI shown in blue and the markers for DNA DSBs (53BP1) are shown in green. SD values display ranges of values in different nuclei. Scale bar = 10 μ m.

The immunofluorescence assay slides were imaged and analyzed. The nuclei were stained with DAPI (4',6-Diamidino-2-Phenylindole, Dihydrochloride), and 53BP1 proteins were tagged with Alexa 488 which is shown in green in Fig.3.3. The slides were imaged along the z-stack to cover the depth of the nuclei. The volume images were produced by 3-Dimensional (3D) reconstruction. The quantitative data was produced by counting the 53BP1 and divided by the 2D projected area of all the nuclei imaged (n=274 for control, n=310 for GNP-RGD). The 53BP1 foci/nuclear area was 0.024 ± 0.0056 and 0.026 ± 0.0059 for the IR control and IR GNP-RGD cells respectively and the difference was small but statistically significant ($p < 0.05$). The cells treated with GNP-RGD prior to the 2 Gy, 6 MV radiation had an increase in the 53BP1 count per nuclei area compared to the cells that were treated with saline (irradiated control) prior to radiation as shown in Fig. 3.3.

3.4 Discussion

In radiation therapy, ionizing radiation is delivered to the tumour through an external beam source and causes damage to various cellular components, including the DNA, which is the target that leads to radiobiological effects. Ionizing radiation interacts with biomolecules and generates free radicals from ionization or excitation. The ejected electrons further travel and collide with atoms to create cascade of free radicals. The local dose or radiation can be improved with high atomic number (Z) particles, such as GNPs, due to dose enhancements from elevated photoelectric absorption. The photoelectric effect predominantly occurs in the kV energy range. However, kV energy radiation lacks in the ability of deep penetration and therefore it is only used to treat superficial tumours. Therefore, MV energy radiation was used in this study for wider clinical

relevance. It is predicted from Monte Carlo studies that the dose enhancement due to GNPs at MV ranges would be insignificant [218]. However, other experimental results were reported to have a higher than predicted dose enhancement in the MV ranges [8, 11, 55, 226, 227, 256]. For example, Liu *et al.* incubated murine cancer cells CT26 with 500 μM of 6.1 nm PEGylated GNPs and observed a dose enhancement of 1.32 with 6 MV X-ray radiation [256]. Jain *et al.* reported a dose enhancement of 1.29 in MDA-MB-231 cells exposed to 12 μM of 1.9 nm GNPs (AurovistTM) [8]. Chithrani *et al.* observed a dose enhancement of 1.17 in HeLa cells exposed to 1 nM of 50 nm citrate-coated (unmodified) GNPs [55]. The decrease in survival fraction by $19 \pm 6\%$ for MDA-MB-231 cells exposed to 0.3 nM of 10 nm peptide modified GNPs indicates that sensitization can be observed even with a relatively low concentration of GNPs incubated. The discrepancy between Monte Carlo predictions and experimental results indicate the presence of mechanisms of GNP radiation other than the physical mode of sensitization, such as chemical and biological enhancements [228]. One of the key biological ways of radiosensitization that have been identified is through DNA repair inhibition [228].

Several types of DNA lesions are produced upon exposure to radiation [228]. Of the many types of DNA lesions, DNA double-strand breaks (DSBs) are considered the most harmful, because unrepaired DSBs are sufficient to trigger permanent growth arrest and cell death [158-160]. Cells respond to DSBs by mounting a complex signaling network that coordinates DNA repair reactions with DNA damage checkpoint activation and chromatin reorganization. This signaling network is called the DSB response and includes both diffusible and chromatin-based signaling events [161]. Experimental analysis of DNA DSBs, such as immunofluorescence assays have identified DNA repair inhibition as biological mechanisms of radiosensitization by GNPs [228]. In this study, p53-Binding Protein 1 (53BP1) was used as a readout indicator of DNA DSBs

from immunofluorescence assays. An important regulator of DSB signaling is 53BP1. 53BP1 was initially identified as a protein that binds to the central DNA binding domain of p53 and enhances p53-mediated transcriptional activation [163]. As an early event in the recognition of the breaks, 53BP1 becomes hyper-phosphorylated after radiation and rapidly redistributes into distinct nuclear foci. The average number of 53BP1 foci peaks 30 min post cell exposure to DNA DSB inducing agents and decreases over time with kinetics that parallel the rate of DNA repair over time returning to baseline 16 hours post exposure [159, 164]. Since the treated cells were fixed 24 hours post treatment, the 53BP1 foci detected are an indicator of the DNA DSBs that have a lower probability of being repaired. A single persistent DNA DSB may be sufficient to induce cell death [165, 166].

In this study, the 53BP1 foci/nuclear area was 0.024 ± 0.0056 and 0.026 ± 0.0059 for the IR control and IR GNP-RGD cells respectively which was found to be statistically different ($p < 0.05$). Other studies have also demonstrated an inhibition of radiation-induced DNA damage repair with the presence of 10 nm peptide modified GNPs at a 0.3 nM concentration. Chithrani *et al.* reported that the incubation of HeLa cells with 50 nm citrate GNPs increased the number of γ H2AX and 53BP1 foci at 4 and 24 hrs post-IR at both 220 kV and 6 MV energies and suggested delayed DNA repair to be a key mode of radiosensitization [55]. Cui *et al.* also presented significant residual DNA damage from a γ -H2AX immunofluorescence assay 24 hrs post IR on MDA-MB-231 cells radiated with 2 Gy and 4 Gy of 250 kV X-rays in the presence of 1.61 μ M or 3.21 μ M of 2.7 nm tiopronin GNPs in MDA-MB-231 cells [9]. Considering the association of DNA repair and radiation, inhibition of DNA damage response pathways is a plausible mechanism of dose enhancement with GNPs [228]. However, there are also reports on a lack of influence of GNPs on DNA repair kinetics. For example, Jain *et al.* observed no significant different in the

number of 53BP1 foci, 1 hr or 24 hrs after with 1 Gy of 160 kV X-rays in cells MDA-MB-231 cells exposed to 12 μ M of 1.9 nm GNPs compared to the control group [8]. Contradictory outcomes for the effect of GNPs on DNA damage upon irradiation reported by the various groups indicate that the role and mechanism of DNA repair inhibition in the presence of GNPs remain inconclusive in the field and further studies are required, taking the difference in parameters such as, physico-chemical properties of GNPs, cell line involved, incubation conditions, and radiation energy and dose, into account.

3.5 Conclusions

Radiosensitization with GNPs at higher energies in the MV range have been theorized to be negligible through previous Monte Carlo studies. However, radiation sensitization was observed for MDA-MB-231 cells with incubation of 0.3 nM concentrations of 10 nm peptide modified colloidal GNPs upon 2 Gy, 6 MV X-rays radiation. Based on clonogenic assays, there was a 19 ± 6 % decrease in cell survival for cells treated with GNP-RGD compared to the cells treated with PBS prior to irradiation. There was also a statistical significant increase in 53BP1 proteins probed for cells treated with GNP-RGD compared to the cells treated with PBS prior to radiation. This indicates increased DNA DSBs for cells treated with GNP-RGD. The radiosensitization with the presence of peptide modified GNPs were observed even with a relatively low incubation concentration (0.3 nM) at 6 MV radiation.

Chapter 4

Gold nanoparticles with combined chemotherapy and radiation therapy

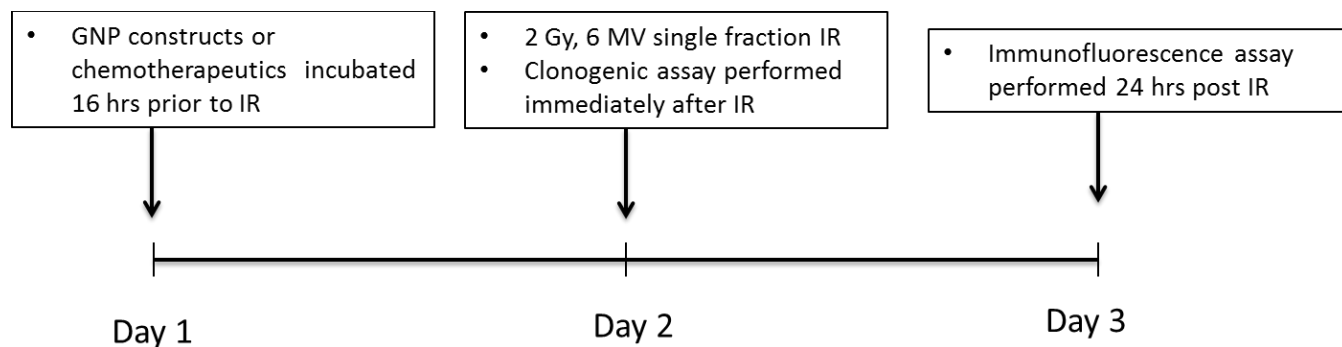
4.1 Introduction

The integration of chemotherapy with local modalities of radiation therapy is a logical and reasonable approach that has greatly improved the cure rates of solid tumours [20, 30]. Clinically, combined chemotherapy and radiation therapy is used for local control of the primary tumour mass through radiation and control of the metastatic disease through systemic chemotherapy [20]. Three basic combinations of chemotherapy and radiotherapy are categorized based on sequencing: chemotherapy before, during, and after radiation therapy [30]. Considering the variety of drugs available for cancer treatment, the possible choice of sequencing of combined chemotherapy and radiation therapy is countless, and the treatment plan differs for each individual patient. The standard treatment sequence refers to chemotherapy regimen before a traditional external beam radiation therapy treatment [30]. Chemotherapy used prior to irradiation is expected to cause maximal tumour regression for locally advanced tumours [30]. Bleomycin is commonly used before or during radiation but it is also used after radiation as a cocktail of other chemotherapeutic drugs [30]. Cisplatin is used to treat variety of solid human tumours and exhibit anti-tumour effects alone, but it is also known for its radiosensitizing effects [186, 257]. The major limitation of combining chemotherapy and radiation therapy is the normal-tissue toxicity, since either modality can cause major normal tissue toxicity [20]. Due to the limitations of the current cancer treatment modalities, methods for improving the therapeutic results are continuously being researched. Gold

nanoparticles (GNPs) are one of the materials that are used extensively in the field of nanomedicine and cancer research [33]. The high surface area-to-volume ratio along with the large surface bio conjugation possibilities has made GNPs as an ideal platform for delivering pharmaceuticals for chemotherapy [58-60] and GNPs have also been used as a radiosensitizer in radiation therapy [33, 55, 61-63]. This allows the possibility of GNP mediated combined cancer therapy. A few studies have used GNPs to observe the effect of combined chemotherapy and radiation therapy. For example, Zhang *et al.* demonstrated that the combination of GNP, cisplatin, and radiation had a 2.95- and 3.22-fold increase in DNA DSBs in a DNA plasmid model [258]. Cui *et al.* evaluated the enhancement effects of 0.5 mg/mL GNPs and 12 μ M of cisplatin with 225 kV radiation in MDA-MB-231 cells and observed a dose enhancement of 1.39. In this chapter, peptide modified GNPs will be used in combination with bleomycin, a chemotherapeutic agent that conjugates onto the surface of GNPs, or cisplatin, a chemotherapeutic agent that also acts as a radiosensitizer, with 2 Gy, 6 MV radiation to demonstrate the presence of relatively low concentrations of peptide modified GNPs improves the therapeutic outcome of the same dosages of chemotherapeutic agents and radiation in MDA-MB-231 cells. This is the first study where enhancement effects of GNPs and chemotherapeutics in combination with MV energy radiation are examined *in vitro*.

4.2 Methods

4.2.1 Sequence of combined treatment



<Fig. 4.1> **Sequence of combined treatment flow chart.** A flow chart schematic of the combined treatment sequence.

The sequences of the triple combined treatments are shown in Fig. 4.1. MDA-MB-231 cells were grown in 6 well tissue culture dishes and were incubated with free BLM, GNP-RGD-BLM, free CIS, or GNP-RGD;CIS for 16 hours before treating with 2 Gy, 6 MV radiation. Clonogenic assays were performed immediately after the radiation and immunofluorescence assays were performed 24 hours post radiation.

4.2.2 Synthesis of colloidal gold nanoparticles

GNPs of size 10 nm were synthesized using the citrate reduction method [65]. First, 300 μ l of 1 % chloroauric acid ($\text{HAuCl}_4 \cdot 3\text{H}_2\text{O}$) (Sigma-Aldrich) was added to 30 ml of double-distilled water and heated on a hot plate while stirring. Once it reached the boiling point, 1 ml of 1 % sodium citrate tribasic dehydrate ($\text{HOC}(\text{COONa})(\text{CH}_2\text{COONa})_2 \cdot 2\text{H}_2\text{O}$) (Sigma-Aldrich) was added to form GNPs of diameter 10 nm. After the colour of the solution changed from dark blue to bright red, the solution was left to boil for another five minutes while being stirred. Finally, the GNP solution was brought to room temperature while being stirred.

4.2.3 Preparation of peptide modified GNP constructs

Peptide modified GNP constructs were assembled by first conjugating the GNPs with a pentapeptide, H-Cys-Ala-Leu-Asn-Asn-OH (CALNN) (AnaSpec, San Jose, USA), with approximately 300 peptides/GNP ratio for stabilization purposes. The peptide with H-Cys-Lys-Lys-Lys-Lys-Lys-Gly-Gly-Arg-Gly-Asp-Met-Phe-Gly-OH (CKKKKKKGGRGDMFG) sequence (AnaSpec, San Jose, USA) was added with a 16 to 20 peptide/GNP ratio. This peptide modified GNP construct will be labelled and referred to as GNP-RGD in this dissertation.

Bleomycin (BioShop) was added to the GNP-RGD at approximately 780 bleomycin molecules/GNP ratio. Conjugation of bleomycin molecules onto the GNP surface occurs through a gold-thiol bond. This construct will be labelled and referred to as GNP-RGD-BLM (BLM refers to bleomycin) in this dissertation.

Cisplatin (Tocris Bioscience) was added to GNP-RGD construct at approximately 620 molecule/GNP ratio. It was expected that cisplatin molecules do not have an interaction with the GNPs and remains in the mixture. This construct will be labelled and referred to as GNP-RGD;CIS (CIS refers to cisplatin). It is expected that the cisplatin does not attach onto the surface of the GNP-RGD, hence using a semicolon instead of a hyphen to indicate addition of cisplatin to the GNP-RGD solution.

4.2.4 Hyperspectral imaging

The CytoViva (CytoViva Inc., Auburn, USA) technology in combination with dark field microscopy was used to image GNP distribution within cells. The microscope is a dark-field imaging system that uses oblique angle lighting. GNPs appear bright due to their high scattering

cross-section. This hyperspectral imaging of GNPs does not require optical labeling of the GNPs. It is also possible to extract spectral information from each pixel for verification purposes.

4.2.5 Cell culture and GNP delivery

MDA-MB-231 (breast cancer cell line) cells were obtained from ATCC and cultured in Dulbecco's Modified Eagle's Medium (DMEM) (Gibco), supplemented with 10 % Fetal Bovine Serum (FBS) (Gibco, USA origin) and 1 % penicillin-streptomycin (Gibco) at 37 °C humidified incubator with 5 % CO₂. The cells were exposed to either (1) 435 nM of CIS, (2) 0.3 nM of GNP-RGD and 435 nM of CIS, (3) 633 nM BLM, or (4) 0.3 nM of GNP-RGD and 633 nM of BLM for sixteen hours prior to radiation and clonogenic assays.

4.2.6 Clonogenic Assay

After the treatments, the cells were trypsinized and diluted to form single-cell suspensions. The required volumes of cell suspension solution were calculated for the control and treatment samples. The required volumes were placed on 60 mm tissue culture dishes and the dishes were rocked for even distribution of the cells. The cells were left in the 37 °C humidified incubator with 5 % CO₂ for 10-14 days for colonies to grow. Once colonies are formed, the dishes were stained and fixed with 0.1 % of methylene blue (BioShop) in 70 % ethyl alcohol (Fisherbrand) for 1 hr. The stained dishes were rinsed in lukewarm water and left to air-dry overnight. The air-dried control dishes were then counted. Colonies were defined as structures containing >50 cells. Survival fractions were then calculated relative to non-irradiated control cells. Survival fraction (SF) was obtained with the following equation:

$$SF = \frac{\text{Number of colonies counted}}{\text{Number of cells plated} \times PE}$$

4.2.7 Immunofluorescence Assay for probing DNA damage

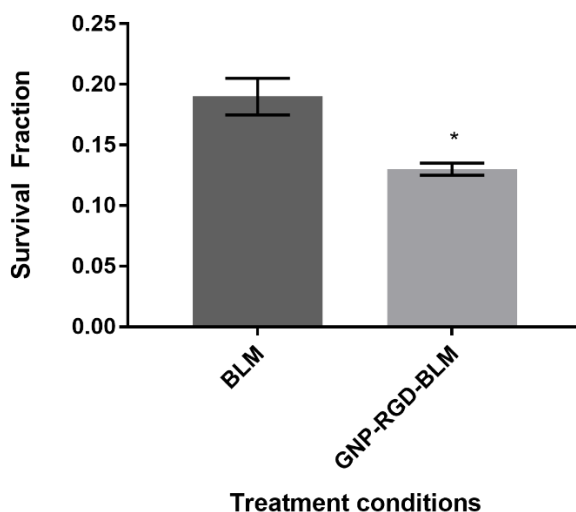
Cells were grown in coverslips (#1.5 18 mm) in 6 well dishes. After the overnight treatment under different experimental conditions, the cells were rinsed three times with PBS. The cells were then treated with 2 % paraformaldehyde/PBS/0.2 % and Triton X-100 for 20 min followed by treatment with 0.5 % NP40 for 20 min. Cover slips were left in 2 % BSA/1 % donkey serum in PBS for 1 h. Cells were washed with PBS three times for 5 min between each treatment. Following this, the coverslips were fixed with primary antibody (53BP1 Ser 1778. 1:200; Cell Signaling Technologies) overnight. The coverslips were then washed with 0.5 % BSA/0.175 % Tween 20/PBS (secondary wash) for 5 min three times before being treated with optically labeled secondary antibody (anti-rabbit IgG Alexa 488. 1:500; Life Technologies) for 45 min. The coverslips were washed with the secondary wash before being treated with 0.1 µg/mL of DAPI for 10 min. The coverslips were then finally washed with PBS for 5 min three times and mounted onto glass slides after adding a drop of antifade solution. The edges were sealed and stored at 4 °C in the dark. The slides were then imaged with a LSM 700 confocal microscope (Carl Zeiss Microscopy, Jena, Germany) and analyzed with the Imaris software (Bitplane, Zurich, Switzerland).

4.2.8 Statistical Analysis

Statistical analyses were performed using the IBM SPSS Statistics (IBM Corporation, New York, USA). A two-sample t-test was used to measure statistical significance between pairs of results. A p-value of less than 0.05 was considered to be significant. The Bliss Independence Criteria was used to analyze synergism between GNP with drug, and radiation.

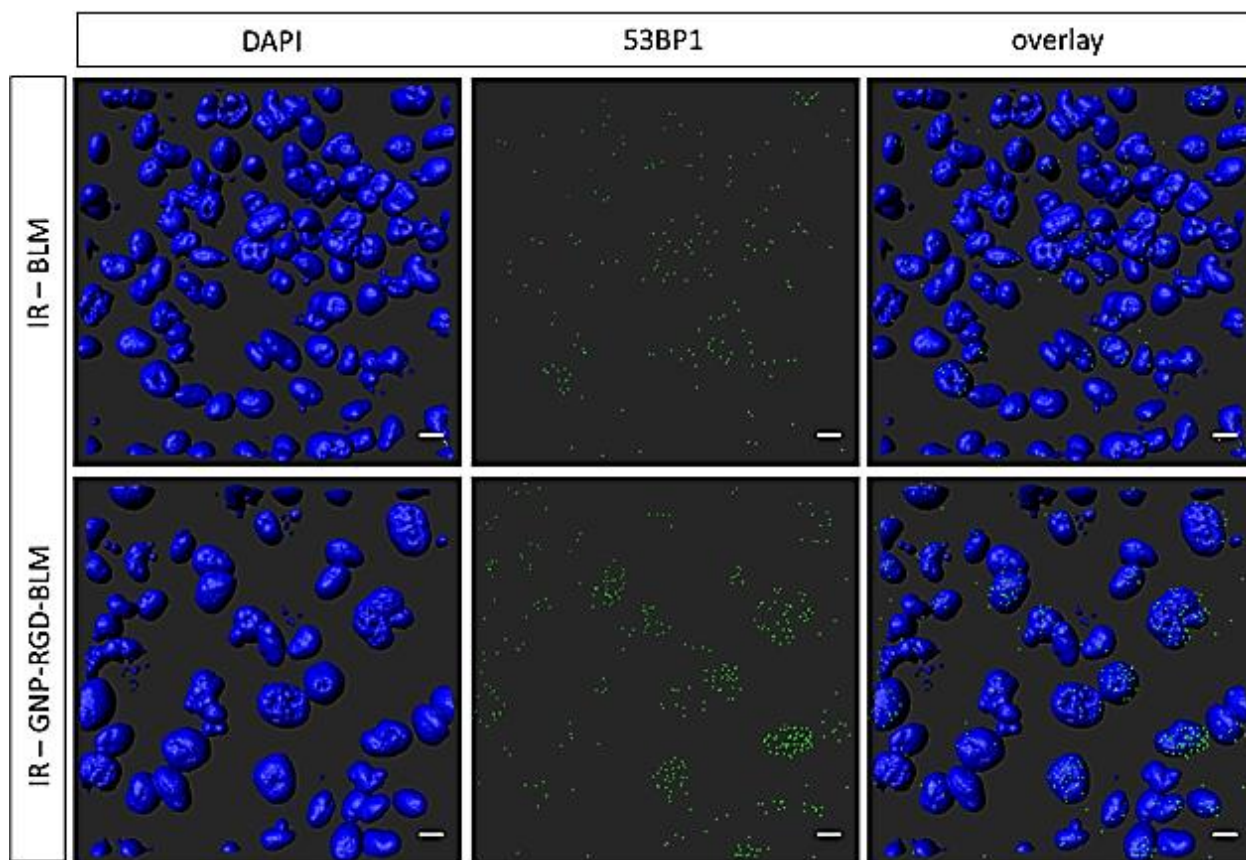
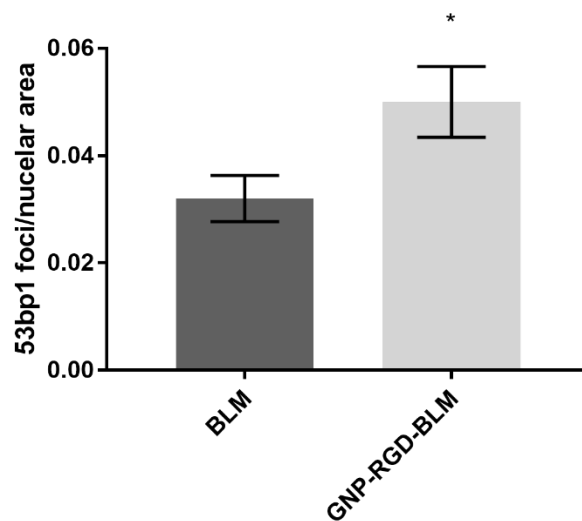
4.3 Results

4.3.1 Combined effect of gold nanoparticles, bleomycin and radiation



<Fig. 4.2> Comparison of cell survival fraction for cells treated IR GNP-RGD-BLM compared to IR BLM. MDA-MB-231 cells treated with peptide modified GNPs conjugated with 633 nM bleomycin (BLM) and treated with 2 Gy, 6 MV (IR-GNP-RGD-BLM) had a 32 ± 9 % decrease in survival compared to cells treated with same dosages of BLM and IR (treated with same volume of saline). Data are means \pm S.E.M. for $n = 4$. * indicates statistically significant difference (unpaired t-test, $p < 0.05$).

To study the effect of GNP mediated combined chemotherapy and radiation therapy, cells were first incubated with GNP-RGD-BLM or free BLM prior to radiation. The cells treated with GNP-RGD-BLM and radiation (referred to as IR GNP-RGD-BLM) had a 32 ± 9 % ($p < 0.05$) decrease in cell survival compared to the cells treated with free bleomycin and radiation (referred to as IR BLM), with the survival fraction of 0.13 ± 0.005 and 0.19 ± 0.015 , respectively as shown in Fig. 4.2. The combination of GNP-RGD-BLM with radiation had a statistically significant increase in cell death compared to the combination of bleomycin and radiation. Immunofluorescence assays were performed in addition to clonogenic assays to probe the DNA damage from the combined treatments as illustrated in Fig. 4.3.

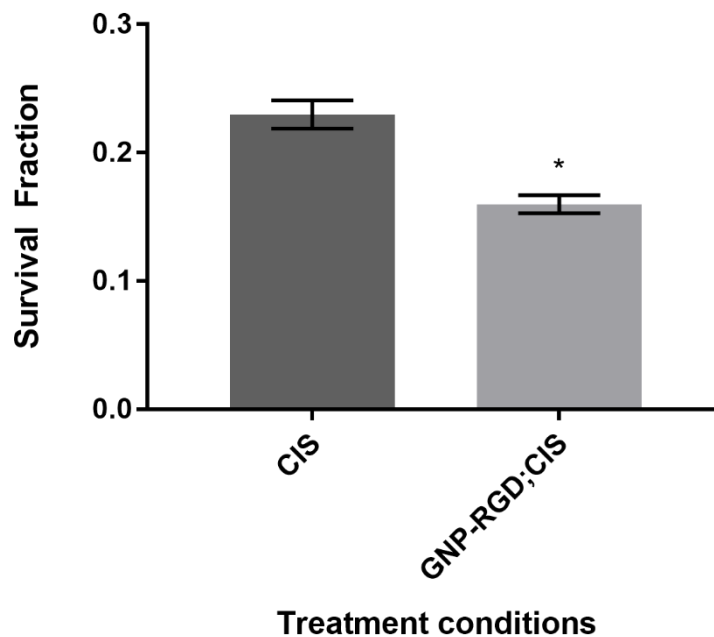


<Fig. 4.3> Comparison of 53BP1 ratio for IR-BLM and IR-GNP-RGD-BLM. MDA-MB-231 cells treated with peptide modified GNPs conjugated with 633 nM BLM and treated with 2 Gy, 6 MV X-ray radiations. The nucleus is stained with DAPI shown in blue and the markers for DNA DSBs (53BP1) are shown in green. SD values display ranges of values in different nuclei. Scale bar = 10 μ m.

The cells treated with GNP-RGD-BLM and cells treated with BLM followed by radiation were both fluorescently tagged with DAPI and 53BP1 antibodies with Alexa 488 probing DNA DSBs 24 hours post-treatment. The fixed cells were then imaged with a confocal microscope and shown in Fig. 4.3. The slides were imaged along the z-stack to cover the depth of the nuclei. The qualitative images were produced by 3-Dimensional (3D) reconstruction of the DAPI stained nucleus (shown in blue in Fig. 4.3) and overlaying with the 53BP1 (shown as green pixels in Fig. 4.3). The quantitative data was produced by counting the 53BP1 and divided by the 2D projected area of all the nuclei imaged (n=389 for BLM, n=307 for GNP-RGD-BLM). The number of 53BP1 foci per 2D projected z-stacked nuclear area for cells treated with BLM and GNP-RGD-BLM prior to radiation were 0.032 ± 0.0043 and 0.050 ± 0.0066 respectively and the difference was statistically significant (t-test, $p < 0.05$). These results indicate that there was an increase in DNA DSBs cells treated with IR GNP-RGD-BLM compared to cells treated with IR BLM.

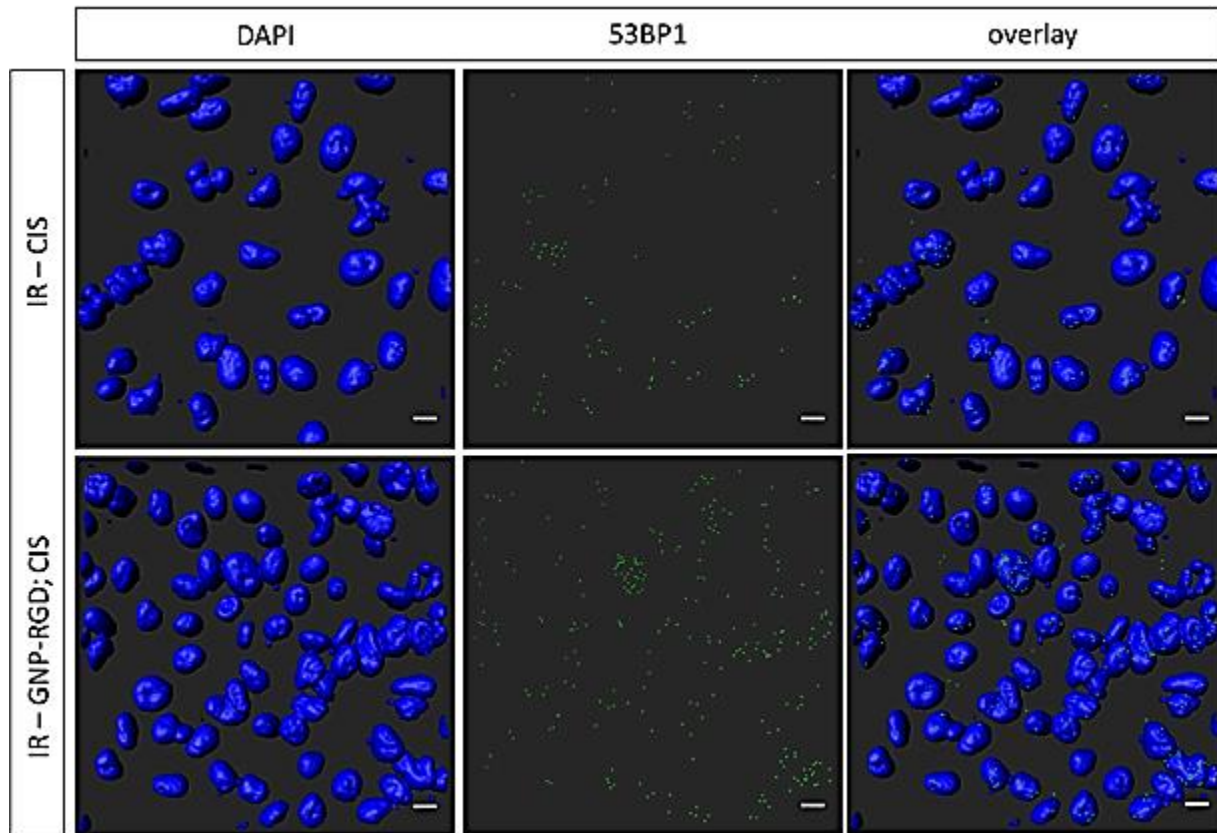
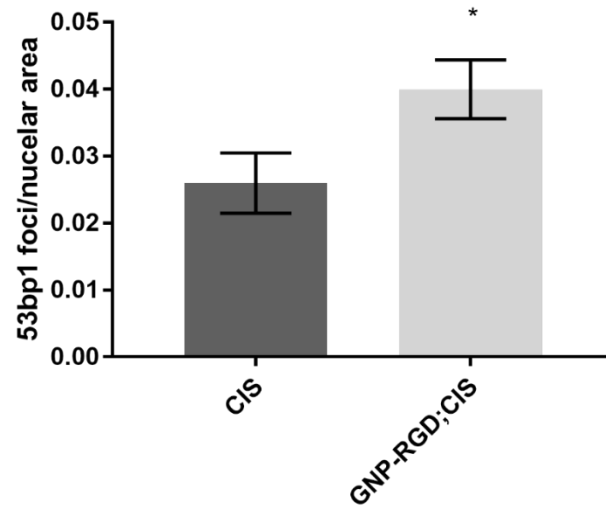
Further therapeutic gains were observed by using GNP-RGD-BLM conjugates in combination with radiation. Combination of chemotherapy and radiation therapy is clinically used to for cancer treatment and utilizing GNPs as a drug carrier and a radiation sensitizer improves therapeutic outcome of the combinational therapy.

4.3.2 Combined effect of gold nanoparticles, cisplatin and radiation



<Fig. 4.4> Comparison of cell survival for cells treated with IR GNP-RGD; CIS compared to IR CIS. MDA-MB-231 cells treated with peptide modified GNPs and 435 nM cisplatin and treated with 2 Gy, 6 MV (IR-GNP-RGD; CIS) had a $30 \pm 6\%$ decrease in survival compared to cells treated with same dosages of cisplatin and radiation (IR CIS) (treated with same volume of saline). Data are means \pm S.E.M for $n = 3$. * indicates statistically significant difference (unpaired t-test, $p < 0.05$).

As illustrated in Fig. 4.4, the cells treated with GNP-RGD; CIS and radiation (referred to as IR GNP-RGD; CIS) had a $30 \pm 6\%$ ($p < 0.05$) decrease in cell survival compared to the cells treated with cisplatin and radiation (referred to as IR CIS), with the survival fraction of 0.16 ± 0.007 and 0.23 ± 0.011 , respectively.



<Fig. 4.5> Comparison of 53BP1 ratio for IR-CIS and IR-GNP-RGD; CIS. MDA-MB-231 treated with peptide modified GNPs conjugated with 435 nM CIS and treated with 2 Gy, 6 MV X-ray radiations. The nucleus is stained with DAPI shown in blue and the markers for DNA DSBs (53BP1) are shown in green. SD values display ranges of values in different nuclei. Scale bar = 10 μ m.

The cells treated with GNP-RGD; CIS and cells treated with CIS followed by radiation were both fluorescently tagged 53BP1 antibodies probing DNA DSBs 24 hours post-treatment. The fixed cells were then imaged with a confocal microscope and shown in Fig. 4.5. The slides were imaged along the z-stack to cover the depth of the nuclei. The qualitative images were produced by 3D reconstruction of the DAPI stained nucleus (shown in blue in Fig. 4.5) and overlaying with the 53BP1 (shown as green pixels in Fig. 4.5). The quantitative data was produced by counting the 53BP1 and divided by the 2D projected area of all the nuclei imaged (n=307 for CIS, n=357 for GNP-RGD; CIS). The number of 53BP1 foci per 2D projected z-stacked nuclear area for cells treated with CIS and GNP-RGD; CIS prior to radiation were 0.026 ± 0.0045 and 0.040 ± 0.0044 respectively and the difference is statistically significant (t-test, $p < 0.05$). These results indicate that the DNA DSBs are increased for cells treated with IR GNP-RGD; CIS compared to cells treated with IR CIS. The triple combinational treatment of cells treated with GNP-RGD; CIS and radiation had an improved therapeutic result compared to the double combined treatment of cisplatin and radiation.

4.4 Discussion

The final goal of this dissertation was to investigate the effect of GNP constructs in combined chemotherapy and radiation therapy. The use of combined chemotherapy and radiation therapy has improved the cure rates of solid tumours [20, 30]. The standard treatment sequence refers to a chemotherapy regimen before a traditional external beam radiation therapy treatment [30]. Chemotherapy used prior to irradiation is expected to cause maximal tumour regression for locally advanced tumours [30]. As discussed before, GNPs can be used as a carrier platform for chemotherapeutic drugs. GNP-drug complexes have higher tumour specificity than free drugs.

Results from this study indicate that the DNA DSBs are increased for cells treated with IR GNP-RGD-BLM compared to cells treated with IR BLM; and cells treated with IR GNP-RGD; CIS compared to cells treated with IR CIS. The triple combinational treatment of cells treated with GNP-RGD-BLM and radiation had a 32 ± 9 % decrease in survival fraction compared to the double combined treatment of bleomycin and radiation; and the triple combinational treatment of cells treated with GNP-RGD; CIS and radiation had a 30 ± 6 % decrease in survival fraction compared to the double combined treatment of cisplatin and radiation. In addition to the decrease in survival fraction, the 53BP1 count per nuclear area was also increased for the triple combinational treated cells.

While the MDA-MB-231 cells incubated with GNP-RGD; CIS had no statistically significant change in SF compared to cells incubated with the same concentration of free cisplatin (CIS), with SF of 0.61 ± 0.005 and 0.60 ± 0.005 , respectively ($p > 0.05$) (Fig. 2.9 in section 2.3.6) without radiation, the triple combinational treatment of cells treated with GNP-RGD; CIS and radiation had a 30 ± 6 % decrease in survival fraction compared to the double combined treatment of cisplatin and radiation. Platinum based chemotherapeutics such as cisplatin are commonly being used clinically in combination with radiation in the treatment of variety of solid tumours [165, 184, 259]. One proposed mechanism of cisplatin radiosensitization is through the cisplatin inhibition of repair of radiation-induced DNA lesions [259]. It has been shown that the most effective combinations between cisplatin and irradiation is achieved with lower dosages (1 $\mu\text{g/ml}$ compared to 3 $\mu\text{g/ml}$ or 6 $\mu\text{g/ml}$ [260] and 2 Gy compared to 6 Gy [261]) of the two modalities [259]. With the addition of peptide modified GNPs in the combined cisplatin and irradiation treatment, the therapeutic results improved even further.

One of the most commonly used models to study combined effects of substances *in vivo* and *in vitro* is the Bliss Independence Criterion as reference [262, 263]. The Bliss criterion for two toxic agents to have an additive effect is expressed by the following equation:

$$E(x, y) = E(x) + E(y) - E(x) * E(y),$$

where E is the fractional effect (between 0 and 1), x and y are the doses of two compounds in a combinational experiment. If the experimental effect is larger than the calculated value, the experimental result indicates a synergistic effect. If the experimental effect is smaller than the calculated value, the experimental result indicates an antagonistic effect. Otherwise, the effect is additive [262-264]. The Bliss equations are applicable to experimental data for single points and entire dose-response curves but the main assumption of the Bliss Independence Criterion is that the toxic agents act independently from one another [262, 263]. The Bliss Independence Criteria have been used to analyze synergism between multiple modes of treatments. Tarapacki *et al.* used the Bliss Independence Criteria to examine the synergism of PEGylated gold nanoparticles combined with ultrasound and microbubbles [265]. The fractional effect (E) for a condition was calculated as ‘1-SF,’ where SF was obtained from clonogenic assays. Since, GNPs by itself did not cause a toxic effect, treatment with GNP-RGD-BLM or GNP-RGD;CIS was considered one effect, and the treatment with radiation was considered another effect. The calculated values are presented in Table 4.1, along with the experimental effect obtained from clonogenic assays.

<Table 4.1> Comparison of predicted effect using the Bliss Independence Criteria with experimental values.

	Calculated effect from Eq (1)	Experimental Effect (1-SF)	Difference between calculated and experimental
IR GNP-RGD-BLM	0.88 ± 0.02	0.87 ± 0.005	0.01 ± 0.02
IR GNP-RGD; CIS	0.82 ± 0.02	0.84 ± 0.007	0.02 ± 0.02

The expected additive effect of IR GNP-RGD-BLM was calculated to be 0.88 ± 0.02 which includes the range of experimental effect of 0.87 ± 0.005 ; the expected additive effect of IR GNP-RGD; CIS was calculated to be 0.82 ± 0.02 which also is within the range of the experimental effect of 0.84 ± 0.007 , as shown in Table 4.1. Since the difference of zero is within the propagated uncertainty range of the difference for both IR GNP-RGD-BLM and IR GNP-RGD; CIS, the calculated effect and the experimental effect can be concluded to agree. The triple combined effect of GNP-RGD-BLM and radiation and the triple combined effect of GNP-RGD; CIS and radiation both indicate an additive effect with the assumption that the chemotherapeutic (GNP-RGD-BLM or GNP-RGD; CIS) and the physical agent (radiation) is independent. The combined chemotherapeutic drug and radiation effect in the presence of GNPs is to be further evaluated at different combination of dosages.

4.5 Conclusion

The results of this section demonstrate that using peptide modified GNPs in combined chemotherapy (633 nM Bleomycin or 435 nM cisplatin) and radiation therapy (single fraction of 2 Gy, 6 MV X-ray) significantly enhanced therapeutic results by $32 \pm 9 \%$ and $30 \pm 6 \%$ respectively. The triple combined effect of GNP-RGD-BLM and radiation and the triple combined effect of GNP-RGD; CIS and radiation both indicated an additive effect examined with the Bliss Independence Criteria. This signifies that the GNP platform can be utilized in combined chemotherapy and radiation therapy with chemotherapeutic agents that do and do not conjugate onto the surface of the GNPs. The results also show that the incubation of RGD modified GNPs at a relatively low concentration (0.3 nM) can improve combined chemotherapy and radiation even at a MV energy radiation. The GNP platform that can be used with conjugated and unconjugated

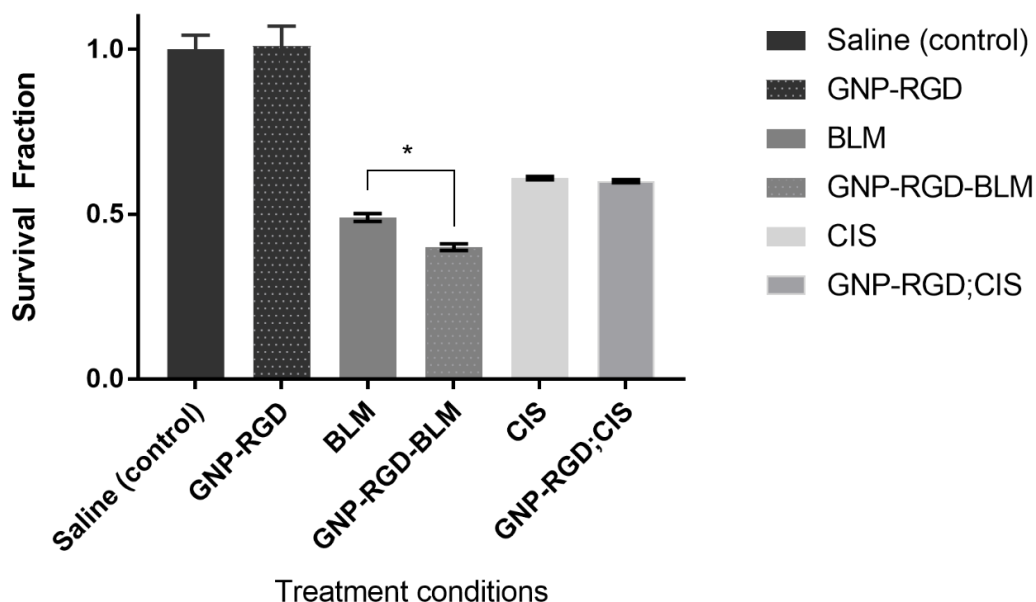
chemotherapeutic agent along with radiation will be beneficial in treatment plans that involve multiple dosages of various chemotherapeutics and multiple fractions of radiation. Further modifications to this GNP-based platform will have to be performed and tested in future *in vivo* studies.

Chapter 5

Summary, discussion, and future work

This chapter contains a summary of the work discussed in previous chapters. The effect of having peptide modified GNPs with chemotherapeutic agents, with radiation, and with combined chemotherapeutic agents and radiation has been discussed. A summary of non-irradiated and irradiated clonogenic assay cell SFs will be listed.

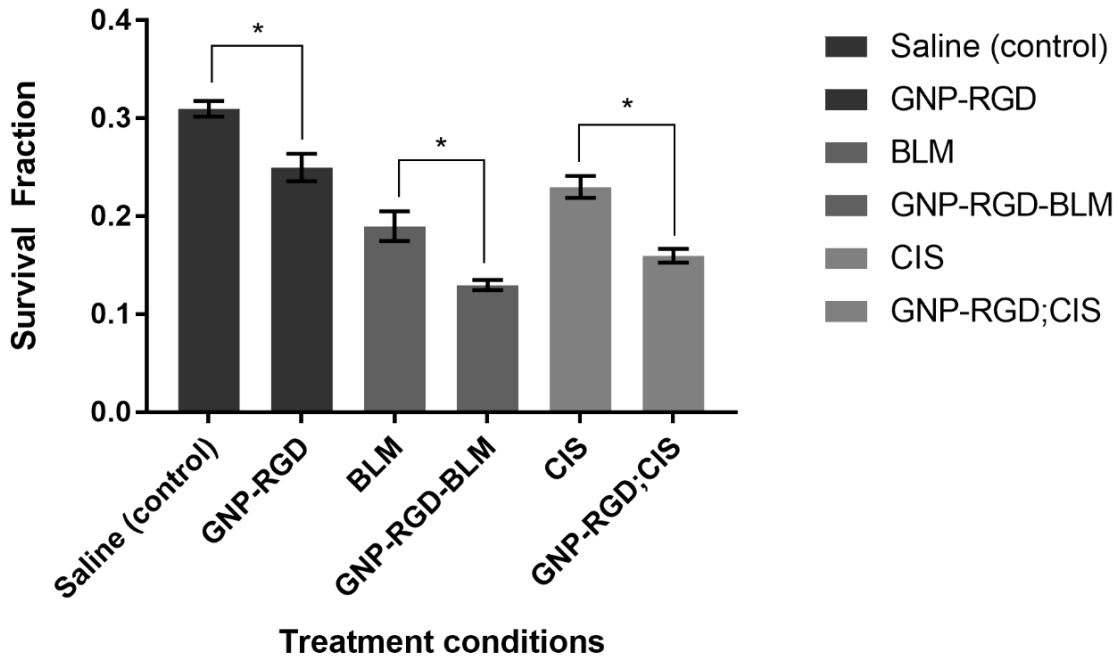
5.1 Summary of GNP mediated combined therapy



<Fig. 5.1> Summary of survival fractions of non-irradiated MDA-MB-231 cells under various treatment conditions. Survival fraction of MDA-MB-231 cells treated with GNPs, chemotherapeutics (BLM and CIS) and GNP with chemotherapeutics. * indicates statistically significant difference between the pair (unpaired t-test, $p < 0.05$).

Fig. 5.1 is a summary of the clonogenic assay survival fractions of MDA MB 231 cells treated with GNP-RGD (SF of 1.01 ± 0.06), BLM (SF of 0.49 ± 0.012), GNP-RGD-BLM (SF of

0.40 ± 0.010), CIS (SF of 0.61 ± 0.005) and GNP-RGD; CIS (SF of 0.60 ± 0.005) with the plating efficiency measured from the control sample treated with the same volume of PBS. While GNP-RGD-BLM had a statistically significant decrease in SF compared to BLM ($p < 0.05$), GNP-RGD; CIS did not have a statistically significant decrease ($p > 0.05$). These results indicate GNPs can carry chemotherapeutics resulting in an efficient delivery than the free counterparts (GNP-RGD-BLM). Moreover, GNPs do not affect the efficacy of the chemotherapeutic if it is not conjugated (GNP-RGD;CIS). The latter result is also important in that GNPs can still be potentially used in combined chemotherapy and radiation therapy treatments just as a radiosensitizer if the drug conjugation is not possible.



<Fig. 5.2> Summary of survival fractions of irradiated MDA-MB-231 cells under various treatment conditions. Survival fraction of MDA-MB-231 cells treated with GNPs, chemotherapeutics (BLM and CIS) and GNP with chemotherapeutics. * represents statistically significant difference. * indicates statistically significant difference between the pair (unpaired t-test, $p < 0.05$).

Fig. 5.2 is a summary of the survival fractions of MDA MB 231 cells irradiated with 2 Gy, 6 MV X-rays that were incubated with PBS (SF of 0.31 ± 0.008), GNP-RGD (SF of 0.25 ± 0.014), BLM (SF of 0.19 ± 0.015), GNP-RGD-BLM (SF of 0.13 ± 0.005), CIS (SF of 0.23 ± 0.011) and GNP-RGD; CIS (SF of 0.16 ± 0.007) with the plating efficiency measured from the non-irradiated control sample treated with the same volume of PBS. Every condition that was incubated with the addition of GNP-RGD had a statistically significant decrease than the non-GNP-RGD counterparts. Clonogenic assays were used as the main measure of treatment effectiveness in *in vitro* studies as the loss of reproductive integrity of tumour cells is the important goal of cancer treatment [21]. A summary list of survival fraction of MDA-MB-231 cells from various treatment combinations are shown in Table 5.1. Sensitization to 6 MV radiation have been observed with a relatively low concentration of GNP constructs in cells. Moreover, to the best of the author's knowledge, this dissertation is the first demonstration of the results of combining chemotherapeutics and radiation with RGD-functionalized GNPs with a MV energy radiation.

<Table 5.1> Summary of Survival fraction of MDA MB 231 cells of various treatment conditions.

Treatment condition		Mean	Standard Error of Mean
Non-Irradiated	Saline (control)	1	0.043
	GNP-RGD	1.01	0.060
	BLM	0.49	0.012
	GNP-RGD-BLM	0.40	0.010
	CIS	0.61	0.005
	GNP-RGD; CIS	0.60	0.005
Irradiated	Saline (control)	0.31	0.008
	GNP-RGD	0.25	0.014
	BLM	0.19	0.015
	GNP-RGD-BLM	0.13	0.005
	CIS	0.23	0.011
	GNP-RGD; CIS	0.16	0.007

5.2 Discussion

The significance of findings from previous chapters (Chapter 2, 3, and 4) will be discussed in section 5.2.1. Future directions will be discussed in section 5.2.2.

5.2.1 Significance of findings

In the clinics, multiple dosages of chemotherapy and multiple dosages of radiation are generally prescribed to the patient, and the schedule, dosage of treatment is different from patient to patient. The usage of GNP-RGD in combination with chemotherapeutic agents, radiation, and combined chemotherapeutic agents with radiation has shown statistically significant improvement in this study and the effectiveness (X) can become more apparent for multiple treatments. Assuming that each treatment is equally effective, and there is no cell proliferation between treatments, the survival following n treatments is given by X^n , which is a concept introduced by Hill and Bristow [266]. The survival fraction post 10, 20, and 30 treatments of the various permutations of GNP-RGD, chemo (BLM or CIS), and radiation and the percentage decrease of the condition pairs are summarized in Table 5.2.

<Table 5.2> Values of Survival Fraction and Percentage Difference of Various Treatments

Treatment condition		Experimental SF	% decrease	Predicted SF post 10 treatment	% decrease	Predicted SF post 20 treatment	% decrease	Predicted SF post 30 treatment	% decrease
Non Irradiated	Saline (control)	statistically no difference in experimental SF study							
	GNP-RGD								
	BLM	0.49	18	8×10^{-4}	87	6×10^{-7}	98	5×10^{-10}	99.8
	GNP-RGD-BLM	0.40		1×10^{-4}		1×10^{-8}		1×10^{-12}	
	CIS	statistically no difference in experimental SF study							
	GNP-RGD; CIS								
Irradiated	Saline (control)	0.31	19	8×10^{-6}	88	7×10^{-11}	99	6×10^{-16}	99.8
	GNP-RGD	0.25		1×10^{-6}		9×10^{-13}		9×10^{-19}	
	BLM	0.19	32	6×10^{-8}	98	4×10^{-15}	99.9	2×10^{-22}	99.99
	GNP-RGD-BLM	0.13		1×10^{-9}		2×10^{-18}		3×10^{-27}	
	CIS	0.23	30	4×10^{-7}	97	2×10^{-13}	99.9	7×10^{-20}	99.99
	GNP-RGD; CIS	0.16		1×10^{-8}		1×10^{-16}		1×10^{-24}	

As shown in Table 5.2, small differences in survival can translate into large differences and therefore a larger significance during a course of multiple treatments [266].

The probability of tumour control can be estimated from the following equation:

$$P_0 = e^{-a}$$

Where P_0 is the probability that a tumour will contain no survival stem cells, a is the average number of cells surviving [266]. To achieve tumour control, all tumour stem cells must be killed [266]. Tumour stem cells are referred to the limited proportion of tumour cells with the capacity for cell proliferation [267]. Cells from human tumours have been found to be able to generate colonies in adequate nutrient environment, however, the proportion of cells that generate

colonies have been found to be low (less than 1 percent) which suggests a low proportion of tumour stem cells [267].

A small difference in survival can translate into large differences over multiple treatments and that can also lead to a significant difference in tumour control probability. An example to show the difference in tumour control probability using cell survival fraction obtained from Chapter 2 is shown in Table 5.3.

< Table 5.3> Comparison of tumour control probability extended from experimental SF values

Treatment condition		Experimental SF	SF post 30 treatment	Average number of cells surviving for a tumour containing 10^9 cells	Tumour control probability
Non-Irradiated	BLM	0.49	5×10^{-10}	0.5	0.6
	GNP-RGD-BLM	0.40	1×10^{-12}	0.001	0.999

It is generally recognized that *in vitro* data cannot be extrapolated directly to *in vivo* or clinical settings since assays in vitro assays do not account for tumour microenvironmental factors and the fact that tumours may contain clonogenic subpopulations of cells with different sensitivity to radiation or chemotherapeutic of interest [266]. However, Table 5.3 shows that a decrease in SF with the presence of GNP-RGD for one dose of chemotherapeutics can potentially mean less number of treatments in an overall treatment regimen. For most solid tumours, the limit of clinical detection is approximately 1 gram of tissue, which corresponds to approximately $10^8 \sim 10^9$ cells [21, 268]. Therefore, the average number of cells surviving for a tumour containing 10^9 cells and the corresponding tumour control probability have been calculated and shown in Table 5.3 for

proof of principle purposes. The principle significance comes from the fact that a small difference in survival can translate into large differences over multiple treatments and that can also lead to a significant difference in tumour control probability.

The results of this dissertation show that peptide modified 10 nm GNPs can be used with chemotherapeutic agents, radiation, or with combined chemotherapeutic agents and radiation. The presence of GNPs showed a statistically significant improvement to the therapeutic result even at a relatively low incubation concentration of 0.3 nM. This is significant because when a GNP system is translated to *in vivo* studies, the number of particles that would reach the cell level with respect to the initial incubation number will substantially decrease.

5.2.2 Future directions

The objective of using any combination of therapeutic agents is to achieve an improved therapeutic result. However, there is no universally acceptable measure of therapeutic result in a clinically setting since lifespan, duration or remission, quality of life are all important and reflect the decision factor of choosing a certain therapeutic regime over another [269]. Studies in this dissertation have shown that GNPs can be used (1) with chemotherapeutic agents, (2) with radiation, and (3) combination of chemotherapeutics and radiation. The usage of GNPs could potentially be another addition to the toolbox of combination therapy that some patients could benefit from since the presence of GNPs improves conjugated chemotherapeutic entry to cells, yet does not hinder unconjugated chemotherapeutics, while acting as a radiosensitizer.

All studies in this dissertation are performed *in vitro*. However, the main goal of this research is to translate the results to *in vivo* and eventually to clinical studies. It is generally recognized that *in vitro* data cannot be extrapolated directly to *in vivo* or clinical settings [266].

Several extra factors must be considered to extend this work to *in vivo*. Accumulation of the nanoparticles into the cells becomes a more complicated process as NPs must pass more barriers before entering the cells. Successful clinical translation of nanomedicine requires NPs to be accumulated in the tumour tissue [88].

In normal organs, circulating NP systems are cleared from the circulation by the mononuclear phagocyte system (MPS) or glomerular filtration in the kidney [270]. Polyethylene glycol (PEG) is a commonly used molecule to decrease the NP surface exposure to proteins, such as opsonin [271]. Opsonin is a protein that binds to foreign microorganisms for enhanced phagocytosis and removal of foreign material from circulation for clearance. Protecting NP surfaces from binding of opsonin can improve blood circulation of the NPs [271, 272]. Prolonged circulation of PEGylated particles promote tumour selectivity of NPs [273]. The GNP construct used for this dissertation is first modified with CALNN peptides. The stability and circulation time of CALNN modified GNPs have yet to be studied, however, if CALNN modified GNPs are not found to be optimal for *in vivo* settings, polyethylene glycol (PEG) could be used as a replacement. The limitations of modifying GNPs with PEG molecules is that accumulation on a cellular level is decreased because the PEG moiety hinders binding of PEGylated NPs to tumour cells receptors [271-273]. Peptides containing the RGD motif, used for modification in this dissertation, can be used to improve the accumulation of PEGylated GNPs to a certain extent [271]. The concentration of the CALNN and RGD modified GNP construct used throughout this dissertation was 0.3 nM. It is predicted that a higher concentration would be required if PEG molecules are used in lieu of RGD peptides. Cruje *et al.* studied the uptake of PEGylated GNPs in MDA-MB-231 cells and observed that a 1:1 ratio of PEG:RGD ratio enhanced the uptake the most [271]. They also observed 14 nm RGD-PEG modified GNP constructs had approximately a 29 % accumulation

than that of unmodified citrated stabilized GNPs in MDA-MB-231 cells [271]. Since the CALNN-RGD modified GNPs used in this dissertation had a 6-7 fold increase in accumulation in MDA-MB-231 cells compared to the unmodified counterpart, if PEG-RGD is to be used in lieu of CALNN-RGD, an approximate increase of 22 times the concentration, or approximately 6 -7 nM is predicted to have a similar effect assuming other parameters remain the same.

Nano-sized agents with long enough circulation time leak preferentially into tumour tissue through the permeable tumour vasculature and are retained in the tumour bed due to reduced lymphatic drainage [89, 270]. Intravenously injected nano-sized drugs are delivered to tissues through arterioles and released from capillaries [90, 270]. Normal capillaries are lined by tightly sealed endothelium, firmly attached with pericytes and further enveloped in a thin layer of basement membrane [270]. In contrast, tumour vasculature usually has incomplete endothelial lining with relatively large pores (0.1 – 3 μm in diameter) that leads to an increased permeability and hydraulic conductivity [270]. Moreover, tumour vasculature has reduced pericyte coverage and the pericytes and basement membranes are loosely associated with the endothelial cells [270]. The NPs are able to enter through leaky and loosely compacted tumour vasculature and remain there due to poor lymphatic drainage [270]. The EPR effect improves the delivery of nanoscale therapeutics to tumours, however, the improvement in delivery is less than a 2-fold increase compared to normal organs [270]. The EPR effect can be improved by manipulating local tumour or systemic conditions through various methods, such as modulating tumour blood flow, tumour vasculature and stroma, and killing of cancer cells [270].

Although the poorly organized tumour vascular architecture and the reduction of lymphatic drainage results in preferential accumulation and retention of NPs in tumour tissue, the tumour cells also have the potential for more rapidly proliferating than the cells that form blood vessels

[274]. This variance in proliferation speed creates population of cells distant ($> 100 \mu\text{m}$) from blood vessels that lead to hypoxic regions and the lack of lymphatic drainage increases interstitial fluid pressure (IFP) which paradoxically can limit delivery of therapeutic agents [274]. Therapeutic agents have to be able to access all of the cells within a tumour that are capable of regeneration to be effective [274]. Counterintuitively, administration of agents that inhibit angiogenesis temporarily improved blood flow and reduced IFP by pruning immature vessels [274, 275]. However, the effect is dependent on tumour model and the anti-angiogenic agents because other studies have reported of a lack of improved oxygenation [274].

Once NPs enter the tumour tissue, they are generally retained in the tissues through the cross-linking of surface bound serum proteins [276]. Most NPs that are not modified are first coated with serum proteins and then met with the plasma membrane of cells [107]. It has been found that a large variety of proteins adsorb to the NP surface irrespective of NP size or composition and even with the presence of polyethylene glycol (PEG) coating, which has been reported to have low serum protein adsorption [276].

The permeability of macromolecules within the tumour can be dependent on the extracellular matrix (ECM) content [277]. The ECM is an essential component of tissues that consists of collagen and elastin fibers immersed in viscoelastic gel that is composed mainly of hyaluronan and proteoglycan [278]. This matrix of collagen network prevents penetration of macromolecules and the delivery of therapeutic agents to cancer cells [277, 279]. Serum proteins that adsorb on the surface of NPs can be cross-linked into tissue through any available amine groups found at the N-terminus of in lysine residues [276]. While this cross-linking helps NPs stay in the tissue, it prevents the NPs of further penetration. A tumour with a well-developed collagen network can be considered to be physically resistant to macromolecule-based therapies [277].

Chithrani's group has previously studied GNP penetration in multicellular models of MDA-MB-231 cells and MCF-7 cells [98]. The ECM for MDA-MB-231 is less organized than ECM of MCF-7 cell line and MDA-MB-231 cell layers were less compartmentalized than MCF-7 cell layers [98]. The more aggressive and invasive tumour cells like MDA-MB-231 secrete matrix-degrading proteinases that serve to break down collagen and attribute to the differences in ECM and cell layer organizations [99, 100]. It was observed that the GNPs penetrated deeper through the MDA-MB-231 MCL than the MCF-7 MCL [98]. This study shows that a better developed ECM prevents penetration of nanoparticles. The development of collagen network varies from cell line to cell line, but degeneration of the collagen network and an abnormal ECM organization can be common features of tumours [277]. This characteristic of tumours can be advantageous in having NPs accumulated more in the tumour tissues than the normal tissues. For tumours with a relatively well-developed collagen network, treatments that reverse or inhibit collagen production and assembly can be performed prior to macromolecule-based therapies [277]. Ji *et al.* down-regulated ECM levels and observed an enhanced penetration of a therapeutic agent, gemcitabine, and suggested that the regulation of ECM may become a promising adjuvant therapeutic strategy for ECM-rich tumours [279]. Other studies have shown that ECM-degrading enzyme collagenase or the hormone relaxin that modifies collagen structure can improve the distribution of macromolecules in solid tumours [280, 281]. Agents with antifibrotic effects, such as Losartan or Pentoxifylline were also reported to be effective in reducing the tumour tissue collagen content and enhance diffusive transport of intravenously administered NPs [273, 282, 283]. By directly degrading the ECM or indirectly by inhibiting the synthesis can not only improve the penetration of nanoscale therapeutics, but it can also decrease solid stress to tumours and reduce interstitial fluid pressure which can further enhance the EPR effect as well [270].

Nanotherapeutic agents can have improved delivery after multiple therapies as the tumour cells themselves act as a barrier to deeper penetration of NPs [270]. Radiation therapy in particular damages cancer cells with less pronounced effect on the vasculature [270]. It has been shown that nano-sized molecules enter radiation treated tumours at a rate 2.2-fold higher than non-irradiated tumours [284]. Radiation killed well-oxygenated cancer cells near tumour vessels, and as a result vascular permeability increased by reduced barrier function of the cancer cells [270]. However, excessive radiation damaged the vessels and shut down blood flow, which affected the nanotherapeutic agent delivery negatively [285]. Moreover, effects of radiation on ECM must also be considered. Mohamed *et al.* found that radiation damaged the long polymer chains of hyaluronan and elastin were damaged, which resulted in premature stiffening of tissue [278]. The effect of radiation on ECM could potentially affect delivery of therapeutic agents.

As discussed, development of cancer nanomedicine requires careful consideration of multiple facets at multiple levels because overcoming the barriers for NP delivery can be complexed and there could be contradictory effects from a single condition or a single treatment. For example, although the lack of lymphatic system in tumour tissue helps NP retention, it also increases the IFP which can limit delivery of NPs; and the killing of cancer cells by radiation can reduce barriers formed by cancer cells and improve NP delivery, but radiation can also damage vessels that could lead to impedance of NP delivery. Although direct *in vivo* assessment has the advantage of duplicating the clinical environment more closely, *in vitro* techniques offer the advantage of being able to examine and evaluate isolated results with less complicated parameters. The benefit of utilizing CALNN-stabilized, RGD modified 10 nm colloidal GNPs with a chemotherapeutic that is conjugated through gold-thiol chemistry (bleomycin) and with a chemotherapeutic that is not conjugated but acts as an additional radiosensitizer (cisplatin) with a

2 Gy single fraction 6 MV X-ray radiation in MDA-MB-231 cells *in vitro* has been reported in this dissertation. The results from this *in vitro* monolayer study using MDA-MB-231 breast cancer cells can be further investigated using different cell lines since wide range of cell lines derived from human tumours have shown intrinsic variation in NP accumulation, radiation sensitivity and in response to certain chemotherapeutics [266]. Then, the results could be expanded to multilayer *in vitro* studies, which take ECM into account. Features of solid cancers that are not modelled by multicellular models are variable IFP, the influence of convection and stromal cells [274]. Eventually, *in vivo* studies can be performed after subsequent optimization. Clinical translation requires further extensive research since patient data would be necessary to ensure the mechanism of action for the NP formulation observed in animal models is effective in human patients [286].

5.3 Future work – preliminary study

The goal of NP-based platforms will be the targeted delivery of therapy to tumours with minimal side effects [287-291]. Optimizing the interface between NPs and biological environment at various levels should be discussed for improving delivery of NPs to the target tumour area. Successful delivery of NPs into tumour depends on efficiency of crossing few boundaries in the tumour microenvironment as discussed in the previous section 5.2.2. For NPs to be delivered to cancer cells, a) NPs needs to be functionalized for circulation through the blood vessels until it reaches tumour vasculature where NPs can make use of the leakiness of the vasculature to enter tumour tissue, penetrate through the tumour matrix, and enter the cancer cells. In this study, accumulation of PEGylated GNPs was first observed in *in vitro* cell models prior to the use in *in vivo* models. Recent studies have shown that the size dependence of GNP uptake may differ between monolayer cultures [292-298]. The Extra Cellular Matrix (ECM) acts as a barrier in NP transport in tissue-like structures [277, 279]. Given that transport through the ECM is diffusion-dependent, GNP transport is predicted to be inversely proportional to GNP size [98]. It has been observed that 20 nm GNPs penetrates better through the multilayer *in vitro* cell models compared to 50 nm NPs [299], but uptake of these smaller NPs has been reported to be lower than the 50 nm counterpart [104]. A smaller 10 nm sized GNP was selected for his study for better penetration through tumour tissue, but the surface was modified with PolyEthylene Glycol (PEG) [271, 272] to improve circulation time by reducing non-specific uptake by the reticuloendothelial system (RES) at *in vivo* models and an integrin binding domain RGD, to improve internalization at the cellular level [300, 301]. Studies have shown that uptake of GNPs at monolayer level is compromised once they are functionalized with PEG, but the Chithrani's group has also demonstrated that NP uptake can be improved by co-functionalizing with a peptide containing

RGD domain [301, 302]. A preliminary study by our group developed a formulation of PEG and RGD conjugated GNPs. The accumulation of this formulation was evaluated in monolayer MIA-PaCa-2 cells and *in vivo* models.

5.3.1 Materials and Methods

Synthesis and characterization of NPs

GNPs were synthesized using the citrate reduction method [65]. First, 300 μ l of 1 % chloroauric acid ($\text{HAuCl}_4 \cdot 3\text{H}_2\text{O}$) (Sigma-Aldrich) was added to 30 ml of double-distilled water and heated on a hot plate while stirring. Once it reached the boiling point, 1 ml of 1 % sodium citrate tribasic dehydrate ($\text{HOC}(\text{COONa})(\text{CH}_2\text{COONa})_2 \cdot 2\text{H}_2\text{O}$) (Sigma-Aldrich) was added. After the colour of the solution changed from dark blue to bright red, the solution was left to boil for another five minutes while being stirred. Finally, the GNP solution was brought to room temperature.

Conjugation of peptides and PEG onto GNPs

A 0.1 % PEG solution was prepared with thiol-terminated polyethylene glycol with a molecular weight of 2 kDa. The solution was added to GNP solutions to achieve a grafting density of 2 PEG molecules per nm^2 . For 10 nm GNPs, approximately 630 PEG molecules were added. A solution of peptide sequence, CKKKKKKGGR**RGDM**FG was mixed with a solution of the PEG molecules at PEG: RGD = 2:1 ratio. To confirm PEGylation of GNPs, DLS measurements were conducted. This was followed by UV-visible spectrophotometry to confirm the stability.

Cellular uptake studies

MIA-PaCa-2 cells were cultured in Dulbecco's Modified Eagle's Medium (DMEM) with 10 % Fetal Bovine Serum grown to confluent so that three wells of a 6-well tissue culture dishes were incubated with the same NP type. For optical imaging purposes, cells were placed on glass coverslips and grown to 60 % confluent. Cell cultures were incubated with 5×10^{10} GNPs per dish. Following incubation, all cell cultures were washed with Phosphate-Buffered Saline (PBS) three times. Those without coverslips were trypsinized and processed for quantification studies. Those with coverslips were rinsed twice with PBS, followed by fixation with 4 % paraformaldehyde in PBS for 10 minutes at room temperature, then rehydration in PBS. Coverslips were mounted onto glass slides and were dried overnight and kept at 4 °C prior to being imaged.

Pancreatic Xenograft Model.

The human pancreas cancer cell line, MIA-PaCa-2 cells, was cultured in Dulbecco DMEM - Dulbecco's Modified Eagle Medium (Life Technologies) with 10 % Fetal Bovine Serum (FBS), 100 units/mL penicillin G and 100 µg/mL streptomycin (Hyclone). Cells were maintained at 37 °C in a humidified atmosphere containing 5 % CO₂. To derive subcutaneous (s.c.) xenografts, 6-8 week-old female SCID mice were injected with 1.5×10^6 cells in the lower left dorsal flank. Injection of GNPs in the tail vein was started when xenografts reached a volume of ~250 mm³. Mice were randomly divided into groups for all studies and subsequently sacrificed at intervals of 24 h, 48 h, and 72 h. Tumour length and width measurements were converted into tumour volume using $(L \times W^2 / 2)$ where L and W are the larger and smaller diameters, respectively; tumours were measured every 2 days with calipers. Animals were monitored for any signs of physical toxicity

over the duration of each study. Experiments were conducted in accordance with the University Health Network (UHN) Animal Care Committee guidelines.

***In vivo* Biodiversity Assay**

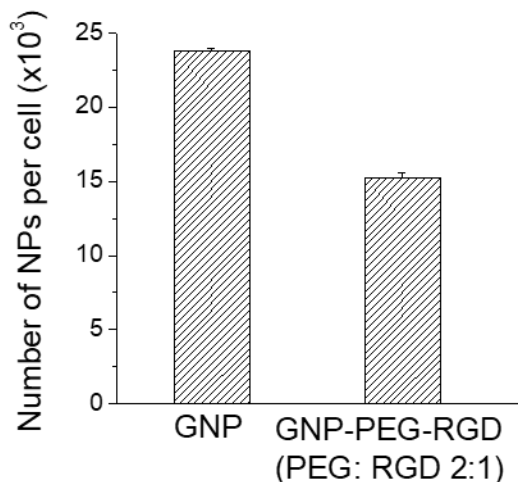
SCID mice were sacrificed at pre-determined time-points as tumour and organs (liver, kidney, pancreas, spleen) were surgically removed and analyzed *ex-vivo*. Subsequently, organs were homogenized using a mechanical homogenizer. All surgical and organ removal techniques were conducted in accordance with UHN Small Animal Surgery Guidelines.

Quantification of GNPs

GNP accumulation in cells or organs was quantified using Inductively Coupled Plasma Atomic Emission Spectroscopy (ICP-AES). Following sixteen hours of incubation with GNPs, the cells were washed three times with PBS and the cells were suspended from the monolayer cultures with 0.25 % trypsin-EDTA (Gibco) for quantification of GNPs present per cell. Cells were counted with either a hemocytometer (Hausser Scientific, Horsham, USA) or a Vi-CELL XR automated cell counter (Beckman Coulter, Brea, USA). The surgically removed organs were weighed and homogenized. Then the samples were treated with aqua regia (mixture of 37 % hydrochloric acid (HCl) (Sigma-Aldrich) and 70 % nitric acid (HNO₃) (Caledon Laboratories Ltd.) a ratio of 3:1) in a silica oil bath. The samples were diluted and concentrations of gold (Au) atoms were measured in [mg/L] with the Optima 7300 DV ICP AES (Perkin Elmer, Waltham, USA). The resulting gold atom counts were converted to GNPs per cell or per organ weight.

5.3.2 Preliminary results

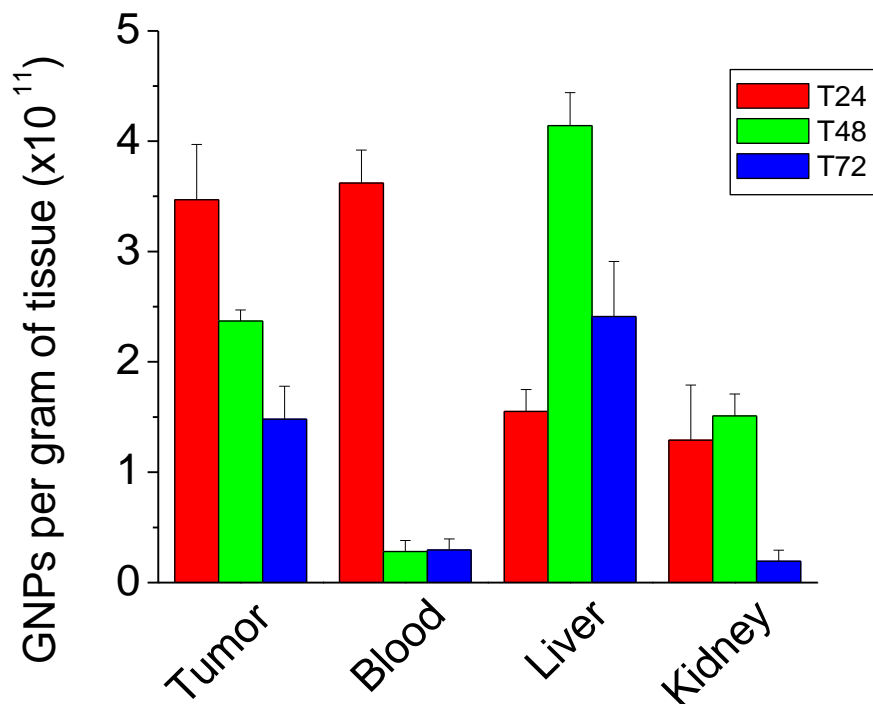
Cellular uptake of gold nanoparticles at monolayer level



<Fig. 5.3> Accumulation of GNP constructs in monolayer MIA-Pa-Ca-2 cells. Decreased accumulation was observed for cells modified with peptide (PEG and RGD) modified GNPs compared to the unmodified (citrate stabilized) GNPs.

The cellular uptake of three GNP complexes (unmodified GNPs and GNP-RGD-PEG) in MIA-PaCa-2 pancreatic cell line was assessed. The cells were incubated with the same concentration (10 nM) of NPs for 16 hrs. Figure 5.3 illustrates the cellular uptake of unmodified (citrate-capped) GNPs, GNP-PEG-RGD with PEG: RGD ratio of 2:1 after 16-hour incubation in MIA-PaCa-2 cells. The accumulated number of unmodified GNPs unmodified (citrate-capped) GNPs and GNP-PEG-RGD (PEG: RGD ratio of 2:1) per cell were 23,800 and 15,250 respectively as shown in Fig. 5.3.

In vivo uptake and pharmacokinetics of GNPs in a pancreatic cancer model



<Fig. 5.4> Accumulation of GNP constructs in various organs of SCID mice. Accumulation of GNP constructs in various organs at 24, 48, 72 hrs post injection.

Figure 5.4 elucidates pharmacokinetic profiles of GNPs at both the tumour and plasma level in the *in vivo* pancreas cancer model of GNP-PEG-RGD with 2:1 ratio. The highest accumulation in tumour was observed 24 hrs after injection of the GNPs at a maximal level of 3.6 $\mu\text{g Au/g}$ of tissue with a subsequent decrease at 48 hrs, and a substantially significant decrease at 72 hrs (Fig. 5.4). Zhang *et al.* reported i.p. injection of similar sized (12.1 nm) PEGylated GNPs to mice resulted in approximately 0.25 $\mu\text{g Au/g}$ in tumour.

A comprehensive review by Wilhelm *et al.* analyzed the NP tumour delivery efficiency from current NP delivery publications [303]. The median and mean of gold material tumour uptake in [% Injected Dose/g] were 3.5, and 6.1 respectively [303]. The discrepancy between the median and mean indicate a high variability of data sets [303]. The large variability between studies

indicate that accumulation of GNPs is dependent of multiple parameters, including the physicochemical properties of the GNPs (size, shape, surface chemistry), presence of targeting molecules, and the tumour environment (size and type of tumour, properties of the tumour blood vessels involved, and properties of ECM involved etc.) as discussed in section 5.2.2. The varied parameters used across different studies make it challenging to compare results in a meaningful way and to identify the optimal parameters.

The concentration of GNPs in blood at 24 hr post injection was 3.5×10^{11} GNPs/ μ L and the GNP levels in blood after 48 and 72 hr significantly decreased. The biological half-life, referring to the time it takes for the blood plasma concentration of a substance to halve, following first order kinetics was calculated to be 7.05 hr. The sufficiently low half-life indicates fast pharmacokinetics, which suggests that toxicity to other organ systems will be minimal with this initial injection dose. Tumour uptake remained approximately 35 % of the 24 hr level at 72 hrs, which shows the GNP retention in tumour is longer than GNP clearance from circulation.

5.3.3 Conclusion

Modifying the GNP constructs with PEG reduced the accumulation at monolayer cell models. These results are expected as it has also been shown from previous studies that GNP modification with PEG decrease cell accumulation [271-273]. Despite the low accumulation at cellular levels, PEG is commonly used to functionalize GNP surfaces as it can decrease the NP surface exposure to proteins, such as opsonin and improve blood circulation in *in vivo* studies [271, 272]. Although varied parameters used across different studies make it challenging to compare results, the tumour accumulation of GNP-PEG-RGD was comparable to a study that used similar sized PEGylated GNPs. Also, the GNP retention was observed to be longer than GNP clearance

from circulation which suggest GNP can be retained in the tumour for the duration of treatments if to be used with other therapeutic modalities. The results from this study have shown that the GNP retention in tumour is significant after 24, 48, and 72 hr post injection, compared to the amount that is cleared from the circulation.

Further work can be performed to incorporate chemotherapeutics and/or radiation to the formulation. It has been demonstrated from previous chapters that the presence of 0.3 nM CALNN/RGD modified GNPs decreased the cell survival of (1) conjugated drug, bleomycin, (2) 2 Gy, 6 MV radiation, and (3) combined chemotherapy (with bleomycin or cisplatin) and radiation. As discussed in section 5.2.2, PEG can be used in lieu of CALNN peptides for stabilization purposes. Although the usage of GNPs in cancer treatment is still at an early stage, with continuous research on various aspects of GNPs under various conditions, the usage of GNPs could potentially be another addition to the toolbox of combination therapy that some patients could benefit from since the presence of GNPs improves conjugated chemotherapeutic entry to cells, yet does not hinder unconjugated chemotherapeutics, while acting as a radiosensitizer.

Appendix

Supplementary

Calculation to confirm TPS

- *The TMR, S_c , and S_p are obtained from beam data for Elekta Agility (the unit that was used for the radiation experiment)*

Dose = 2 Gy (200 cGy), Energy = 6 MV, Field Size (FS) = 20x20 cm²

$$\text{MU setting} = \frac{\text{Prescribed Dose}}{RDR \times S_c \times S_p \times TMR \times \text{inhom CF}}$$

RDR = reference dose rate = 1cGy/MU

TMR = tissue maximum ratio = ratio of dose at depth d to the dose at d_{max} for a given FS

* TMR (6 MV, 20x20, d=10) = 0.814

S_c = collimator scatter factor * $S_c(20) = 1.026$

S_p = phantom scatter factor * $S_p(20) = 1.027$

$$\text{Inhomogeneity Correction Factor (Ratio of TPR)} = \frac{TPR(d', FS)}{TRP(d, FS)} = \frac{TPR(9.02, 20 \times 20)}{TRP(10, 20 \times 20)} = 1.03$$

MU = 226 MU

In Vitro dosage in comparison to clinical dosage

According to Cancer Care Ontario, general dosing of

BLM: 10-20 mg/m² weekly or 2x weekly (max. dose 400 mg/m²)

CIS: 20 mg/m² daily 4-5 days, every 3-4 weeks

$$\text{Body surface area (BSA) [m}^2\text{]} = \sqrt{\text{height [cm]} \times \text{weight [kg]} / 3600}$$

According to Statistics Canada 2008,

	Avg. height [cm]	Avg. weight [kg]	BSA [m ²]
Female	163	66	1.72
Male	175	74	1.90

Estimated blood volume (EBV) based on BSA:

For female: EBV [L] = 3.29 BSA [m²] – 1.229 (*Avg. Canadian 4.0144 L)

For male: EBV [L] = 3.47 BSA [m²] – 1.954 (*Avg. Canadian 5.022 L)

BLM clinical dose:

Female: 10 – 20 mg/m² = 10-20 mg/1.516 L = 6.6-13.2 mg/L

Male: 10 – 20 mg/m² = 10-20 mg/2.061 L = 4.85-9.7 mg/L

Concentration used for expt: 633 nM x 1415 g/mol = 8.96x10⁻⁴g/L (approx 10 % of clinical dose)

CIS clinical dose

Female: 20 mg/m² = 20 mg/1.516 L = 13.2 mg/L

Male: 20 mg/m² = 20 mg/2.061 L = 9.7 mg/L

Concentration used for expt: 435 nM x 300.01g/mol = 1.305x10⁻⁴g/L (approx 1 % of clinical dose)

Bibliography

1. Vogelstein, B. and K.W. Kinzler, *The multistep nature of cancer*. Trends in Genetics, 1993. **9**(4): p. 138-141.
2. Dai, X., H. Cheng, Z. Bai, and J. Li, *Breast cancer cell line classification and its relevance with breast tumor subtyping*. J Cancer, 2017.
3. Pardal, R., M.F. Clarke, and S.J. Morrison, *Applying the principles of stem-cell biology to cancer*. Nature reviews. Cancer, 2003. **3**(12): p. 895.
4. Pece, S., M. Serresi, E. Santolini, M. Capra, E. Hulleman, V. Galimberti, . . . P.P. Di Fiore, *Loss of negative regulation by Numb over Notch is relevant to human breast carcinogenesis*. The Journal of cell biology, 2004. **167**(2): p. 215-221.
5. Politi, K., N. Feirt, and J. Kitajewski. *Notch in mammary gland development and breast cancer*. in *Seminars in Cancer Biology*. 2004. Elsevier.
6. Al-Hajj, M., M.S. Wicha, A. Benito-Hernandez, S.J. Morrison, and M.F. Clarke, *Prospective identification of tumorigenic breast cancer cells*. Proceedings of the National Academy of Sciences, 2003. **100**(7): p. 3983-3988.
7. Holliday, D.L. and V. Speirs, *Choosing the right cell line for breast cancer research*. Breast cancer research, 2011. **13**(4): p. 215.
8. Jain, S., J.A. Coulter, A.R. Hounsell, K.T. Butterworth, S.J. McMahon, W.B. Hyland, . . . F.J. Currell, *Cell-specific radiosensitization by gold nanoparticles at megavoltage radiation energies*. International Journal of Radiation Oncology Biology Physics, 2011. **79**(2): p. 531-539.
9. Cui, L., K. Tse, P. Zahedi, S.M. Harding, G. Zafarana, D.A. Jaffray, . . . C. Allen, *Hypoxia and cellular localization influence the radiosensitizing effect of gold nanoparticles (AuNPs) in breast cancer cells*. Radiation Research, 2014. **182**(5): p. 475-488.
10. Butterworth, K., J. Coulter, S. Jain, J. Forker, S. McMahon, G. Schettino, . . . D. Hirst, *Evaluation of cytotoxicity and radiation enhancement using 1.9 nm gold particles: potential application for cancer therapy*. Nanotechnology, 2010. **21**(29): p. 295101.

11. Wang, C., Y. Jiang, X. Li, and L. Hu, *Thioglucose-bound gold nanoparticles increase the radiosensitivity of a triple-negative breast cancer cell line (MDA-MB-231)*. *Breast cancer*, 2015. **22**(4): p. 413-420.
12. Jain, S., J.A. Coulter, K.T. Butterworth, A.R. Hounsell, S.J. McMahon, W.B. Hyland, . . . F.J. Currell, *Gold nanoparticle cellular uptake, toxicity and radiosensitisation in hypoxic conditions*. *Radiotherapy and Oncology*, 2014. **110**(2): p. 342-347.
13. McMahon, S.J., W.B. Hyland, M.F. Muir, J.A. Coulter, S. Jain, K.T. Butterworth, . . . J.M. O'Sullivan, *Nanodosimetric effects of gold nanoparticles in megavoltage radiation therapy*. *Radiotherapy and Oncology*, 2011. **100**(3): p. 412-416.
14. *Treatment*. 2017; Available from: <http://www.cancer.ca/en/cancer-information/diagnosis-and-treatment/treatment/?region=on>.
15. *Types of Cancer Treatment*. 2017 April 6, 2017; Available from: <https://www.cancer.gov/about-cancer/treatment/types>.
16. Podgorsak, E.B., *Radiation Physics for Medical Physicists*. Vol. 2. 2010: Springer.
17. Podgorsak, E.B., *Radiation Oncology Physics: A Handbook for Teachers and Students*. 2005, Vienna: International Atomic Energy Agency.
18. Delaney, G. and M. Barton, *Evidence-based estimates of the demand for radiotherapy*. *Clinical Oncology*, 2015. **27**(2): p. 70-76.
19. Orth, M., K. Lauber, M. Niyazi, A.A. Friedl, M. Li, C. Maihöfer, . . . C. Belka, *Current concepts in clinical radiation oncology*. *Radiation and environmental biophysics*, 2014. **53**(1): p. 1-29.
20. Herscher, L.L., J.A. Cook, R. Pacelli, H. Pass, A. Russo, and J. Mitchell, *Principles of chemoradiation: theoretical and practical considerations*. *Oncology* (Williston Park, NY), 1999. **13**(10 Suppl 5): p. 11-22.
21. Boyer, M.J.T., Ian F., *Cellular and molecular basis of drug treatment of cancer in The basic science of oncology*, I.F.H. Tannock, Richard P.; Bristrow, Robert G.; Harrington, Lea, Editor. 2005, McGraw-Hill: Toronto. p. 349-375.

22. Hanahan, D. and R.A. Weinberg, *Hallmarks of cancer: the next generation*. Cell, 2011. **144**(5): p. 646-674.
23. Crawford, S., *Is it time for a new paradigm for systemic cancer treatment? Lessons from a century of cancer chemotherapy*. Frontiers in pharmacology, 2013. **4**: p. 68.
24. Jain, R.K., *Transport of molecules, particles, and cells in solid tumors*. Annual Review of Biomedical Engineering, 1999. **1**(1): p. 241-263.
25. Helm, E., *Nanotechnology may replace existing treatments for cancer*. Eukaryon, 2007. **3**(1): p. 255-62.
26. Georgelin, T., S. Bombard, J.M. Siaugue, and V. Cabuil, *Nanoparticle-Mediated Delivery of Bleomycin*. Angewandte Chemie International Edition, 2010. **49**(47): p. 8897-8901.
27. Strebhardt, K. and A. Ullrich, *Paul Ehrlich's magic bullet concept: 100 years of progress*. Nature Reviews Cancer, 2008. **8**(6): p. 473-480.
28. Gullotti, E. and Y. Yeo, *Extracellularly activated nanocarriers: a new paradigm of tumor targeted drug delivery*. Molecular Pharmaceutics, 2009. **6**(4): p. 1041-1051.
29. Vincent, A., S. Babu, E. Heckert, J. Dowding, S.M. Hirst, T.M. Inerbaev, . . . T.S. Rahman, *Protonated nanoparticle surface governing ligand tethering and cellular targeting*. ACS nano, 2009. **3**(5): p. 1203-1211.
30. Rubin, P. and S.K. Carter, *Combination radiation therapy and chemotherapy: A logical basis for their clinical use*. CA: a cancer journal for clinicians, 1976. **26**(5): p. 274-292.
31. Seiwert, T.Y., J.K. Salama, and E.E. Vokes, *The concurrent chemoradiation paradigm—general principles*. Nature clinical practice Oncology, 2007. **4**(2): p. 86-100.
32. Ma, B.B., R.G. Bristow, J. Kim, and L.L. Siu, *Combined-modality treatment of solid tumors using radiotherapy and molecular targeted agents*. Journal of Clinical Oncology, 2003. **21**(14): p. 2760-2776.
33. Chithrani, B.D., *Optimization of Bio-Nano Interface Using Gold Nanostructures as a Model Nanoparticle System*. Insciences J, 2011. **1**: p. 136-156.

34. Xu, Z.P., Q.H. Zeng, G.Q. Lu, and A.B. Yu, *Inorganic nanoparticles as carriers for efficient cellular delivery*. Chemical Engineering Science, 2006. **61**(3): p. 1027-1040.
35. Moghimi, S.M., A.C. Hunter, and J.C. Murray, *Nanomedicine: current status and future prospects*. The FASEB Journal, 2005. **19**(3): p. 311-330.
36. Baltzer, N. and T. Copponnex, *Precious Metals for Biomedical Applications*. 2014: Elsevier.
37. Cho, K., X. Wang, S. Nie, and D.M. Shin, *Therapeutic nanoparticles for drug delivery in cancer*. Clinical Cancer Research, 2008. **14**(5): p. 1310-1316.
38. ud Din, F., W. Aman, I. Ullah, O.S. Qureshi, O. Mustapha, S. Shafique, and A. Zeb, *Effective use of nanocarriers as drug delivery systems for the treatment of selected tumors*. International Journal of Nanomedicine, 2017. **12**: p. 7291.
39. Allen, T.M. and P.R. Cullis, *Drug delivery systems: entering the mainstream*. Science, 2004. **303**(5665): p. 1818-1822.
40. Green, M., G. Manikhas, S. Orlov, B. Afanasyev, A. Makhson, P. Bhar, and M. Hawkins, *Abraxane[®], a novel Cremophor[®]-free, albumin-bound particle form of paclitaxel for the treatment of advanced non-small-cell lung cancer*. Annals of Oncology, 2006. **17**(8): p. 1263-1268.
41. Singer, J.W., B. Baker, P. De Vries, A. Kumar, S. Shaffer, E. Vawter, . . . P. Garzone, *Poly-(l)-glutamic acid-paclitaxel (CT-2103)[XYOTAX[™]], a biodegradable polymeric drug conjugate, in Polymer drugs in the clinical stage*. 2004, Springer. p. 81-99.
42. Steinmetz, N.F., *Viral nanoparticles as platforms for next-generation therapeutics and imaging devices*. Nanomedicine: Nanotechnology, Biology and Medicine, 2010. **6**(5): p. 634-641.
43. Jiang, Y.-Y., G.-T. Tang, L.-H. Zhang, S.-Y. Kong, S.-J. Zhu, and Y.-Y. Pei, *PEGylated PAMAM dendrimers as a potential drug delivery carrier: in vitro and in vivo comparative evaluation of covalently conjugated drug and noncovalent drug inclusion complex*. Journal of drug targeting, 2010. **18**(5): p. 389-403.
44. Malik, N., E.G. Evagorou, and R. Duncan, *Dendrimer-platininate: a novel approach to cancer chemotherapy*. Anti-cancer drugs, 1999. **10**(8): p. 767-776.

45. Madaan, K., S. Kumar, N. Poonia, V. Lather, and D. Pandita, *Dendrimers in drug delivery and targeting: Drug-dendrimer interactions and toxicity issues*. Journal of pharmacy & bioallied sciences, 2014. **6**(3): p. 139.
46. Rohovie, M.J., M. Nagasawa, and J.R. Swartz, *Virus-Like Particles: Next-Generation Nanoparticles for Targeted Therapeutic Delivery*. Bioengineering & Translational Medicine, 2016.
47. Davis, M.E., *Nanoparticle therapeutics: an emerging treatment modality for cancer*. Nature reviews Drug discovery, 2008. **7**(9): p. 771-782.
48. Zamboni, W.C., *Liposomal, nanoparticle, and conjugated formulations of anticancer agents*. Clinical Cancer Research, 2005. **11**(23): p. 8230-8234.
49. Lytton-Jean, A.K., K.J. Kauffman, J.C. Kaczmarek, and R. Langer, *Cancer nanotherapeutics in clinical trials, in Nanotechnology-Based Precision Tools for the Detection and Treatment of Cancer*. 2015, Springer. p. 293-322.
50. Steinmetz, N.F., *Viral nanoparticles in drug delivery and imaging*. 2013, ACS Publications.
51. Yildiz, I., S. Shukla, and N.F. Steinmetz, *Applications of viral nanoparticles in medicine*. Current opinion in biotechnology, 2011. **22**(6): p. 901-908.
52. Mody, V.V., R. Siwale, A. Singh, and H.R. Mody, *Introduction to metallic nanoparticles*. Journal of Pharmacy and Bioallied Sciences, 2010. **2**(4): p. 282.
53. Chithrani, B.D. and W.C. Chan, *Elucidating the mechanism of cellular uptake and removal of protein-coated gold nanoparticles of different sizes and shapes*. Nano Letters, 2007. **7**(6): p. 1542-1550.
54. Fratoddi, I., I. Venditti, C. Cametti, and M. Russo, *Gold nanoparticles and gold nanoparticle-conjugates for delivery of therapeutic molecules. Progress and challenges*. Journal of Materials Chemistry B, 2014. **2**(27): p. 4204-4220.
55. Chithrani, D.B., S. Jelveh, F. Jalali, M. van Prooijen, C. Allen, R.G. Bristow, . . . D.A. Jaffray, *Gold nanoparticles as radiation sensitizers in cancer therapy*. Radiation Research, 2010. **173**(6): p. 719-728.

56. Park, S.-H., S.-G. Oh, J.-Y. Mun, and S.-S. Han, *Loading of gold nanoparticles inside the DPPC bilayers of liposome and their effects on membrane fluidities*. *Colloids and Surfaces B: Biointerfaces*, 2006. **48**(2): p. 112-118.
57. Garcia, M.E., L.A. Baker, and R.M. Crooks, *Preparation and characterization of dendrimer-gold colloid nanocomposites*. *Analytical Chemistry*, 1999. **71**(1): p. 256-258.
58. Paciotti, G.F., D.G. Kingston, and L. Tamarkin, *Colloidal gold nanoparticles: a novel nanoparticle platform for developing multifunctional tumor-targeted drug delivery vectors*. *Drug Development Research*, 2006. **67**(1): p. 47-54.
59. Paciotti, G.F., L. Myer, D. Weinreich, D. Goia, N. Pavel, R.E. McLaughlin, and L. Tamarkin, *Colloidal gold: a novel nanoparticle vector for tumor directed drug delivery*. *Drug Delivery*, 2004. **11**(3): p. 169-183.
60. Ghosh, P., G. Han, M. De, C.K. Kim, and V.M. Rotello, *Gold nanoparticles in delivery applications*. *Advanced drug delivery reviews*, 2008. **60**(11): p. 1307-1315.
61. Jelveh, S. and D.B. Chithrani, *Gold nanostructures as a platform for combinational therapy in future cancer therapeutics*. *Cancers*, 2011. **3**(1): p. 1081-1110.
62. Bergen, J.M., H.A. van Recum, T.T. Goodman, A.P. Massey, and S.H. Pun, *Gold Nanoparticles as a Versatile Platform for Optimizing Physicochemical Parameters for Targeted Drug Delivery*. *Macromol Biosci*, 2006. **6**: p. 506-516.
63. Souza, G.R., D.R. Christianson, F.I. Staquicini, M.G. Ozawa, E.Y. Snyder, R.L. Sidman, . . . R. Pasqualini, *Networks of gold nanoparticles and bacteriophage as biological sensors and cell-targeting agents*. *Proceedings of the National Academy of Sciences of the United States of America*, 2006. **103**(5): p. 1215-1220.
64. Perrault, S.D., C. Walkey, T. Jennings, H.C. Fischer, and W.C. Chan, *Mediating tumor targeting efficiency of nanoparticles through design*. *Nano Letters*, 2009. **9**(5): p. 1909-1915.
65. Turkevich, J., P.C. Stevenson, and J. Hillier, *A study of the nucleation and growth processes in the synthesis of colloidal gold*. *Discussions of the Faraday Society*, 1951. **11**: p. 55-75.

66. Frens, G., *Controlled nucleation for the regulation of the particle size in monodisperse gold suspensions*. *nature*, 1973. **241**(105): p. 20-22.
67. Khlebtsov, N. and L. Dykman, *Biodistribution and toxicity of engineered gold nanoparticles: a review of in vitro and in vivo studies*. *Chemical Society Reviews*, 2011. **40**(3): p. 1647-1671.
68. Tran, M., R. DePenning, M. Turner, and S. Padalkar, *Effect of citrate ratio and temperature on gold nanoparticle size and morphology*. *Materials Research Express*, 2016. **3**(10): p. 105027.
69. Frens, G., *Particle size and sol stability in metal colloids*. *Colloid & Polymer Science*, 1972. **250**(7): p. 736-741.
70. Kimling, J., M. Maier, B. Okenve, V. Kotaidis, H. Ballot, and A. Plech, *Turkevich method for gold nanoparticle synthesis revisited*. *The Journal of Physical Chemistry B*, 2006. **110**(32): p. 15700-15707.
71. Piella, J.B., Neus G.; Puentes, Victor, *Size-Controlled Synthesis of Sub-10-nanometer Citrate-Stabilized Gold Nanoparticles and Related Optical Properties*. *Chem. Mater*, 2016. **28**(4): p. 1066-1075.
72. Brust, M., M. Walker, D. Bethell, D.J. Schiffrin, and R. Whyman, *Synthesis of thiol-derivatised gold nanoparticles in a two-phase liquid-liquid system*. *Journal of the Chemical Society, Chemical Communications*, 1994(7): p. 801-802.
73. Alkilany, A.M. and C.J. Murphy, *Toxicity and cellular uptake of gold nanoparticles: what we have learned so far?* *Journal of nanoparticle research*, 2010. **12**(7): p. 2313-2333.
74. Shukla, R., V. Bansal, M. Chaudhary, A. Basu, R.R. Bhonde, and M. Sastry, *Biocompatibility of gold nanoparticles and their endocytotic fate inside the cellular compartment: a microscopic overview*. *Langmuir*, 2005. **21**(23): p. 10644-10654.
75. Connor, E.E., J. Mwamuka, A. Gole, C.J. Murphy, and M.D. Wyatt, *Gold nanoparticles are taken up by human cells but do not cause acute cytotoxicity*. *Small*, 2005. **1**(3): p. 325-327.
76. Fratoddi, I., I. Venditti, C. Cametti, and M.V. Russo, *How toxic are gold nanoparticles? The state-of-the-art*. *Nano Research*, 2015. **8**(6): p. 1771-1799.

77. Haume, K., S. Rosa, S. Grellet, M.A. Śmiałek, K.T. Butterworth, A.V. Solov'yov, . . . N.J. Mason, *Gold nanoparticles for cancer radiotherapy: a review*. *Cancer Nanotechnology*, 2016. **7**(1): p. 8.
78. Patra, H.K., S. Banerjee, U. Chaudhuri, P. Lahiri, and A.K. Dasgupta, *Cell selective response to gold nanoparticles*. *Nanomedicine: Nanotechnology, Biology and Medicine*, 2007. **3**(2): p. 111-119.
79. Tsoli, M., H. Kuhn, W. Brandau, H. Esche, and G. Schmid, *Cellular uptake and toxicity of Au55 clusters*. *Small*, 2005. **1**(8-9): p. 841-844.
80. Goodman, C.M., C.D. McCusker, T. Yilmaz, and V.M. Rotello, *Toxicity of gold nanoparticles functionalized with cationic and anionic side chains*. *Bioconjugate Chemistry*, 2004. **15**(4): p. 897-900.
81. Pan, Y., S. Neuss, A. Leifert, M. Fischler, F. Wen, U. Simon, . . . W. Jahnen-Dechent, *Size-dependent cytotoxicity of gold nanoparticles*. *Small*, 2007. **3**(11): p. 1941-1949.
82. Pan, Y., A. Leifert, D. Ruau, S. Neuss, J. Bornemann, G. Schmid, . . . W. Jahnen-Dechent, *Gold nanoparticles of diameter 1.4 nm trigger necrosis by oxidative stress and mitochondrial damage*. *Small*, 2009. **5**(18): p. 2067-2076.
83. Zhang, X.-D., D. Wu, X. Shen, J. Chen, Y.-M. Sun, P.-X. Liu, and X.-J. Liang, *Size-dependent radiosensitization of PEG-coated gold nanoparticles for cancer radiation therapy*. *Biomaterials*, 2012. **33**(27): p. 6408-6419.
84. Zhang, Z., A. Berg, H. Levanon, R.W. Fessenden, and D. Meisel, *On the interactions of free radicals with gold nanoparticles*. *Journal of the American Chemical Society*, 2003. **125**(26): p. 7959-7963.
85. Ionita, P., M. Conte, B.C. Gilbert, and V. Chechik, *Gold nanoparticle-initiated free radical oxidations and halogen abstractions*. *Organic & biomolecular chemistry*, 2007. **5**(21): p. 3504-3509.
86. Xia, T., M. Kovochich, J. Brant, M. Hotze, J. Sempf, T. Oberley, . . . A.E. Nel, *Comparison of the abilities of ambient and manufactured nanoparticles to induce cellular toxicity according to an oxidative stress paradigm*. *Nano Letters*, 2006. **6**(8): p. 1794-1807.

87. Soenen, S.J., P. Rivera-Gil, J.-M. Montenegro, W.J. Parak, S.C. De Smedt, and K. Braeckmans, *Cellular toxicity of inorganic nanoparticles: common aspects and guidelines for improved nanotoxicity evaluation*. *Nano Today*, 2011. **6**(5): p. 446-465.
88. Bae, Y.H. and K. Park, *Targeted drug delivery to tumors: myths, reality and possibility*. *Journal of Controlled Release*, 2011. **153**(3): p. 198.
89. Danhier, F., O. Feron, and V. Préat, *To exploit the tumor microenvironment: passive and active tumor targeting of nanocarriers for anti-cancer drug delivery*. *Journal of Controlled Release*, 2010. **148**(2): p. 135-146.
90. Surk, C.D., Daniel, *Angiogenesis*, in *The Basic Science of Oncology*, I.F.H. Tannock, Richard P.; Bristow, Robert G.; Harrington, Lea, Editor. 2005, McGraw-Hill Companies: Toronto. p. 231-248.
91. Hashizume, H., P. Baluk, S. Morikawa, J.W. McLean, G. Thurston, S. Roberge, . . . D.M. McDonald, *Openings between defective endothelial cells explain tumor vessel leakiness*. *The American journal of pathology*, 2000. **156**(4): p. 1363-1380.
92. Puri, A., K. Loomis, B. Smith, J.-H. Lee, A. Yavlovich, E. Heldman, and R. Blumenthal, *Lipid-based nanoparticles as pharmaceutical drug carriers: from concepts to clinic*. *Critical Reviews™ in Therapeutic Drug Carrier Systems*, 2009. **26**(6).
93. Ranganathan, R., S. Madanmohan, A. Kesavan, G. Baskar, Y.R. Krishnamoorthy, R. Santosham, . . . G. Venkatraman, *Nanomedicine: towards development of patient-friendly drug-delivery systems for oncological applications*. *Int J Nanomedicine*, 2012. **7**(1043): p. e1060.
94. Torchilin, V.P., *Drug targeting*. *European Journal of Pharmaceutical Sciences*, 2000. **11**: p. S81-S91.
95. Multhoff, G. and P. Vaupel, *Radiation-induced changes in microcirculation and interstitial fluid pressure affecting the delivery of macromolecules and nanotherapeutics to tumors*. *Frontiers in oncology*, 2012. **2**: p. 165.
96. Jain, R.K., *Normalizing tumor vasculature with anti-angiogenic therapy: a new paradigm for combination therapy*. *Nature Medicine*, 2001. **7**(9): p. 987.

97. Yameen, B., W.I. Choi, C. Vilos, A. Swami, J. Shi, and O.C. Farokhzad, *Insight into nanoparticle cellular uptake and intracellular targeting*. Journal of Controlled Release, 2014. **190**: p. 485-499.
98. Yohan, D., C. Cruje, X. Lu, and D. Chithrani, *Elucidating the uptake and distribution of nanoparticles in solid tumors via a multilayered cell culture model*. Nano-Micro Letters, 2015. **7**(2): p. 127-137.
99. Liotta, L.A., U.P. Thorgeirsson, and S. Garbisa, *Role of collagenases in tumor cell invasion*. Cancer and Metastasis Reviews, 1982. **1**(4): p. 277-288.
100. Gross, J. and Y. Nagai, *Specific degradation of the collagen molecule by tadpole collagenolytic enzyme*. Proceedings of the National Academy of Sciences, 1965. **54**(4): p. 1197-1204.
101. Yohan, D., *Gold Nanoparticle Transport in Multilayered Cell Cultures*, in *Biomedical Physics*. 2015, Ryerson University: Toronto.
102. Fröhlich, E., *The role of surface charge in cellular uptake and cytotoxicity of medical nanoparticles*. Int J Nanomedicine, 2012. **7**(1): p. 5577-91.
103. Trono, J.D., K. Mizuno, N. Yusa, T. Matsukawa, K. Yokoyama, and M. Uesaka, *Size, concentration and incubation time dependence of gold nanoparticle uptake into pancreas cancer cells and its future application to X-ray drug delivery system*. Journal of radiation research, 2010. **52**(1): p. 103-109.
104. Chithrani, B.D., A.A. Ghazani, and W.C. Chan, *Determining the size and shape dependence of gold nanoparticle uptake into mammalian cells*. Nano Letters, 2006. **6**(4): p. 662-668.
105. Bajaj, A., O.R. Miranda, I.-B. Kim, R.L. Phillips, D.J. Jerry, U.H. Bunz, and V.M. Rotello, *Detection and differentiation of normal, cancerous, and metastatic cells using nanoparticle-polymer sensor arrays*. Proceedings of the National Academy of Sciences, 2009. **106**(27): p. 10912-10916.
106. Gal, N., S. Massalha, O. Samuelli-Nafta, and D. Weihs, *Effects of particle uptake, encapsulation, and localization in cancer cells on intracellular applications*. Medical engineering & physics, 2015. **37**(5): p. 478-483.
107. Oh, N.P., Ji-Ho, *Endocytosis and exocytosis of nanoparticles in mammalian cells*. International Journal of Nanomedicine, 2014. **9**: p. 51-63.

108. Alberts, B., A. Johnson, J. Lewis, M. Raff, K. Roberts, and P. Walter, *Transport into the cell from the plasma membrane: endocytosis*. 2002.
109. Kirchhausen, T., *Three ways to make a vesicle*. *Nature reviews Molecular cell biology*, 2000. **1**(3): p. 187-198.
110. Kam, N.W., Z. Liu, and H. Dai, *Carbon nanotubes as intracellular transporters for proteins and DNA: an investigation of the uptake mechanism and pathway*. *Angewandte Chemie*, 2006. **45**(4): p. 577-581.
111. Mukherjee, S., R.N. Ghosh, and F.R. Maxfield, *Endocytosis*. *Physiological Reviews*, 1997. **77**(3): p. 759-803.
112. Jin, H., D.A. Heller, R. Sharma, and M.S. Strano, *Size-dependent cellular uptake and expulsion of single-walled carbon nanotubes: single particle tracking and a generic uptake model for nanoparticles*. *ACS nano*, 2009. **3**(1): p. 149-158.
113. Schroter, C.J., M. Braun, J. Englert, H. Beck, H. Schmid, and H. Kalbacher, *A rapid method to separate endosomes from lysosomal contents using differential centrifugation and hypotonic lysis of lysosomes*. *Journal of Immunological Methods*, 1999. **227**(1-2): p. 161-168.
114. Silverstein, S.C., R.M. Steinman, and Z.A. Cohn, *Endocytosis*. *Annual Review of Biochemistry*, 1977. **46**(1): p. 669-722.
115. Liu, M., Q. Li, L. Liang, J. Li, K. Wang, J. Li, . . . J. Lee, *Real-time visualization of clustering and intracellular transport of gold nanoparticles by correlative imaging*. *Nature Communications*, 2017. **8**: p. 1-10.
116. Jiang, Y., S. Huo, T. Mizuhara, R. Das, Y.-W. Lee, S. Hou, . . . V.M. Rotello, *The interplay of size and surface functionality on the cellular uptake of sub-10 nm gold nanoparticles*. *ACS nano*, 2015. **9**(10): p. 9986-9993.
117. Iversen, T.-G.S., Tore; Sandvig, Kirsten, *Endocytosis and intracellular transport of nanoparticles: Present knowledge and need for future studies*. *Nano Today*, 2011. **6**: p. 176-185.

118. Selby, L.I., C.M. Cortez-Jugo, G.K. Such, and A.P. Johnston, *Nanoescapology: Progress toward understanding the endosomal escape of polymeric nanoparticles*. Wiley Interdisciplinary Reviews: Nanomedicine and Nanobiotechnology, 2017. **9**(5).
119. Lévy, R., N.T. Thanh, R.C. Doty, I. Hussain, R.J. Nichols, D.J. Schiffrin, . . . D.G. Fernig, *Rational and combinatorial design of peptide capping ligands for gold nanoparticles*. Journal of the American Chemical Society, 2004. **126**(32): p. 10076-10084.
120. El-Sayed, A., I.A. Khalil, K. Kogure, S. Futaki, and H. Harashima, *Octaarginine-and octalysine-modified nanoparticles have different modes of endosomal escape*. Journal of Biological Chemistry, 2008. **283**(34): p. 23450-23461.
121. Levy, R., U. Shaheen, Y. Cesbron, and V. See, *Gold nanoparticles delivery in mammalian live cells: a critical review*. Nano reviews, 2010. **1**(1): p. 4889.
122. Qian, W., T. Curry, Y. Che, and R. Kopelman. *Targeted delivery of peptide-conjugated biocompatible gold nanoparticles into cancer cell nucleus*. in *SPIE BiOS*. 2013. International Society for Optics and Photonics.
123. Li, D., Q. Li, X. Hao, Y. Zhang, Z. Zhang, and C. Li, *Assembled Core-Shell Nanostructures of Gold Nanoparticles with Biocompatible Polymers Toward Biology*. Current Topics in Medicinal Chemistry, 2014. **14**(5): p. 595-616.
124. Tkachenko, A.G., H. Xie, D. Coleman, W. Glomm, J. Ryan, M.F. Anderson, . . . D.L. Feldheim, *Multifunctional gold nanoparticle-peptide complexes for nuclear targeting*. Journal of the American Chemical Society, 2003. **125**(16): p. 4700-4701.
125. Fernandez-Martinez, J. and M.P. Rout, *Nuclear pore complex biogenesis*. Current Opinion in Cell Biology, 2009. **21**(4): p. 603-612.
126. Wentz, S.R. and M.P. Rout, *The nuclear pore complex and nuclear transport*. Cold Spring Harbor perspectives in biology, 2010. **2**(10).
127. Suntharalingam, M. and S.R. Wentz, *Peering through the pore: nuclear pore complex structure, assembly, and function*. Developmental Cell, 2003. **4**(6): p. 775-789.

128. Alberts, B., A. Johnson, J. Lewis, M. Raff, K. Roberts, and P. Walter, *The transport of molecules between the nucleus and the cytosol*. 2002.
129. Yang, C., J. Uertz, D. Yohan, and B. Chithrani, *Peptide modified gold nanoparticles for improved cellular uptake, nuclear transport, and intracellular retention*. *Nanoscale*, 2014. **6**(20): p. 12026-12033.
130. Bartczak, D., S. Nitti, T.M. Millar, and A.G. Kanaras, *Exocytosis of peptide functionalized gold nanoparticles in endothelial cells*. *Nanoscale*, 2012. **4**(15): p. 4470-4472.
131. Chithrani, B.D. and W.C.W. Chan, *Elucidating the Mechanism of Cellular Uptake and Removal of Protein-Coated Gold Nanoparticles of Different Sizes and Shapes*. *Nano Lett*, 2007. **7**: p. 1542-1550.
132. Bartczak, D., T. Sanchez-Elsner, F. Louafi, T.M. Millar, and A.G. Kanaras, *Receptor-mediated interactions between colloidal gold nanoparticles and human umbilical vein endothelial cells*. *Small*, 2011. **7**: p. 388–394.
133. Wang, Z., N. Li, J. Zhao, J.C. White, P. Qu, and B. Xing, *CuO nanoparticle interaction with human epithelial cells: cellular uptake, location, export, and genotoxicity*. *Chem Res Toxicol*, 2012. **25**: p. 1512–1521.
134. Chu, Z., Y. Huang, Q. Tao, and Q. Li, *Cellular uptake evolution, and excretion of silica nanoparticles in human cells*. *Nanoscale*, 2011. **3**: p. 3291–3299.
135. Pengo, P., Q.B. Broxterman, B. Kaptein, L. Pasquato, and P. Scrimin, *Synthesis of a stable helical peptide and grafting on gold nanoparticles*. *Langmuir*, 2003. **19**(6): p. 2521-2524.
136. D'Souza, S.E., M.H. Ginsberg, and E.F. Plow, *Arginyl-glycyl-aspartic acid (RGD): a cell adhesion motif*. *Trends in Biochemical Sciences*, 1991. **16**: p. 246-250.
137. Gehlsen, K.R., W.S. Argraves, M.D. Pierschbacher, and E. Ruoslahti, *Inhibition of in vitro tumor cell invasion by Arg-Gly-Asp-containing synthetic peptides*. *The Journal of cell biology*, 1988. **106**(3): p. 925-930.
138. Ruoslahti, E. and M.D. Pierschbacher, *New perspectives in cell adhesion: RGD and integrins*. *Science*, 1987. **238**(4826): p. 491-498.

139. Wang, F., Y. Li, Y. Shen, A. Wang, S. Wang, and T. Xie, *The functions and applications of RGD in tumor therapy and tissue engineering*. International journal of molecular sciences, 2013. **14**(7): p. 13447-13462.
140. Ruoslahti, E., *Peptides as targeting elements and tissue penetration devices for nanoparticles*. Advanced Materials, 2012. **24**(28): p. 3747-3756.
141. Gao, H., W. Shi, and L.B. Freund, *Mechanics of receptor-mediated endocytosis*. Proceedings of the National Academy of Sciences of the United States of America, 2005. **102**(27): p. 9469-9474.
142. Alberts, B., D. Bray, J. Lewis, M. Raff, K. Roberts, and J.D. Watson, *Molecular biology of the cell*. 4 ed. Garland, New York. 2002.
143. Naik, S., D. Patel, K. Chuttani, A.K. Mishra, and A. Misra, *In vitro mechanistic study of cell death and in vivo performance evaluation of RGD grafted PEGylated docetaxel liposomes in breast cancer*. Nanomedicine: Nanotechnology, Biology and Medicine, 2012. **8**(6): p. 951-962.
144. Xu, Q., Y. Liu, S. Su, W. Li, C. Chen, and Y. Wu, *Anti-tumor activity of paclitaxel through dual-targeting carrier of cyclic RGD and transferrin conjugated hyperbranched copolymer nanoparticles*. Biomaterials, 2012. **33**(5): p. 1627-1639.
145. Zhang, L., S. Zhu, L. Qian, Y. Pei, Y. Qiu, and Y. Jiang, *RGD-modified PEG–PAMAM–DOX conjugates: in vitro and in vivo studies for glioma*. European Journal of Pharmaceutics and Biopharmaceutics, 2011. **79**(2): p. 232-240.
146. Zhang, Y.-f., J.-c. Wang, D.-y. Bian, X. Zhang, and Q. Zhang, *Targeted delivery of RGD-modified liposomes encapsulating both combretastatin A-4 and doxorubicin for tumor therapy: in vitro and in vivo studies*. European journal of pharmaceutics and biopharmaceutics, 2010. **74**(3): p. 467-473.
147. Shayakhmetov, D.M., A.M. Eberly, Z.-Y. Li, and A. Lieber, *Deletion of penton RGD motifs affects the efficiency of both the internalization and the endosome escape of viral particles containing adenovirus serotype 5 or 35 fiber knobs*. Journal of Virology, 2005. **79**(2): p. 1053-1061.
148. Tkachenko, A.G., H. Xie, Y. Liu, D. Coleman, J. Ryan, W.R. Glomm, . . . D.L. Feldheim, *Cellular trajectories of peptide-modified gold particle complexes: comparison of nuclear localization signals and peptide transduction domains*. Bioconjugate Chemistry, 2004. **15**(3): p. 482-490.

149. Park, S.H., S.G. Oh, J.Y. Mun, and S.S. Han, *Loading of gold nanoparticles inside the DPPC bilayers of liposome and their effects on membrane fluidities*. Colloids and surfaces.B, Biointerfaces, 2006. **48**(2): p. 112-118.
150. Nativo, P., I.A. Prior, and M. Brust, *Uptake and intracellular fate of surface-modified gold nanoparticles*. ACS nano, 2008. **2**(8): p. 1639-1644.
151. Chen, P.C., S.C. Mwakwari, and A.K. Oyelere, *Gold nanoparticles: from nanomedicine to nanosensing*. Nanotechnology, science and applications, 2008. **1**: p. 45.
152. Gao, H., W. Shi, and L.B. Freund, *Mechanics of receptor-mediated endocytosis*. . Proc Natl Acad Sci USA, 2005. **102**: p. 9469-9474.
153. Shi, W., Wang J, Fan X, Gao H, *Size and shape effects on diffusion and absorption of colloidal particles near a partially absorbing sphere: Implications for uptake of nanoparticles in animal cells*. Phy Rev E, 2008. **78**: p. 061914-061925.
154. Zhang, S., J. Li, G. Lykotrafitis, G. Bao, and S. Suresh, *Size-dependent Endocytosis of Nanoparticles*. Adv Mater, 2009. **21**: p. 419-424.
155. Chakarov, S., R. Petkova, G.C. Russev, and N. Zhelev, *DNA damage and mutation. Types of DNA damage*. BioDiscovery, 2014. **11**.
156. Lindahl, T., *Instability and decay of the primary structure of DNA*. nature, 1993. **362**(6422): p. 709-715.
157. De Bont, R. and N. Van Larebeke, *Endogenous DNA damage in humans: a review of quantitative data*. Mutagenesis, 2004. **19**(3): p. 169-185.
158. Rodier, F. and J. Campisi, *Four faces of cellular senescence*. The Journal of cell biology, 2011. **192**: p. 547-556.
159. Harding, S.M. and R.G. Bristow, *Discordance between phosphorylation and recruitment of 53BP1 in response to DNA double-strand breaks*. Cell Cycle, 2012. **11**(7): p. 1432-1444.
160. Banáth, J.P., D. Klovov, S.H. MacPhail, C.A. Banuelos, and P.L. Olive, *Residual γ H2AX foci as an indication of lethal DNA lesions*. BMC Cancer, 2010. **10**(1): p. 4.

161. Jackson, S.P. and J. Bartek, *The DNA-damage response in human biology and disease*. nature, 2009. **461**(7267): p. 1071.
162. Menon, V. and L. Povirk, *Involvement of p53 in the repair of DNA double strand breaks: multifaceted Roles of p53 in homologous recombination repair (HRR) and non-homologous end joining (NHEJ)*, in *Mutant p53 and MDM2 in Cancer*. 2014, Springer. p. 321-336.
163. Panier, S. and S.J. Boulton, *Double-strand break repair: 53BP1 comes into focus*. Nature Reviews Molecular Cell Biology, 2014. **15**(1): p. 7-18.
164. Schultz, L.B., N.H. Chehab, A. Malikzay, and T.D. Halazonetis, *p53 binding protein 1 (53BP1) is an early participant in the cellular response to DNA double-strand breaks*. The Journal of cell biology, 2000. **151**(7): p. 1381-1390.
165. Boeckman, H.J., K.S. Trego, and J.J. Turchi, *Cisplatin sensitizes cancer cells to ionizing radiation via inhibition of nonhomologous end joining*. Molecular Cancer Research, 2005. **3**(5): p. 277-285.
166. Huang, L.-C., K.C. Clarkin, and G.M. Wahl, *Sensitivity and selectivity of the DNA damage sensor responsible for activating p53-dependent G1 arrest*. Proceedings of the National Academy of Sciences, 1996. **93**(10): p. 4827-4832.
167. Dasari, S. and P.B. Tchounwou, *Cisplatin in cancer therapy: molecular mechanisms of action*. European Journal of Pharmacology, 2014. **740**: p. 364-378.
168. Kroemer, G., L. Galluzzi, P. Vandenabeele, J. Abrams, E. Alnemri, E. Baehrecke, . . . D. Green, *Classification of cell death: recommendations of the Nomenclature Committee on Cell Death 2009*. Cell death & differentiation, 2009. **16**(1): p. 3-11.
169. Umezawa, Y., H. Morishima, S. Saito, T. Takita, H. Umezawa, S. Kobayashi, . . . M. Ohno, *Synthesis of the pyrimidine moiety of bleomycin*. Journal of the American Chemical Society, 1980. **102**(21): p. 6630-6631.
170. Hecht, S.M., *The chemistry of activated bleomycin*. Accounts of Chemical Research, 1986. **19**(12): p. 383-391.
171. Umezawa, H.M., K., Takeuchi T.; Okami Y., *New Antibiotics: Bleomycin A and B*. Journal of Antibiotics, 1966. **19**: p. 200-209.

172. Siu, L.L.M., Malcolm J., *Pharmacology of anticancer drugs*, in *The basic science oncology*, I.F.H. Tannock, Richard P.; Bristow, Robert G.; Harrington, Lea, Editor. 2005, McGraw-Hill: Toronto. p. 322-348.
173. Kuramochi, H.T., Katsutoshi; Takita, Tomohisa, *An Active Intermediate Formed in the Reaction of Bleomycin-Fe(II) Complex with Oxygen*. *The Journal of Antibiotics* 1981. **34**(5): p. 576-582.
174. Jamieson, E.R. and S.J. Lippard, *Structure, recognition, and processing of cisplatin-DNA adducts*. *Chemical Reviews*, 1999. **99**(9): p. 2467-2498.
175. Lippard, S.J., *New chemistry of an old molecule: cis-[Pt(NH₃)₂Cl₂]*. *Science (New York, N.Y.)*, 1982. **218**(4577): p. 1075-1082.
176. Rosenberg, B., L. VanCamp, J.E. Trosko, and V.H. Mansour, *Platinum compounds: a new class of potent antitumour agents*. *nature*, 1969. **222**(5191): p. 385-386.
177. Rosenberg, B. and L. VanCamp, *The successful regression of large solid sarcoma 180 tumors by platinum compounds*. *Cancer Research*, 1970. **30**(6): p. 1799-1802.
178. Kociba, R.J., S.D. Sleight, and B. Rosenberg, *Inhibition of Dunning asc itic leukemia and Walker 256 carcinosarcoma with cis-diamminedichloroplatinum (NSC-119875)*. *Cancer chemotherapy reports.Part 1*, 1970. **54**(5): p. 325-328.
179. Keys, H.M., B.N. Bundy, F.B. Stehman, L.I. Muderspach, W.E. Chafe, C.L. Suggs, 3rd, . . . D. Gersell, *Cisplatin, radiation, and adjuvant hysterectomy compared with radiation and adjuvant hysterectomy for bulky stage IB cervical carcinoma*. *The New England journal of medicine*, 1999. **340**(15): p. 1154-1161.
180. Loehrer, P.J. and L.H. Einhorn, *Drugs five years later. Cisplatin*. *Annals of Internal Medicine*, 1984. **100**(5): p. 704-713.
181. Morris, M., P.J. Eifel, J. Lu, P.W. Grigsby, C. Levenback, R.E. Stevens, . . . D.G. Mutch, *Pelvic radiation with concurrent chemotherapy compared with pelvic and para-aortic radiation for high-risk cervical cancer*. *The New England journal of medicine*, 1999. **340**(15): p. 1137-1143.

182. Rose, P.G., B.N. Bundy, E.B. Watkins, J.T. Thigpen, G. Deppe, M.A. Maiman, . . . S. Insalaco, *Concurrent cisplatin-based radiotherapy and chemotherapy for locally advanced cervical cancer*. The New England journal of medicine, 1999. **340**(15): p. 1144-1153.
183. Bosl, G.J. and R.J. Motzer, *Testicular germ-cell cancer*. The New England journal of medicine, 1997. **337**(4): p. 242-253.
184. Hayes, D.M., E. Cvitkovic, R.B. Golbey, E. Scheiner, L. Helson, and I.H. Krakoff, *High dose Cis-platinum diammine dichloride. Amelioration of renal toxicity by mannitol diuresis*. Cancer, 1977. **39**(4): p. 1372-1381.
185. Andrews, P.A., S. Velury, S.C. Mann, and S.B. Howell, *cis-Diamminedichloroplatinum(II) accumulation in sensitive and resistant human ovarian carcinoma cells*. Cancer Research, 1988. **48**(1): p. 68-73.
186. Eljack, N.D., H.-Y.M. Ma, J. Drucker, C. Shen, T.W. Hambley, E.J. New, . . . R.J. Clarke, *Mechanisms of cell uptake and toxicity of the anticancer drug cisplatin*. Metallomics, 2014. **6**(11): p. 2126-2133.
187. Safaei, R., *Role of copper transporters in the uptake and efflux of platinum containing drugs*. Cancer Letters, 2006. **234**(1): p. 34-39.
188. Hall, M.D., M. Okabe, D.-W. Shen, X.-J. Liang, and M.M. Gottesman, *The role of cellular accumulation in determining sensitivity to platinum-based chemotherapy*. Annual Review of Pharmacology and Toxicology, 2008. **48**: p. 495-535.
189. Arnesano, F., M. Losacco, and G. Natile, *An updated view of cisplatin transport*. European Journal of Inorganic Chemistry, 2013. **2013**(15): p. 2701-2711.
190. Ivy, K.D. and J.H. Kaplan, *A re-evaluation of the role of hCTR1, the human high-affinity copper transporter, in platinum-drug entry into human cells*. Molecular Pharmacology, 2013. **83**(6): p. 1237-1246.
191. Cohen, G.L., W.R. Bauer, J.K. Barton, and S.J. Lippard, *Binding of cis-and trans-dichlorodiammineplatinum (II) to DNA: evidence for unwinding and shortening of the double helix*. Science, 1979. **203**(4384): p. 1014-1016.

192. Macquet, J.-P. and J.-L. Butour, *Modifications of the DNA secondary structure upon platinum binding: a proposed model*. *Biochimie*, 1978. **60**(9): p. 901-914.
193. Sorenson, C.M. and A. Eastman, *Influence of cis-diamminedichloroplatinum(II) on DNA synthesis and cell cycle progression in excision repair proficient and deficient Chinese hamster ovary cells*. *Cancer Research*, 1988. **48**(23): p. 6703-6707.
194. Sorenson, C.M. and A. Eastman, *Mechanism of cis-diamminedichloroplatinum(II)-induced cytotoxicity: role of G2 arrest and DNA double-strand breaks*. *Cancer Research*, 1988. **48**(16): p. 4484-4488.
195. Sorenson, C.M., M.A. Barry, and A. Eastman, *Analysis of events associated with cell cycle arrest at G2 phase and cell death induced by cisplatin*. *Journal of the National Cancer Institute*, 1990. **82**(9): p. 749-755.
196. Psyrri, A., M. Kwong, S. DiStasio, L. Lekakis, M. Kassir, C. Sasaki, . . . D. Ross, *Cisplatin, fluorouracil, and leucovorin induction chemotherapy followed by concurrent cisplatin chemoradiotherapy for organ preservation and cure in patients with advanced head and neck cancer: long-term follow-up*. *Journal of Clinical Oncology*, 2004. **22**(15): p. 3061-3069.
197. Kavanagh, J.N., K.M. Redmond, G. Schettino, and K.M. Prise, *DNA double strand break repair: a radiation perspective*. *Antioxidants & redox signaling*, 2013. **18**(18): p. 2458-2472.
198. Nikjoo, H., P. O'Neill, W. Wilson, and D. Goodhead, *Computational approach for determining the spectrum of DNA damage induced by ionizing radiation*. *Radiation Research*, 2001. **156**(5): p. 577-583.
199. Kwatra, D., A. Venugopal, and S. Anant, *Nanoparticles in radiation therapy: a summary of various approaches to enhance radiosensitization in cancer*. *Translational Cancer Research*, 2013. **2**(4): p. 330-342.
200. Pan, X., P. Cloutier, D. Hunting, and L. Sanche, *Dissociative electron attachment to DNA*. *Physical Review Letters*, 2003. **90**(20): p. 208102.
201. Kobayashi, K., N. Usami, E. Porcel, S. Lacombe, and C. Le Sech, *Enhancement of radiation effect by heavy elements*. *Mutation Research/Reviews in Mutation Research*, 2010. **704**(1): p. 123-131.

202. Das, I.J. and K.L. Chopra, *Backscatter dose perturbation in kilovoltage photon beams at high atomic number interfaces*. Medical physics, 1995. **22**(6): p. 767-773.
203. Das, I.J., *Forward dose perturbation at high atomic number interfaces in kilovoltage x-ray beams*. Medical physics, 1997. **24**(11): p. 1781-1787.
204. Santos Mello, R., H. Callisen, J. Winter, A.R. Kagan, and A. Norman, *Radiation dose enhancement in tumors with iodine*. Medical physics, 1983. **10**(1): p. 75-78.
205. Nath, R., P. Bongiorno, and S. Rockwell, *Iododeoxyuridine radiosensitization by low- and high-energy photons for brachytherapy dose rates*. Radiation Research, 1990. **124**(3): p. 249-258.
206. Kim, D., S. Park, J.H. Lee, Y.Y. Jeong, and S. Jon, *Antibiofouling polymer-coated gold nanoparticles as a contrast agent for in vivo X-ray computed tomography imaging*. Journal of the American Chemical Society, 2007. **129**(24): p. 7661-7665.
207. Haller, C. and I. Hizoh, *The cytotoxicity of iodinated radiocontrast agents on renal cells in vitro*. Investigative radiology, 2004. **39**(3): p. 149-154.
208. Hizoh, I. and C. Haller, *Radiocontrast-induced renal tubular cell apoptosis: hypertonic versus oxidative stress*. Investigative radiology, 2002. **37**(8): p. 428-434.
209. Regulla, D.F., L.B. Hieber, and M. Seidenbusch, *Physical and biological interface dose effects in tissue due to X-ray-induced release of secondary radiation from metallic gold surfaces*. Radiation Research, 1998. **150**(1): p. 92-100.
210. Herold, D.M., I.J. Das, C.C. Stobbe, R.V. Iyer, and J.D. Chapman, *Gold microspheres: a selective technique for producing biologically effective dose enhancement*. International Journal of Radiation Biology, 2000. **76**(10): p. 1357-1364.
211. Rahman, W.N., N. Bishara, T. Ackerly, C.F. He, P. Jackson, C. Wong, . . . M. Geso, *Enhancement of radiation effects by gold nanoparticles for superficial radiation therapy*. Nanomedicine : nanotechnology, biology, and medicine, 2009. **5**(2): p. 136-142.
212. Hainfeld, J.F., D.N. Slatkin, and H.M. Smilowitz, *The use of gold nanoparticles to enhance radiotherapy in mice*. Physics in medicine and biology, 2004. **49**(18): p. N309.

213. Neshatian, M., S. Chung, D. Yohan, C. Yang, and D.B. Chithrani, *Determining the size dependence of colloidal gold nanoparticle uptake in a tumor-like interface (hypoxic)*. *Colloids and Interface Science Communications*, 2014. **1**: p. 57-61.
214. Lewinski, N., V. Colvin, and R. Drezek, *Cytotoxicity of nanoparticles*. *Small* (Weinheim an der Bergstrasse, Germany), 2008. **4**(1): p. 26-49.
215. Matsudaira, H., A.M. Ueno, and I. Furuno, *Iodine contrast medium sensitizes cultured mammalian cells to X rays but not to gamma rays*. *Radiation Research*, 1980. **84**(1): p. 144-148.
216. Norman, A., M. Ingram, R.G. Skillen, D.B. Freshwater, K.S. Iwamoto, and T. Solberg, *X-ray phototherapy for canine brain masses*. *Radiation Oncology Investigations*, 1997. **5**(1): p. 8-14.
217. Unezaki, S., K. Maruyama, J.-I. Hosoda, I. Nagae, Y. Koyanagi, M. Nakata, . . . S. Tsuchiya, *Direct measurement of the extravasation of polyethyleneglycol-coated liposomes into solid tumor tissue by in vivo fluorescence microscopy*. *International Journal of Pharmaceutics*, 1996. **144**(1): p. 11-17.
218. Cho, S.H., *Estimation of tumour dose enhancement due to gold nanoparticles during typical radiation treatments: a preliminary Monte Carlo study*. *Physics in medicine and biology*, 2005. **50**(15): p. N163.
219. Carter, J.D., N.N. Cheng, Y. Qu, G.D. Suarez, and T. Guo, *Nanoscale energy deposition by X-ray absorbing nanostructures*. *The Journal of Physical Chemistry B*, 2007. **111**(40): p. 11622-11625.
220. Cho, S.H., B.L. Jones, and S. Krishnan, *The dosimetric feasibility of gold nanoparticle-aided radiation therapy (GNRT) via brachytherapy using low-energy gamma-/x-ray sources*. *Physics in medicine and biology*, 2009. **54**(16): p. 4889.
221. Jones, B.L., S. Krishnan, and S.H. Cho, *Estimation of microscopic dose enhancement factor around gold nanoparticles by Monte Carlo calculations*. *Medical physics*, 2010. **37**(7): p. 3809-3816.
222. Lechtman, E., N. Chattopadhyay, Z. Cai, S. Mashouf, R. Reilly, and J. Pignol, *Implications on clinical scenario of gold nanoparticle radiosensitization in regards to photon energy, nanoparticle size, concentration and location*. *Physics in medicine and biology*, 2011. **56**(15): p. 4631.

223. Kong, T., J. Zeng, X. Wang, X. Yang, J. Yang, S. McQuarrie, . . . J.Z. Xing, *Enhancement of Radiation Cytotoxicity in Breast-Cancer Cells by Localized Attachment of Gold Nanoparticles*. *Small*, 2008. **4**(9): p. 1537-1543.
224. Butterworth, K.T., S.J. McMahon, L.E. Taggart, and K.M. Prise, *Radiosensitization by gold nanoparticles: effective at megavoltage energies and potential role of oxidative stress*. *Translational Cancer Research*, 2013. **2**(4): p. 269-279.
225. Leung, M.K., J.C. Chow, B.D. Chithrani, M.J. Lee, B. Oms, and D.A. Jaffray, *Irradiation of gold nanoparticles by x-rays: Monte Carlo simulation of dose enhancements and the spatial properties of the secondary electrons production*. *Medical physics*, 2011. **38**(2): p. 624-631.
226. Wang, C., X. Li, Y. Wang, Z. Liu, L. Fu, and L. Hu, *Enhancement of radiation effect and increase of apoptosis in lung cancer cells by thio-glucose-bound gold nanoparticles at megavoltage radiation energies*. *Journal of nanoparticle research*, 2013. **15**(5): p. 1642.
227. Wolfe, T., D. Chatterjee, J. Lee, J.D. Grant, S. Bhattarai, R. Taylor, . . . S. Krishnan, *Targeted gold nanoparticles enhance sensitization of prostate tumors to megavoltage radiation therapy in vivo*. *Nanomedicine: Nanotechnology, Biology and Medicine*, 2015. **11**(5): p. 1277-1283.
228. Her, S., D.A. Jaffray, and C. Allen, *Gold nanoparticles for applications in cancer radiotherapy: Mechanisms and recent advancements*. *Advanced drug delivery reviews*, 2017. **109**: p. 84-101.
229. Yao, X., C. Huang, X. Chen, Y. Zheng, and L. Sanche, *Chemical radiosensitivity of DNA induced by gold nanoparticles*. *Journal of biomedical nanotechnology*, 2015. **11**(3): p. 478-485.
230. Misawa, M. and J. Takahashi, *Generation of reactive oxygen species induced by gold nanoparticles under x-ray and UV Irradiations*. *Nanomedicine: Nanotechnology, Biology and Medicine*, 2011. **7**(5): p. 604-614.
231. Cheng, N.N., Z. Starkewolf, R.A. Davidson, A. Sharmah, C. Lee, J. Lien, and T. Guo, *Chemical enhancement by nanomaterials under X-ray irradiation*. *Journal of the American Chemical Society*, 2012. **134**(4): p. 1950-1953.
232. Yang, C., J. Uertz, and D.B. Chithrani, *Colloidal Gold-Mediated Delivery of Bleomycin for Improved Outcome in Chemotherapy*. *Nanomaterials*, 2016. **6**(3): p. 48.

233. Yang, C. and B. Chithrani. *Gold-mediated Drug Delivery for Improved Outcome in Chemotherapy*. in *Proc. of SPIE Vol.* 2017.
234. Yang, C., K. Bromma, and B.D. Chithrani. *Cancer nanomedicine: gold nanoparticle mediated combined cancer therapy*. in *Proc. of SPIE Vol.* 2018.
235. Emerich, D.F. and C.G. Thanos, *Targeted nanoparticle-based drug delivery and diagnosis*. Journal of drug targeting, 2007. **15**(3): p. 163-183.
236. Groneberg, D.A., M. Giersig, T. Welte, and U. Pison, *Nanoparticle-based diagnosis and therapy*. Current Drug Targets, 2006. **7**(6): p. 643-648.
237. Duncan, B., C. Kim, and V.M. Rotello, *Gold nanoparticle platforms as drug and biomacromolecule delivery systems*. Journal of Controlled Release, 2010. **148**(1): p. 122-127.
238. Ferrari, M., *Cancer nanotechnology: opportunities and challenges*. Nature Reviews Cancer, 2005. **5**(3): p. 161-171.
239. Lavan, D.A., T. McGuire, and R. Langer, *Small-scale systems for in vivo drug delivery*. Nature Biotechnology, 2003. **21**(10): p. 1184-1191.
240. Zhang, L., F. Gu, J. Chan, A. Wang, R. Langer, and O. Farokhzad, *Nanoparticles in medicine: therapeutic applications and developments*. Clinical pharmacology & therapeutics, 2008. **83**(5): p. 761-769.
241. Libutti, S.K., G.F. Paciotti, A.A. Byrnes, H.R. Alexander, W.E. Gannon, M. Walker, . . . L. Tamarkin, *Phase I and pharmacokinetic studies of CYT-6091, a novel PEGylated colloidal gold-rhTNF nanomedicine*. Clinical Cancer Research, 2010. **16**(24): p. 6139-6149.
242. Frens, G., *Controlled nucleation for the particle size in monodisperse gold suspensions*. nature, 1973. **241**: p. 20-22.
243. Stoeva, S.I.P., B.L.V.; Uma, Sitharaman; Stoimenov, Peter K.; Zaikovski, Vladimir; Sorensen, Christopher M.; Klabunde, Kenneth J., *Face-Centered Cubic and Hexagonal Closed-Packed Nanocrystal Superlattices of Gold Nanoparticles Prepared by Different Methods*. J. Phys. Chem. B, 2003. **107**: p. 7441-7448.

244. Chithrani, B.D., J. Stewart, C. Allen, and D.A. Jaffray, *Intracellular uptake, transport, and processing of nanostructures in cancer cells*. *Nanomedicine: Nanotechnology, Biology and Medicine*, 2009. **5**(2): p. 118-127.
245. Haiss, W., N.T. Thanh, J. Aveyard, and D.G. Fernig, *Determination of size and concentration of gold nanoparticles from UV-vis spectra*. *Analytical Chemistry*, 2007. **79**(11): p. 4215-4221.
246. Amendola, V. and M. Meneghetti, *Size evaluation of gold nanoparticles by UV-vis spectroscopy*. *The Journal of Physical Chemistry C*, 2009. **113**(11): p. 4277-4285.
247. Coulter, J.A., S. Jain, K.T. Butterworth, L.E. Taggart, G.R. Dickson, S.J. McMahon, . . . A.R. Hounsell, *Cell type-dependent uptake, localization, and cytotoxicity of 1.9 nm gold nanoparticles*. *International Journal of Nanomedicine*, 2012. **7**: p. 2673.
248. Mankovskii, G. and A. Pejovic-Milic, *Total reflection X-Ray Fluorescence based quantification of gold nanoparticles in cancer cells*. *Journal of Analytical Atomic Spectrometry*, 2018.
249. Hakem, R.H., Lea, *Cell Death*, in *The Basic Science of Oncology*, I.F.H. ock, Richard P.; Bristow, Robert G.; Harrington, Lea, Editor. 2005, The McGraw-Hill Companies: Toronto. p. 194-204.
250. Povirk, L.F.W., W.; Kohnlein, W.; Hutchinson, F., *DNA double-strand breaks and alkali-labile bonds produced by bleomycin*. *Nucleic Acids Research*, 1977. **4**: p. 3573-3579.
251. Goodwin, K.D.L., M.K.; Long, E.C.; Georgiadis, M.M., *Crystal structure of DNA-bound Co(III) bleomycin B2: Insights on intercalation and minor groove binding*. *PNAS*, 2008. **105**: p. 5052-5056.
252. Allal, A.S., M. Richter, M. Russo, M. Rouzaud, P. Dulguerov, and J.M. Kurtz, *Dose variation at bone/titanium interfaces using titanium hollow screw osseointegrating reconstruction plates*. *International Journal of Radiation Oncology Biology Physics*, 1998. **40**(1): p. 215-219.
253. Melian, E., M. Fatyga, P. Lam, M. Steinberg, S.P. Reddy, G.J. Petruzzelli, and G.P. Glasgow, *Effect of metal reconstruction plates on cobalt-60 dose distribution: a predictive formula and clinical implications*. *International Journal of Radiation Oncology Biology Physics*, 1999. **44**(3): p. 725-730.

254. Li, X.A., J.C. Chu, W. Chen, and T. Zusag, *Dose enhancement by a thin foil of high-Z material: a Monte Carlo study*. Medical physics, 1999. **26**(7): p. 1245-1251.
255. Almond, P.R., P.J. Biggs, B.M. Coursey, W. Hanson, M.S. Huq, R. Nath, and D. Rogers, *AAPM's TG-51 protocol for clinical reference dosimetry of high-energy photon and electron beams*. Medical physics, 1999. **26**(9): p. 1847-1870.
256. Liu, C.-J., C.-H. Wang, S.-T. Chen, H.-H. Chen, W.-H. Leng, C.-C. Chien, . . . T.-C. Lai, *Enhancement of cell radiation sensitivity by pegylated gold nanoparticles*. Physics in medicine and biology, 2010. **55**(4): p. 931.
257. Begg, A., *Cisplatin and radiation: interaction probabilities and therapeutic possibilities*. International Journal of Radiation Oncology Biology Physics, 1990. **19**(5): p. 1183-1189.
258. Zheng, Y. and L. Sanche, *Gold nanoparticles enhance DNA damage induced by anti-cancer drugs and radiation*. Radiation Research, 2009. **172**(1): p. 114-119.
259. Wilson, G.D., S.M. Bentzen, and P.M. Harari. *Biologic basis for combining drugs with radiation*. in *Seminars in radiation oncology*. 2006. Elsevier.
260. Myint, W., C. Ng, and G. Raaphorst, *Examining the non-homologous repair process following cisplatin and radiation treatments*. International Journal of Radiation Biology, 2002. **78**(5): p. 417-424.
261. Gorodetsky, R., F. Levy-Agababa, X. Mou, and A.M. Vexler, *Combination of cisplatin and radiation in cell culture: effect of duration of exposure to drug and timing of irradiation*. International Journal of Cancer, 1998. **75**(4): p. 635-642.
262. Goldoni, M.J., Carolina, *A mathematical approach to study combined effects of toxicants in vitro: evaluation of the Bliss independence criterion and the Loewe additivity model*. Toxicology in vitro, 2007. **21.5**: p. 759-769.
263. Bliss, C., *The toxicity of poisons applied jointly*. Annals of applied biology, 1939. **26**(3): p. 585-615.

264. Lee, J.J.K., M.; Ayers, G.D.; Lotan, R., *Interaction index and different methods for determining drug interaction in combination therapy*. Journal of biopharmaceutical statistics, 2007. **17**: p. 461-480.
265. Tarapacki, C.K., Raffi, *Enhancing laser therapy using PEGylated gold nanoparticles combined with ultrasound and microbubbles*. Ultrasonics, 2014. **57**: p. 36-43.
266. Hill, R.P.B., Robert B., *The scientific basis of radiotherapy*, in *The basic science of oncology*, I.F.H. Tannock, Richard P.; Bristrow, Robert G.; Harrington, Lea, Editor. 2008, McGraw-Hill: Toronto. p. 289-321.
267. Donovan, J.C.H.S., Joyce; Tannock, Ian F., *Cell proliferation and tumor growth*, in *The basic science of oncology*, I.F.H. Tannock, Richard P.; Bristrow, Robert G.; Harrington, Lea, Editor. 2005, McGraw-Hill: Toronto. p. 167-193.
268. Del Monte, U., *Does the cell number 10^9 still really fit one gram of tumor tissue?* Cell Cycle, 2009. **8**(3): p. 505-506.
269. steel, G.G.P., Michael J., *Exploitable mechanisms in combined radiotherapy-chemotherapy: The concept of additivity*. Int. J. Radiation Oncology Biol. Phys., 1979. **5**: p. 85-91.
270. Nakamura, Y.M., Ai; Choyke, Peter L.; Kobayashi, Hisataka, *Nanodrug Delivery: Is the Enhanced Permeability and Retention Effect Sufficient for Curing Cancer*. Bioconjugate Chemistry, 2016. **27**(10): p. 2225-2238.
271. Cruje, C. and B. Chithrani, *Integration of peptides for enhanced uptake of PEGylated gold nanoparticles*. Journal of nanoscience and nanotechnology, 2015. **15**(3): p. 2125-2131.
272. Cruje, C. and D.B. Chithrani, *Polyethylene Glycol Functionalized Nanoparticles for Improved Cancer Treatment*. Reviews in Nanoscience and Nanotechnology, 2014. **3**(1): p. 20-30.
273. Khawar, I.A.K., Jung Ho; Kuh, Hyo-Jeong, *Improving drug delivery to solid tumors: Priming the tumor microenvironment*. Journal of Controlled Release, 2015. **201**: p. 78-89.
274. Minchinton, A.I.T., Ian F., *Drug penetration in solid tumours*. Nature Reviews Cancer, 2006. **6**(8): p. 583-592.

275. Tong, R.T.B., Yves; Kozin, Sergey V.; Winkler, Frank; Hicklin, Daniel J.; Jain, Rakesh K., *Vascular normalization by vascular endothelial growth factor receptor 2 blockade induces a pressure gradient across the vasculature and improves drug penetration in tumors* Cancer Research, 2004. **64**(11): p. 3731-3736.
276. Sindhvani, S.S., Abdullah Muhammad; Wilhelm, Stefan; Glancy, Dylan R.; Chen, Yih Yang; Dobosz, Michael; Chan, Warren C.W., *Three-Dimensional Optical Mapping of Nanoparticle Distribution in Intact Tissues*. ACS nano, 2016. **10**(5): p. 5468-5478.
277. Netti, P.A.B., David A.; Swartz, Melody A.; Grodzinsky, Alan J.; Jain, Rakesh K., *Role of extracellular matrix assembly in interstitial transport in solid tumors*. Cancer Research, 2000. **60**(9): p. 2497-2503.
278. Mohamed, F.B., D.A.; Winlove, C.P., *Effects of ionizing radiation on extracellular matrix*. Nuclear Instruments and Methods in Physics Research Section A, 2007. **580**(1): p. 566-569.
279. Ji, T.L., Jiayan; Wang, Jing; Cai, Rong; Zhang, Yinlong; Qi, Feifei; Zhang, Lijing; Zhao, Xiao; Wu, Wenjing; Hao, Jihui; Qin, Zhihai; Zhao, Ying; Nie, Guangjun, *Designing liposomes to suppress extracellular matrix expression to enhance drug penetration and pancreatic tumor therapy*. ACS nano, 2017. **11**(9): p. 8668-8678.
280. Jain, R.K.s., Triantafyllos, *Delivering nanomedicine to solid tumors*. Nature reviews Clinical Oncology, 2010. **7**(11): p. 653-664.
281. Goodman, T.T.O., Peggy L.; Pun, Suzie H., *Increased nanoparticle penetration in collagenase-treated multicellular spheroids*. Int J Nanomedicine, 2007. **2**(2): p. 265-274.
282. Chauhan, V.P.M., John D.; Liu, Hao; Lacorre, Delphine A.; Jain, Saloni; Kozin, Sergey V.; Stylianopoulos, Triantafyllos; Mousa, Ahmed S.; Han, Xiaozing; Adstamongkonkul, Pichet; Popovic, Zoran; Huang, Peigen; Bawendi, Mounqi G.; Boucher, Yves; Jain, Rakesh K, *Angiotensin inhibition enhances drug delivery and potentiates chemotherapy by decompressing tumour blood vessels*. Nature Communications, 2013. **4**.
283. Diop-Frimpong, B.C., Vikash P.; Krane, Stephen; Boucher, Yves; Jain, Rakesh K. *Losartan inhibits collagen I synthesis and improves the distribution and efficiency of nanotherapeutics in tumors*. in *Proceedings of the National Academy of Sciences (PNAS)*. 2011.

284. Kobayashi, H.R., Koen; English, Sean; Yordanov, Alexander T.; Milenic, Diane E.; Sowers, Anastasia L.; Citrin, Deborah; Krishna, Murali C.; Waldmann, Thomas A.; Mitchell, James B.; Brechbiel, Martin W., *Application of a macromolecular contrast agent for detection of alteration of tumor vessel permeability induced by radiation*. *Clinical Cancer Research*, 2004. **10**(22): p. 7712-7720.
285. Kobayashi, H.T., Baris; Watanabe, Rira; Choyke, Peter L., *Cancer drug delivery: considerations in the rational design of nanosized bioconjugates*. *Bioconjugate Chemistry*, 2014. **25**(12): p. 2093-2100.
286. Syed, A.M., S. Sindhvani, and W.C. Chan, *Making vessels more permeable*. *Nature Biomedical Engineering*, 2017. **1**(8): p. 629.
287. Alivisatos, P., *The use of nanocrystals in biological detection*. *Nat Biotech.*, 2003. **22**: p. 47-51.
288. Liong, M., Lu J, Kovichich M, Xia T, Ruehm SG, Nel AE, Tamanoi F, Zink JJ., *Multifunctional Inorganic Nanoparticles for Imaging, Targeting, and Drug Delivery*. *ACS nano*, 2008. **2**: p. 889-896.
289. Langereis, S., Keupp J, van Velthoven JIJ, de Roos IHC, Burdinski D, Pikkemaat JA, Gru" H, *A Temperature-Sensitive Liposomal 1H CEST and 19F Contrast Agent for MR Image-Guided Drug Delivery*. *J. Am. Chem. Soc.*, 2009. **9**: p. 1380-1381.
290. Perrault, S.D., Walkey C, Jennings T, Fischer HC, Chan WCW, *Mediating Tumor Targeting Efficiency of Nanoparticles Through Design*. *Nano Lett*, 2009. **9**: p. 1909-1915.
291. Lee, J.E., Lee N, Kim H, Kim J, Choi SH, Kim JH, Kim T, Song IC, Park SP, Moon WK, Hyeon T., *Uniform Mesoporous Dye-Doped Silica Nanocrystals for Simultaneous Enhanced Magnetic Resonance Imaging, Fluorescence Imaging, and Drug Delivery*. *J Am Chem Soc*, 2010. **132**: p. 552-557.
292. Goodman, T.T., P.L. Olive, and S.H. Pun, *Increased nanoparticle penetration in collagenase-treated multicellular spheroids*. *International Journal of Nanomedicine*, 2007. **2**(2): p. 265-274.
293. Ramanujan, S., A. Pluen, T.D. McKee, E.B. Brown, Y. Boucher, and R.K. Jain, *Diffusion and convection in collagen gels: implications for transport in the tumor interstitium*. *Biophys J.*, 2002. **83**(3): p. 1650-1660.

294. Grantab, R., S. Sivananthan, and I.F. Tannock, *The penetration of anticancer drugs through tumor tissue as a function of cellular adhesion and packing density of tumor cells*. *Cancer Res.*, 2006. **66**(2): p. 1033-1039.
295. Minchinton, A.I. and I.F. Tannock, *Drug penetration in solid tumours*. *Nat Rev Cancer*, 2006. **6**(8): p. 583-592.
296. Tannock, I.F., C.M. Lee, J.K. Tunggal, D.S. Cowan, and M.J. Egorin, *Limited penetration of anticancer drugs through tumor tissue: a potential cause of resistance of solid tumors to chemotherapy*. *Clin Cancer Res.*, 2002. **8**(3): p. 878-884.
297. Dreher, M.R., W. Liu, C.R. Michelich, M.W. Dewhirst, F. Yuan, and A. Chilkoti, *Tumor vascular permeability, accumulation, and penetration of macromolecular drug carriers*. *J Natl Cancer Inst.*, 2006. **98**(5): p. 335-344.
298. Alexandrakis, G., E. Brown, R. Tong, T. McKee, R. Campbell, Y. Boucher, and R.K. Jain, *Two-photon fluorescence correlation microscopy reveals the two-phase nature of transport in tumors*. *Nat Med.*, 2004. **10**(1078-8956): p. 203-207.
299. Yohan, D., C. Cruje, X. Lu, and D. Chithrani, *Size-Dependent Gold Nanoparticle Interaction at Nano–Micro Interface Using Both Monolayer and Multilayer (Tissue-Like) Cell Models*. *Nano-Micro Letters*, 2015: p. 1-10.
300. Yang, C., J. Uertz, D. Yohan, and B.D. Chithrani, *Peptide modified gold nanoparticles for improved cellular uptake, nuclear transport, and intracellular retention*. *Nanoscale*, 2014. **6**: p. 12026-12033.
301. Cruje, C., C. Yang, J. Uertz, M. van Prooijen, and B.D. Chithrani, *Optimization of PEG coated nanoscale gold particles for enhanced radiation therapy*. *RSC Advances*, 2015. **5**: p. 101525-101532.
302. Cruje, C. and B.D. Chithrani, *Integration of Peptides for Enhanced Uptake of PEGylated Gold Nanoparticles* *Journal of Nanoscience and Technology*, 2015. **15**: p. 2125-2131.
303. Wilhelm, S., A.J. Tavares, Q. Dai, S. Ohta, J. Audet, H.F. Dvorak, and W.C. Chan, *Analysis of nanoparticle delivery to tumours*. *Nature Reviews Materials*, 2016. **1**: p. 16014.